UNIVERSITY OF INSUBRIA

Doctoral School of Biological and Medical Sciences

Ph.D. Program in Neurobiology

Functional and molecular defects of human induced pluripotent stem cell-derived neurons from patients with the neurodegenerative disorder ataxia-telangiectasia

Tutor: **Dr. Domenico Delia**

Supervisor and Coordinator: **Prof. Daniela Parolaro**

Ph.D. thesis of

Dr. Elena Fusar Poli

XXVII Cycle – 2011/2014

The research work presented in this thesis was carried out at the

Fondazione IRCCS Istituto Nazionale dei Tumori

Department of Experimental Oncology

Via Amadeo, 42

Milano

Acknowledgements

I would like to express my very great appreciation to Dr. Domenico Delia for his valuable and constructive suggestions during the planning and development of this research work, to Dr. Luigi Carlessi for precious collaboration throughout all aspects of the project and to Prof. Daniela Parolaro for her professional guidance and valuable support.

I wish to acknowledge the help provided by Dr. Giulia Bechi, Department of Neurophysiopathology, Fondazione IRCCS Istituto Neurologico Carlo Besta, Milan, Italy, for electrophysiological recordings and analysis and by Dr. Barbara Pascucci, CNR Institute of Crystallography, Rome, Italy, for base excision repair analysis. I also wish to thank Dr. Chiara Verpelli, CNR Institute of Neuroscience and Department of Biotechnology and Translational Medicine, Milan, Italy, for providing us with control primary dermal fibroblasts and Dr. Christian Unger, Centre for Stem Cell Biology, University of Sheffield, UK, for providing us with anti-SSEA4 and anti-TRA-1-81 antibodies.

This work was financially supported by Comitato Telethon Fondazione Onlus, grant no. GGP10066, and by the Italian Association for Cancer Research (AIRC), grant no. IG10248.

Table of contents

Abstract

Ataxia-telangiectasia (A-T) is a rare hereditary, early onset neurodegenerative disorder caused by inactivation of the ATM serine/threonine protein kinase, which is the major regulator of the DNA damage response to double-strand breaks (DSBs) and works in sensing and signaling oxidative stress. Disease models are essential for unraveling the mechanisms underlying the neuropathology, but ATM knockout mice do not recapitulate the central nervous system phenotype and neural stem cells are very heterogeneous. In this work we applied a reprogramming approach to generate an *in vitro* human A-T model in order to investigate the outcome of ATM ablation in neurons.

We derived induced pluripotent stem cells from A-T and normal control fibroblasts by introducing the reprogramming factors *OCT3/4*, *KLF4*, *SOX2* and *l-MYC* and from these we obtained expandable nestin-positive neural precursor cells (NPCs) via embryoid body and neural rosette formation. Following differentiation, NPCs gave rise to a high percentage of mature neurons expressing β-tubulin III and microtubule-associated protein 2. Our results show that electrophysiological properties were similar in control and A-T cells. Also, base excision repair, which is important for the removal of DNA single strand breaks caused by oxidative stress, and single strand break repair were normal in A-T cells. On the other hand, A-T neurons displayed attenuated DNA damage response and repair following irradiation and were resistant to apoptosis induced by genotoxic agents, but not by oxidative agents. Moreover, mutant neurons displayed deficits in the expression of the synaptic markers synaptophysin and postsynaptic density protein 95 as well as of the neuronal growth-associated protein SCG10 and K^+ channel-interacting proteins KChIP. Notably, A-T neurons exhibited abnormal accumulation of topoisomerase 1-DNA covalent complexes, which may cause impairment of transcription elongation. These findings reveal that, in neural cells, ATM deficiency suppresses the response and repair of DNA DSBs, impairs neuronal maturation and could promote transcriptional decline, possibly contributing to neurodegeneration in A-T.

This previously undocumented functional and molecular characterization of patient-derived neuronal cells represents the first step in the employment of these cells as the most informative *in vitro* model to investigate neurodegeneration in A-T. Moreover, this model represent a powerful tool for further exploring the mechanisms that cause degeneration of human ATM-deficient neurons and it may be exploited for identifying therapeutic targets and for screening molecules with potential neuroprotective properties.

List of abbreviations

A-T, ataxia-telangiectasia

ATM, ataxia-telangiectasia mutated

BER, base excision repair

bFGF, basic fibroblast growth factor

CHK2, checkpoint kinase 2

CPT, camptothecin

DAPI, 4',6-diamidino-2-phenylindole

DSB, double-strand break

EB, embryoid body

EGF, epidermal growth factor

ESC, embryonic stem cell

HR, homologous recombination

iPSC, induced pluripotent stem cell

IR, ionizing radiation

MRN, MRE11-RAD50-NBS1

NHEJ, non-homologous end joining

NPC, neural precursor cell

NSC, neural stem cell

PMEF-CFL, primary mouse embryonic fibroblasts, strain CF-1

RADAR, rapid approach to DNA adduct recovery

ROS, reactive oxygen species

SSB, single strand break

Top1, topoisomerase I

Top1cc, Top1 cleavage complex

1. Introduction

1.1 Ataxia-telangiectasia

Ataxia-telangiectasia (A-T, also known as Louis-Bar syndrome) is a rare autosomal recessive disorder which leads to a complex and variably severe combination of disease phenotypes, including neurodegeneration, telangiectasia, cancer predisposition, radiosensitivity, chromosomal instability and immunodeficiency (1). A-T was first reported in three patients by Syllaba and Henner in 1926 (2), further described in an additional patient by Louis-Bar in 1941 (3) and finally recognized as a separate disease entity in 1957 by Boder and Sedgwick (4). The disease is broadly distributed throughout the world and occurs equally among males and females of all races, with an incidence of about 1 in 40,000-100,000 live births and a carrier frequency estimated to be approximately 1% (5). The monogenic nature of the disorder was only established in 1995, when Savitsky et al. discovered that A-T is caused by varying degrees of mutational inactivation of the ataxia-telangiectasia mutated (ATM) serine/threonine protein kinase (6).

1.1.1 Neurological manifestations and neuropathological findings

The clinical hallmark and most devastating feature of A-T is early onset cerebellar ataxia, which characterizes all cases and is usually the first presenting symptom, becoming manifest between 12 and 24 months of age and affecting sitting, balance and walking (7,8). Cerebellar dysfunction subsequently spreads to involve the extremities and speech, with consequent dysarthria, oculomotor apraxia, nystagmus, impassive facies, dysphagia and impairment of fine motor functions. Choreoathetosis and dystonia are also typical manifestations during the progression of the disease. Although the gross milestones of early motor development are usually acquired on time thanks to developmental progress, the slowly advancing neurodegeneration causes affected children to require a wheelchair by their early teens.

Strikingly, the relentless neurological impairment seems to spare cognitive function and most A-T individuals appear to have a normal IQ, although there are indications of mental decline with ongoing disease course (7,8).

From a histo-anatomical point of view, the devastating neurodegeneration which leads to the complex neurological phenotype induces severe abnormalities in many districts of the central and peripheral nervous system of affected individuals (7,8,9). According with the fact that A-T is primarily a syndrome of progressive cerebellar ataxia, histological studies of autopsy samples from patients show atrophy of all cerebellar cortical layers, with a thinning of cerebellar hemispheric foliae and cerebellar vermis and frequent vascular changes. These degenerative modifications are accompanied by extensive and progressive loss of Purkinje neurons and, to a lesser extent, of granule neurons (7,8,9). Interestingly, while sometimes displaced in the molecular layer of the cerebellum (10), the majority of the remaining atrophic Purkinje cells are found in the single cell layer of Purkinje cells (Figure 1), indicating that they are able to migrate correctly in the developing brain, and indeed the basket cells that only form around them are in their proper place (11,12). This suggests that Purkinje cells are affected at an early stage, but only after they are fully developed. These observations are in accordance with magnetic resonance imaging studies of the cerebellum, which are generally without pathological findings during early childhood, but show significant thinning of the molecular layer and cerebellar atrophy by the end of the first decade of life (13).

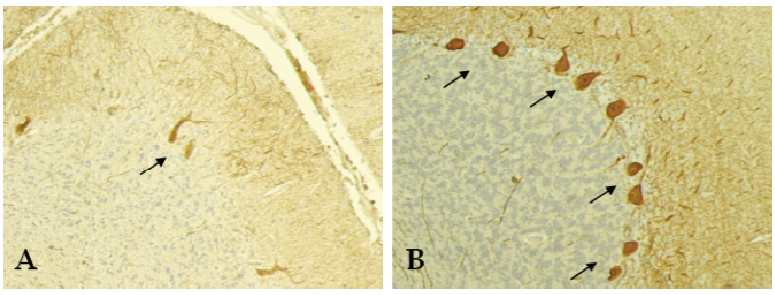

Fig. 1: Comparison of Purkinje cells from an A-T patient (A) and an age-matched control subject (B) detected by anti-calbindin immunostaining of cerebellar sections.

As children grow into adulthood, degenerative changes become more extensive. Autopsy studies report neuronal loss in the striatum and substantia nigra, neurodegeneration of cranial nerves, atrophy of the posterior columns and of the anterior horn, loss of myelinated fibers in corticospinal and spinocerebellar tracts, decreased number of myelinated fibers and severe atrophic changes in peripheral nerves, leading to severe sensorimotor axonal degeneration, peripheral neuropathy, and consecutive spinal muscular atrophy (8,9,14-18).

1.1.2 Non-neurological clinical features

Oculocutaneous telangiectasia, which consists in chronic dilation of capillaries leading to the development of dark red spots especially in the bulbar conjunctivae and in the butterfly area of the face, is the second cardinal feature of A-T and develops several years after the onset of the neurological symptoms (1,7). Fortunately, it is not associated to further complications and is thus medically irrelevant. Another tragic manifestation of A-T is the greatly increased risk of developing cancer, primarily leukemias and lymphomas, with a lifetime frequency that approaches 40% (1,19). It is noteworthy that also carriers of disease-causing mutations have an increased risk of contracting breast tumors, suggesting dominance of the defective gene (20). Importantly, missing the diagnosis of A-T may lead to administration of chemotherapy or even radiotherapy with severe and fatal clinical consequences: indeed patients are hypersensitive to genotoxic agents and ionizing radiation (IR), which renders these therapeutic approaches particularly hazardous and complicates the management of any malignancy (21). Patients also display variable cellular and humoral immunodeficiency with absent or low levels of IgA and IgE, abnormalities in IgG and IgM and an atrophic or absent thymus (7,21). Consequently, affected individuals are particularly vulnerable to infections and suffer from recurrent bronchopulmonary diseases. In addition, the disorder is characterized by rising levels of alpha-fetoprotein (22), chromosomal instability involving primarily the loci of immunoglobulin and T-

cell receptor genes on chromosomes 7 and 14 (21,23), growth retardation (1,7), insulin resistance which causes susceptibility to type II diabetes (24) and gonadal atrophy (7,8). Expected life span is between 15 and 25 years of age and death is caused predominantly by cancer, chronic lung disease resulting from immunodeficiency and defects in chewing and swallowing due to progressive neurological impairment (25).

1.1.3 Diagnosis and treatment

It is important to accurately diagnose A-T as rapidly as possible in order to allow appropriate care and genetic counseling, especially given the increased risk of malignancies and the higher risk of side effects of subsequent cancer treatment not only in patients, but also in heterozygous relatives. The presence of A-T is usually recognized by the combination of neurological features with telangiectasia and infections, but unfortunately in very young children the phenotype is often incomplete and telangiectasia only appears around six years of age, making early differential diagnosis difficult (26). Moreover, it must be noted that the A-T phenotype includes a wide and continuous spectrum of manifestations that span from the previously described severe classical form to a less severe adult-onset disorder, referred to as variant A-T, which is characterized by milder symptoms, extrapyramidal signs and extended lifespan, with consequent further difficulty in recognizing the disease (9).

Laboratory investigations in patients who are suspected to suffer from A-T can accelerate diagnosis. These include measurement of AFP levels, cytogenetic analysis of chromosomal instabilities with special attention to translocations involving chromosomes 7 and 14, evaluation of serum immunoglobulin levels, assessment of the levels of ATM protein or of ATM protein kinase activity, colony survival assay after exposure to γ-radiation and, most recently, mutation detection (27).

Sadly, there is currently no treatment available to cure, prevent or postpone the progression of A-T. Patients are only offered symptomatic and supportive therapies, such as physiotherapy, logopedics, antibiotic treatment, gastrostomy and respiratory support when needed (27).

1.2 ATM gene and protein

The gene responsible for A-T was initially localized to chromosomal region 11q22.3-23.1 in 1988 by Gatti et al. (28), and in 1995 was definitely identified by Savitsky et al. (6) as the *ATM* gene, which extends over 150 kb of genomic DNA and contains 66 exons encoding a 13 kb transcript (29). Since then, more than 400 unique gene mutations reported throughout the whole sequence of *ATM* have been associated to A-T (9,30,31). These mainly comprise truncating mutations, which have detrimental effects on the protein and are associated with the most severe early-onset form of the disorder, while a lower percentage of mutations allowing for residual ATM activity, such as missense mutations or in-frame deletions or insertions, cause milder forms of the disease.

The *ATM* gene encodes a large serine/threonine protein kinase made up of 3056 residues and with a molecular weight of 350 kDa which is constitutively expressed in all tissues and is predominantly located in the nucleus, although a small amount is also present in the cytoplasm of many cell types (6,32). In account of its carboxy-terminus, which contains a catalytically active phosphatidylinositol-3-kinase (PI3K) domain, the ATM protein has been classified as member of the PI3K-related protein kinase (PIKK) family, which also includes ATM and RAD3-related (ATR), DNA-dependent protein kinase (DNA-PK), mammalian target of rapamycin (mTOR), suppressor of mutagenesis in genitalia 1 (SMG1) and transformation/transcription domain-associated protein (TRRAP) (33). ATM phosphorylates its substrates on a serine or threonine that is followed by glutamine, namely an SQ or TQ ([S/T]Q)

motif (34). In addition to the kinase domain, three regulatory domains are also conserved in the PIKK family and are thus found in ATM: a FRAP-ATM-TRAP (FAT) domain, a FAT-C-terminal (FATC) domain and a PIKK-regulatory domain (PRD), which is the N-terminal portion of the FATC domain (33). Other protein regions which have been characterized include sites of interaction with other proteins, such as the substrate-binding site (SBS) near the N-terminus of the protein, and post-translational modification sites, such as Ser367, Ser1893, Ser1981, Ser2996 and Lys3016 (35) (Figure 2), but unfortunately the structure of the protein has not yet been entirely defined, complicating the full comprehension of ATM function.

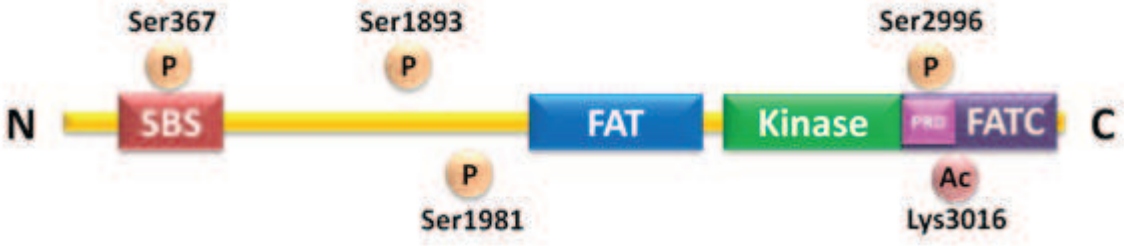

Fig. 2: Schematic representation of ATM.

1.3 Functions of ATM and possible causes of neurodegeneration in ataxia-telangiectasia

It has long been known that ATM plays a central role in the cellular response to DNA damage and in cell cycle checkpoint control, and it is now evident that its activity is essential in an increasing number of other cellular pathways involved in the maintenance of cellular homeostasis (32). Accordingly, the multiple functions of ATM account for the complex phenotypic manifestations deriving from inactivating mutations in the gene. Nonetheless, our current knowledge on ATM activity cannot yet fully explain the tragic neurological decay which affects A-T patients. The relentless neurodegeneration caused by ATM deficiency presumably results from the concurrence of different pathogenetic mechanisms which arise

following the disruption of the multiple pathways in which the serine/threonine kinase is involved (32). Therefore, it is extremely important that ATM functions be defined in detail in order to be able to thoroughly characterize the pathogenesis of the disorder and consequently delineate potential therapeutic strategies.

1.3.1 Role of ATM in the DNA damage response and in cell cycle control

As cells are constantly exposed to a multitude of stresses, including many of which threaten genome stability, several different signal-transduction pathways are readily activated when necessary in order to protect cellular integrity. In particular, DNA double-strand breaks (DSBs) represent the most dangerous form of DNA damage and can lead to cell death, deleterious chromosomal instability and malignant transformation (36). These lesions are generated following exposure to exogenous agents such as IR and radiomimetic chemicals, but can also be caused by endogenous products like oxygen radicals or occur during normal physiological cell processes such as DNA replication, meiotic recombination and V(D)J recombination. The repair of DSBs can occur either by non-homologous end joining (NHEJ) or by homologous recombination (HR) (37). The first is the major DNA repair process in mammalian cells, being active throughout the cell cycle, and consists in the direct ligation of the two DNA ends; the latter intervenes in the late S phase or G2 phase of the cell cycle and repairs the damaged DNA strand with the aid of the intact sister chromatid. Notably, not all DSBs are repaired at the same speed: approximately 85% are repaired with fast kinetics while 15–20% are repaired more slowly (38).

When DNA cannot be readily repaired, as when the lesion is situated in a tightly compacted heterochromatic area or when high levels of damage occur, an ATM-dependent DSB response becomes necessary (35,39). Indeed, the ATM protein kinase participates in the slower repair of DNA lesions and, most importantly, plays a crucial role in the initiation of the cellular

response to DSBs, being able to create a complex yet coordinated signaling network that triggers arrest of cell cycle progression through checkpoint activation. This is crucial for allowing the cell to process the DNA damage and, when this is not possible, for inducing senescence or apoptotic death.

In undamaged cells, ATM is found in the nucleus in the form of inactive homodimers (40). Following the induction of DSBs, ATM is activated through intermolecular autophosphorylation at Ser1981, which causes conformational changes leading to monomerization (40), and is recruited to the lesions by the primary sensor complex MRE11-RAD50-NBS1 (MRN), which assembles at the damaged sites, unwinds the DNA ends and binds and retains ATM through the C-terminal domain of NBS1 (41). Although it is clear that these events are essential for triggering ATM activation, their precise sequence is still debated. Moreover, other processes including chromatin remodeling (40) and post-translational modifications such as autophosphorylation on the three additional sites Ser367, Ser1893 and Ser2996 (42), TIP60-mediated acetylation at Lys3016 (43) and PP5-dependent dephosphorylation (44) of ATM all cooperate in the initiation of its kinase activity. Once activated, ATM functions as the apical kinase in the complex intracellular signaling cascade that characterizes the DNA damage response to DSBs (32).

At the damaged sites, ATM phosphorylates the MRN complex (45) and histone H2AX at Ser139 (producing γH2AX) (46), inducing chromatin modifications that allow the recruitment and phosphorylation of the mediator proteins mediator of DNA damage checkpoint protein 1 (MDC1) (47), p53-binding protein 1 (53BP1) (48) and breast cancer type 1 susceptibility protein (BRCA1) (49), which assemble on the DNA creating autoalimented foci that form a scaffold for the recruitment of repair proteins, sustain and amplify damage signaling and maintain the activation of ATM in a positive feedback loop (35,50). Intriguingly, the assembly of foci at the site of DNA DSBs can also occur in the absence of ATM activity thanks to the redundant

phosphorylation of H2AX operated by DNA-PK, another PIKK involved in DSB processing (51). Nevertheless, being a large amount of the proteins in each focus an ATM substrate, the functional significance of their ATM-dependent phosphorylation is lost when the kinase is missing or inactive.

Furthermore, ATM directly cooperates in the repair of DSBs in heterocromatic DNA by phosphorylating the transcriptional co-repressor Krüppel-associated box-associated protein-1 (KAP1) at the damaged site, consequently easing the entry of the DNA repair machinery (52), and by hyperphosphorylating the endonuclease Artemis, which is responsible for the processing of the damaged ends (53). Importantly, the ATM-dependent DSB-repair also relies on the MRN complex, γH2AX, MDC1 and 53BP1 (52).

Away from the damaged site, ATM phosphorylates the main transducer of the ATM signaling pathway, the checkpoint kinase CHK2, inducing a signaling cascade that leads to cell cycle arrest through DNA damage checkpoint activation (54). Importantly, CHK2 is only one of the numerous diffusible substrates of the apical kinase. Indeed, ATM is able to reach the same endpoints by triggering different pathways, therefore guaranteeing a strict regulation of each process (32). Hence, the G1/S checkpoint is also activated through direct phosphorylation, stabilization and accumulation of the p53 transcription factor, the intra-S phase checkpoint can also be elicited through phosphorylation of SMC1 or BRCA1, and the G2/M checkpoint can be triggered through phosphorylation of BRCA1 (35,55).

This ATM-dependent DNA damage signaling pathway gives rise to a cellular response to DSBs that goes beyond repair, activating both cell survival and cell death pathways through the modulation of gene expression and of protein synthesis and degradation . The outcome is a very meticulous DNA damage response, resulting either in damage removal, cell senescence or apoptosis (32,35) (Figure 3).

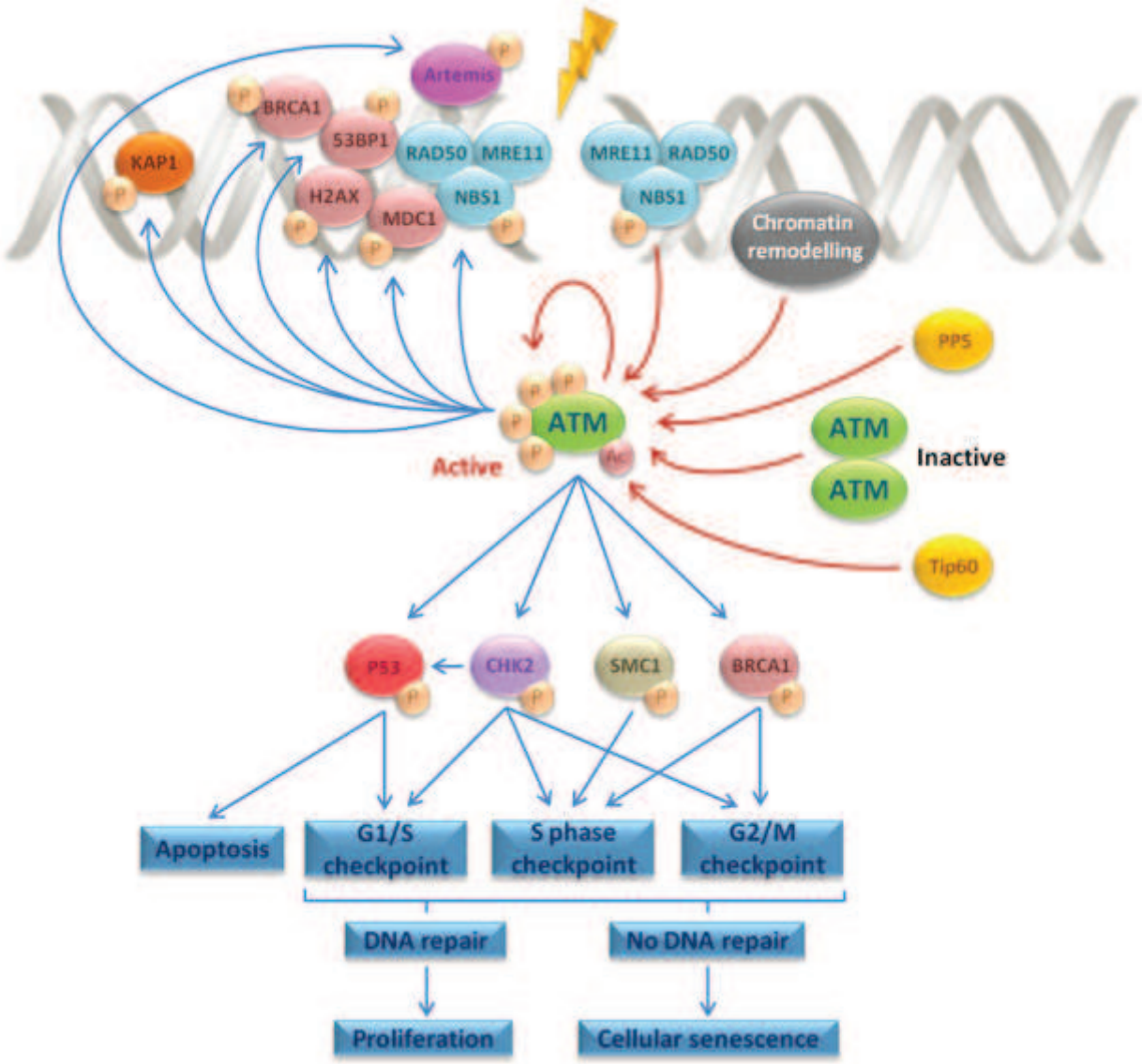

Fig. 3: Schematic representation of the ATM-dependent DNA damage response.

The absence of ATM activity during neuronal development at very early stages may cause the emergence of genomic damage that becomes fixed in the nervous system and, at later stages, it may allow terminally differentiated neurons to further accumulate damaged DNA without an efficient repair mechanism (8,56). ATM-deficient damaged neurons may enter apoptosis or may be retained in the nervous system and as a consequence degenerate due to accumulation of toxic proteins or dysfunctional genes. Moreover, loss of ATM-dependent cell cycle control could also cause unscheduled re-entry of differentiated post-mitotic neurons into the cell cycle, which results in cell death (57).

1.3.2 Additional roles of ATM in the cytoplasm and in the nucleus

Although the most striking function of ATM is certainly its central role in the response to DSBs, which is carried out in the nucleus, the serine/threonine protein kinase is also present in the cytoplasm and plays an important part in other cellular processes in the undamaged cell, participating in signaling pathways that maintain cellular homeostasis and respond to physiological stimuli (32). Indeed, ATM can be activated in a DSB- and MRN-independent manner and has been found to phosphorylate over a hundred substrates, many of which differ from those involved in the DNA damage response.

One of the most important cytoplasmic functions of ATM regards the sensing and signaling of reactive oxygen species (ROS) (32). ROS are chemically reactive molecules which are formed as byproduct of the physiological activity of many endogenous enzymes and of the respiratory chain in the mitochondria, and have important roles in cell signaling and homeostasis (58). When there is an overproduction of ROS, for example following mitochondrial dysfunction or the exposure to exogenous factors such as UV light and IR, or when the effectiveness of cellular antioxidant defenses decreases, intracellular ROS levels can increase dramatically leading to oxidative stress, which produces significant lesions to cellular structures and causes DNA damage in the form of oxidized DNA bases, apurinic/apyrimidinic sites, single strand breaks (SSBs) and DSBs (58). It has long been known that ATM-deficient cells are more susceptible to oxidative damage produced by both exogenous and endogenous factors (59-62) and that they display elevated levels of oxidative damage-responsive pathways (63-66) and reduced levels of antioxidants (67), suggesting that ATM is a sensor for redox homeostasis and that A-T is a disorder related to oxidative stress. Indeed, it has recently been shown that ATM can be directly activated through autophosphorylation in response to the oxidizing agent hydrogen peroxide (H_2O_2) in the absence of DNA damage and in an MRN-independent fashion (68). This is possible thanks to the formation of an intermolecular disulfide bond at Cys2991 in

the C-terminus of the protein, which gives rise to an active covalent dimer. ATM appears to regulate the antioxidant capacity of cells also by indirectly participating in the correct regeneration of the antioxidant glutathione (69). Indeed, ATM is able to enhance the pentose phosphate pathway and therefore the synthesis of the antioxidant cofactor NADPH, which is required by the glutathione reductase enzyme for the reduction of the oxidized form of glutathione back to its reduced active version. As neurons have an intensive metabolic activity, they physiologically accumulate elevated levels of ROS (70) and since the absence of ATM causes the loss of redox balance, A-T neurons may be hypersensitive to endogenous oxidative stress and exogenous oxidative stress-inducing agents(8). This may contribute to the accumulation of DNA damage in these cells and neurodegeneration in A-T could therefore also result from deficient-ROS homeostasis.

Moreover, ATM plays an important role in mitochondrial homeostasis (32). Mitochondria are organelles which have their own DNA and are the sites of cellular respiration, which is essential for the generation of ATP and therefore for supplying energy to the cell (71). Importantly, this process can lead to the endogenous production of damaging ROS species, which is exacerbated by mitochondrial dysfunction. Early reports have described impaired mitochondrial functions in ATM-deficient cells (72,73), and a more recent investigation has shown that indeed a fraction of ATM localizes to mitochondria in thymocytes (74). In particular, according to this study, ATM loss results in deficiencies in mitochondrial electron transport chain activity, impaired ATP levels, elevated mitochondrial ROS and increased mitochondrial number, which is due to defects in the selective clearance of abnormal mitochondria by autophagy, a process also known as mitophagy. It has also been shown that ATM plays an important role in maintaining the integrity of mitochondrial DNA (75). Indeed, the lack of ATM causes decreased protein levels of DNA ligase III, which is the only known DNA ligase operating in mitochondria. This impairs the base excision repair (BER) pathway and thus the

removal of oxidative lesions from mitochondrial DNA, with consequent persistent mitochondrial DNA damage and mitochondrial dysfunction. Hence, these findings indicate that ATM is involved in the regulation of mitochondrial activity and mitochondrial dysfunction may be responsible for elevated ROS production and oxidative stress in A-T neurons.

Cytoplasmic ATM also participates in insulin signaling pathways (32). Insulin is a crucial hormone in the regulation of mitogenic and metabolic actions as it stimulates cell proliferation, boosts protein synthesis, inhibits breakdown of fat and regulates glucose homeostasis by inhibiting its hepatic output and promoting its uptake especially into striated muscle cells and adipocytes (76). It has been shown that ATM participates in the cellular response to insulin by phosphorylating the translation repressor eIF4E-binding protein 1 (4EBP1), which binds to and inhibits the eukaryotic translation initiation factor 4E (eIF4E) (77). Following phosphorylation, 4EBP1 dissociates from eIF4E, with consequent enhancement of protein synthesis. ATM also responds to insulin by phosphorylating and fully activating the protein kinase AKT (78), which participates in multiple physiological processes and is involved in the enhancement of glucose uptake by inducing translocation of the glucose transporter GLUT4 to the plasma membrane (79). The metabolic effects of insulin appear to be regulated by ATM also in an oxidative stress-dependent manner through the phosphorylation of p53 Ser15, which induces changes in gene expression in order to maintain insulin sensitivity and glucose homeostasis (80). Indeed, loss of the ATM phosphorylation site in p53 induces insulin resistance and glucose intolerance, which can be ameliorated by treatment with the antioxidant N-acetylcysteine (NAC). Therefore, the disruption of an insulin-dependent regulation of gene expression, of protein synthesis and of glucose uptake in the absence of ATM can explain some of the symptoms associated with A-T such as metabolic abnormalities, growth retardation and insulin-resistant diabetes. In addition, because insulin serves as a survival and differentiation

factor for the developing neuronal tissue, the impairment of insulin signaling in ATM-deficient neural cells may contribute to neurodegeneration in A-T (81).

Furthermore, ATM plays an important role in the mitotic spindle checkpoint (32). This checkpoint regulates the transition from metaphase to anaphase and is essential for the correct partition of sister chromosomes during mitosis, in order to avoid aneuploidy in daughter cells (82). Recent findings have demonstrated that many proteins involved in the maintenance of genomic stability through the DNA damage response also participate in the regulation of the mitotic spindle checkpoint, including ATM (83-86). Indeed, during mitosis ATM is phosphorylated and activated by the aurora B kinase, and in turn phosphorylates critical components of the mitotic spindle checkpoint such as the budding uninhibited by benzimidazoles homolog 1 (BUB1) protein kinase (87) and the mitotic arrest-deficient protein 1 (MAD1) (88), inducing activation of the first and dimerization of latter, altogether halting the cell cycle until all chromosomes are correctly attached to the mitotic spindle. In case of ATM deficiency, defects in the regulation of the transition from metaphase to anaphase cause aneuploidy (89-91), thus further supporting the role of ATM in the maintenance of genomic and chromosomal stability.

Finally, ATM has been linked to the response to and processing of topoisomerase 1 (Top1)-DNA cleavage complexes (Top1ccs) in neural cells (92,93). Top1 is an enzyme that relaxes DNA supercoiling during replication and transcription by generating transient DNA SSBs and religating the strands (94). Top1ccs are thus temporary intermediates consisting of Top1 covalently linked to a nicked DNA molecule and must be readily removed. The presence of altered DNA bases, for example due to oxidation, or treatment with Top1 inhibitors, such as camptothecin (CPT), stabilize the cleavage complexes and consequently block DNA transcription (94). It has been shown that the trapping of transcription-dependent Top1ccs prevent DNA religation and induce DNA DSBs, which lead to the activation of the ATM-

dependent DNA damage response (93). Moreover, ATM has also been reported to prevent the accumulation of Top1ccs by regulating the turnover of Top1 in a kinase-independent manner (92). Therefore, in the absence of ATM, defective Top1cc processing can increase levels of DNA damage and impair transcription, thus participating in causing neuronal death in A-T.

1.3.3 Specific roles of ATM in neurons

Concordant with the fact that A-T is characterized by selective death of neurons, an increasing number of findings support the notion that in neuronal cells ATM carries out specific cytoplasmic and nuclear functions which are essential for the survival and well-being of these cells (95). Consequently, the disruption of these processes due to ATM deficiency adds to the loss of ubiquitous ATM activities and participates in the onset of neurodegeneration.

The first neuronal-specific function of ATM to be described was its association with and regulation of synaptic vesicle cycling (96). Synaptic vesicles and their recycling are essential in neurons as they store neurotransmitters which, following stimulation, are released at the synapse for the propagation of the nerve impulse (97). In the axon terminals ATM, together with ATR, associates with the two synaptic vesicle proteins synapsin 1 and vesicle-associated membrane protein 2 (VAMP2), also known as synaptobrevin (96). These four proteins thus form a complex in which ATM and ATR regulate the release of vesicles by phosphorylating synapsin 1 and VAMP2, respectively, therefore modulating synaptic function. More recently, it has been reported that ATM cooperates with ATR and possibly other kinases in the generation of a specific [S/T]Q phosphoproteome that localizes to dendrites, synapses and soma (98). Indeed, ATM has been found to be activated in response to depolarizing post-synaptic stimuli in the soma and in the proximal portion of dendrites, consequently driving the phosphorylation of a

vast number of substrates which participate in the regulation of neuronal gene expression, cell viability and synaptic plasticity. The disruption of these cytoplasmic functions of the serine/threonine kinase could contribute to the neurological symptoms of A-T by inducing synaptic degeneration, as it has been shown that in the absence of ATM neurons display defective vesicle trafficking and reduced long term potentiation, which is involved in synaptic plasticity (96).

Another role of ATM in the neuron regards its involvement in the protection against glutamatergic excitotoxicity (99), a pathological process that leads to neuronal death following excessive stimulation by excitatory neurotransmitters and substances (100). It has been shown that during neuronal differentiation induced by retinoic acid, ATM phosphorylates and activates the cAMP-responsive element-binding protein CREB, which binds to the promoter region of the zinc finger homeobox 3 (*ZFHX3*) transcription factor gene and induces its expression (99). In turn, ZFHX3 promotes the transcription of the platelet-derived growth factor tyrosine kinase receptor β (PDGFRB) (99), which participates in the cellular defense against excitotoxicity and thus promotes neuronal survival (101). Accordingly, in response to oxidative stress generated by excessive excitation of neurons, PDGFRB activates ATM in a DNA damage-independent manner to inhibit mTORC1, thus promoting autophagy for the maintenance of cellular homeostasis (99). All together, these findings further indicate that a defective protection of neurons against oxidative stress in the absence of ATM can play a role in inducing chronic neuronal degeneration.

ATM is also engaged in preserving the neuronal epigenetic signature through the regulation of histone modification, which is of pivotal importance for maintaining proper gene expression in neurons (102). Specifically, one of the cytoplasmic roles of ATM in neurons consists in phosphorylating and downregulating the protein phosphatase PP2A, thus mediating the retention of the phosphorylated form of histone deacetylase HDAC4 in the cytoplasm and

consequently preventing histone deacetylation due to its accumulation in the nucleus (103). Furthermore, ATM reduces polycomb repressive complex 2 (PRC2)-dependent trimethylation of histone H3 on Lys27 (H3K27me3) by phosphorylating and downregulating the histone-lysine N-methyltransferase enhancer of zeste homolog 2 (EZH2), which is a catalytic component of PRC2 (104). These histone modifications favor a more open chromatin conformation, which facilitates DNA repair and promotes the transcription of genes involved in neuronal survival and function. ATM deficiency could impede DNA repair and cause transcriptional repression of multiple neuronal genes through decrease of histone acetylation and increase of histone methylation, thus promoting the neurodegenerative phenotype of A-T.

1.4 Models of neurodegeneration in ataxia-telangiectasia

For the purpose of gaining insights into the mechanisms underlying the neuropathology of A-T, the design and use of experimental models is essential. Indeed, studies conducted *in vivo*, in whole animals, and *in vitro*, in cell cultures, have provided invaluable information on the cellular and molecular defects that characterize the neurological phenotype. Nonetheless, the lack of appropriate animal and cellular models is one of the major drawbacks of researching the causes of neurodegeneration in A-T.

1.4.1 ATM-deficient animal models

The use of genetically engineered animal models is extremely important for increasing the knowledge on the pathophysiological mechanisms of neurodegenerative diseases (105). These models aim to recapitulate the causes, the pathological lesions and the symptoms of a specific disease and are generally useful for assessing the efficacy of potential therapeutic strategies before conducting clinical trials in humans.

Drosophila melanogaster is an invertebrate which is often used as a model organism for neurodegenerative disorders (106). Indeed, its short life cycle and simple genome allow rapid construction of transgenic animals which succeed in partially reproducing the lesions found in different diseases. *D. melanogaster* has proven instrumental in dissecting basic disease mechanisms in A-T (107-109), but its use in medical research is limited by the great physiological differences between flies and humans.

Since mice display striking anatomical and physiological similarities to humans, with whom they share 99% of their genes, they are widely considered to be the prime model of inherited human disease (110). Indeed, the ability to engineer the mouse genome enables the generation of transgenic mice which ideally should faithfully represent the human phenotype. The identification of the ATM gene in 1995 (6) allowed the development of ATM-deficient knockout mice, in which the *ATM* gene is disrupted and no ATM protein is produced, and knockin mouse models, in which a deletion is introduced into the ATM gene resulting in the production of an ATM protein that lacks kinase activity (111-117). The goal was to achieve a greater understanding of the disorder and provide a means of screening for drugs to prevent or alleviate the defects in A-T patients, particularly the neurological decay. Unfortunately, while these mice exhibit the major characteristics of human A-T, including immunological abnormalities, radiosensitivity, cancer predisposition and infertility, they barely show the most cardinal features of A-T: neurodegeneration and associated ataxia (118,119). Indeed, although mice lacking ATM display some neurobehavioral defects and subtle neurological abnormalities consistent with a central nervous system that is not totally normal (116,117,120,121), they fail to develop severe neuronal degeneration and neuromotor dysfunction. The difference between the neuronal phenotypes in A-T patients and in ATM-deficient mice is probably caused by differences in the amounts of DNA damage that cause neuronal demise and the short life expectancy of the mouse, which do not allow the degenerative process to develop as it does in

humans (119). It is true that these mouse models and the cell lines derived from them have provided greater insight into the pathophysiology of the disorder, including the role of ATM in proliferating and post-mitotic cells and defects in signalling pathways (118). Nonetheless, the disappointing phenotype has cast a shadow over the use of these animals for studying the neurological aspects of A-T and clearly there is a need for a model that more closely reflects the human disorder.

1.4.2 ATM-deficient human cellular models

As a key limitation to the study of the A-T nervous system is the inappropriateness of the mouse model of the disease, various *in vitro* human cellular models have been employed for investigating the cellular and molecular mechanisms that characterize ATM-deficient neuronal cells in order to overcome this obstacle (122). Indeed, *in vitro* models of neurodegenerative diseases are useful for exploring the pathological processes leading to the defective phenotype and can also be employed for evaluating possible deleterious or protective roles of specific molecules and compounds. Unfortunately, live adult human neurons are not readily available for functional and interventional studies, thus cellular models of A-T are based on induced neuronal differentiation of pluripotent or multipotent cells in culture.

Cell lines that are widely used to study mechanisms of neurodegeneration, and which are also used in the field of A-T research (123-125), are those derived from human neuroblastoma cells. These cell lines are often used as *in vitro* models of neuronal function and differentiation because, being transformed cell lines, they can be propagated *in vitro* and differentiated to a more mature neuron-like phenotype (126). However, to investigate the role of ATM in neurodegeneration, it is desirable to have model systems more representative of human neurons.

A more pertinent *in vitro* model system to study neurodegeneration in A-T is represented by human neural precursor cells and mature neurons derived from the differentiation of pluripotent embryonic stem cells (ESCs) (127-129). Indeed, these cells are derived from the inner cell mass of a blastocyst and are pluripotent, having the potential to generate all the cell types of the human organism. Unfortunately, isolating the inner cell mass results in destruction of the blastocyst, which raises ethical issues that hamper the use of human ESCs in biomedical research (130).

Another potent experimental tool to study neurodegeneration is offered by genetically stable human neural stem cells (NSCs), which reside in specific regions of the fetal and adult central nervous system and participate in its homeostasis (131). These cells retain long-term *in vitro* self-renewal capacity and can differentiate into neurons, astrocytes and oligodendrocytes, in proportions that mirror their physiological distribution (131), but have been argued to be heterogeneous (132).

The impact of ATM deficiency on the biological properties of these cells is studied either by chemical inhibition of ATM kinase activity with the specific inhibitor KU-55933 (133) or by stable knockdown of ATM mediated by lentiviral short hairpin RNA vectors (124,127,134). However, it appears that inhibition of ATM activity and knockdown of the protein do not fully mirror the broad spectrum of A-T-causing mutations (135,136).

Interestingly, neuronal models of A-T based on the use of patient-derived tissues are currently being developed. For example, olfactory mucosa-derived neurospheres, obtained by biopsy through the nostril, have recently been established from several A-T patients and have been shown to differentiate *in vitro* into neurons, astrocytes and oligodendrocytes (137). Howerver, one of the most promising human *in vitro* models of neurodegenerative diseases, including A-T, is represented by patient-derived neural-specified induced pluripotent stem cells.

1.5 Human induced pluripotent stem cell-derived neural cells from patients with ataxia-telangiectasia

Investigation of the causes of many human neurological disorders, including A-T, has been hampered by the inadequacy of animal and cellular models and by the difficulty in obtaining patient-derived neural cells or tissues because of the limited accessibility to the brain. A major breakthrough in research came in recent years, when Professor Shinya Yamanaka of Kyoto University established a reprogramming method for the generation of pluripotent stem cells from mouse and human adult cells through retroviral delivery of four genes that encode the transcription factors OCT3/4, SOX2, KLF4 and cMYC (138,139). These cells were designated as induced pluripotent stem cells (iPSCs) and resemble ESCs in their self-renewal capacity and pluripotency, being able to propagate indefinitely as well as give rise to every other cell type in the body. This technology, which is nowadays based on non-viral, integration-free delivery of reprogramming factors (140), has made it possible to establish iPSCs from the somatic cells of any individual, irrespective of race, genetic background and state of health, thus creating great hope not only in terms of applications in regenerative medicine, such as cell transplantation therapy, but also for modeling human diseases and for new drug development (141). Indeed, protocols established for the *in vitro* differentiation of ESCs toward all three embryonic germ layers can be applied to iPSCs, granting the production of a variety of iPSC-derived cells, including hepatocytes, cardiomyocytes and neurons (139) (Figure 4).

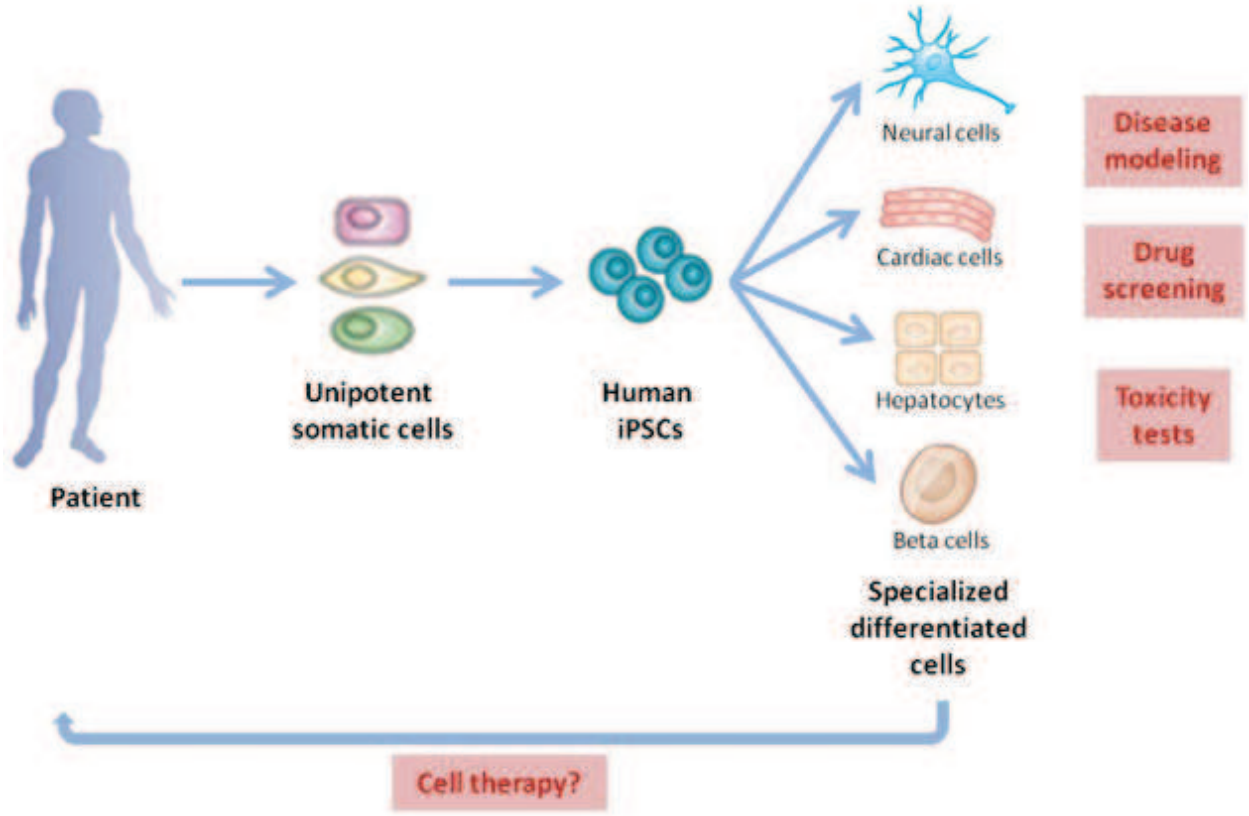

Fig. 4: Schematic representation of human iPSC generation, differentiation and potential applications.

As a result, the iPSC technology has rapidly expanded worldwide and the possibility to reprogram patient-derived cells to become pluripotent and their subsequent differentiation into pure populations of disease-relevant somatic cells has allowed the construction of *in vitro* disease models that contain patient-specific genetic information (141), thus providing an unlimited source of informative material to investigate the disease of interest. In particular, the reprogramming of adult human somatic cells to alternative fates has enabled the generation of novel cellular models of central nervous system disorders such as Alzheimer's disease (142,143), Parkinson's disease (144,145), amyotrophic lateral sclerosis (146,147), Huntington's disease (148,149), spinal muscular atrophy (150), and Rett syndrome (151,152).

In the case of A-T, the establishment of patient-derived iPSCs and their conversion to functional neurons has been recently achieved (153,154). Access to these cell types can provide a means of enhancing our knowledge regarding the role of ATM in the neuronal cellular

environment and represents a powerful tool for exploring the mechanisms that cause degeneration of human ATM-deficient neurons. This, in turn, may be exploited for detecting therapeutic targets and for future *in vitro* screenings for the identification of neuroprotective molecules of pharmacological relevance. Nevertheless, a thorough characterization of the neural progeny of A-T patient-derived induced pluripotent stem cells has not yet been reported. Therefore, in this study, we performed a previously undocumented functional and molecular analysis of human iPSC-derived A-T neuronal cells harboring patient-specific mutations, in order to shed light on the causes of the neuropathology in A-T.

2. *Aim of the Project*

This study aims to clarify the mechanistic link between ATM and neurodegeneration. Indeed, aside from defective DNA damage response and consequent accumulation of genotoxic lesions in pre- and postmitotic neurons, other factors seemingly contribute to neuronal cell death. Unfortunately, mouse models of A-T and *in vitro* ATM-deficient cell lines do not fully recapitulate the human central nervous system defects, hampering studies on neurological decay in A-T. Therefore, the purpose of this project is to investigate the relationship between ATM deficiency and neurodegeneration using a novel *in vitro* model of A-T: patient-derived iPSCs. In particular, the specific aims of this thesis are the following:

1. Generation of human iPSCs through the reprogramming of healthy control and A-T patient-derived skin fibroblasts.
2. Differentiation of human iPSCs into neural precursor cells and terminally differentiated neurons.
3. Determination of the outcome of ATM deficiency on neuronal differentiation, survival and electrophysiological activity in order to evaluate possible maturation or functional defects.
4. Analysis of DNA repair activities and responses to genotoxic or oxidant agents in postreplicative differentiated neurons in relation to ATM deficiency.
5. Assessment of the viability of ATM-deficient postreplicative differentiated neuronal cells following exposure to various doses of genotoxic or oxidant agents.

3. Materials and Methods

3.1 Primary cell cultures

GM03487 and GM02530 A-T patient-derived primary dermal fibroblasts were purchased from the Coriell Institute for Medical Research (Camden, NJ, USA). Both cell lines carried compound heterozygous mutations in the *ATM* gene, in particular GM03487, c.8266A>T and c.1141_1142ins4; GM02530, c.5675_5762del in trans with c.2251-1G>A and c.6573_6653del. Primary dermal fibroblasts from the skin biopsy of a healthy donor were kindly provided by Dr. Chiara Verpelli (CNR Institute of Neuroscience and Department of Biotechnology and Translational Medicine, Milan, Italy). Primary mouse embryonic fibroblasts, strain CF-1, were purchased from Millipore (PMEF-CFL).

All primary fibroblasts were cultured at 37°C in a humidified 5% CO_2 incubator in conventional atmospheric O_2. The A-T and control primary dermal fibroblasts were maintained and expanded in EMEM (Lonza) supplemented with 15% heat-inactivated fetal calf serum (FCS) (Life Technologies), while PMEF-CFL were maintained and expanded in DMEM/F12 (Life Technologies) supplemented with 20% heat-inactivated FCS. Both media also contained 100 units/ml penicillin, 100 µg/ml streptomycin (Lonza), 100 µM non-essential amino acids (Lonza) and 2 mM glutamine (Lonza). All fibroblasts were passaged in uncoated T75 flasks when they reached 80% confluence. Briefly, all culture medium was removed from the flask, cells were rinsed with PBS (Lonza) and 6 ml of trypsin/EDTA solution (170.000 U/l trypsin, 200 mg/l EDTA; Lonza) were added so that the entire surface was covered. The flask was incubated at 37°C for 3-5 min and when the cells became partially detached and rounded, they where dislodged from the surface of the flask by gently tapping the side of it. Trypsin was neutralized by adding 6 ml of medium to the flask and the detached cells were transferred to a sterile 15 ml conical tube. The cells were then centrifuged at 1200 rpm for 5 min. The supernatant was discarded from the tube without dislodging the cell pellet, which was

resuspended in fresh growth medium. The cells were pipetted up and down to ensure a homogeneous cell suspension and plated in new culture flasks at a split ratio of 1:4.

In order to prepare a feeder layer for the generation and/or maintenance of human iPSCs, PMEF-CFL in a confluent flask were mitotically inactivated with 1 µg/ml mitomycin C (Kyowa Hakko Kirin, Milan, Italy) in DMEM high glucose (Euroclone, Pero, Italy) for 3 h at 37°C. Meanwhile, the appropriate number of wells of a 6-well plate or 10 cm dishes were coated with 0.1% gelatin solution for 30 min at 37°C ad set aside until ready to receive the inactivated PMEF-CFL. After treatment, the flask containing the PMEF-CFL was washed with prewarmed DMEM/F12 three times, aspirating after each wash. Cells were collected as previously described with tripsin/EDTA solution, centrifuged and resuspended in a small volume of medium and their concentration was determined. The gelatin solution was aspirated from the wells or dishes which were then seeded with 3.6 x 10^5 cells/well or 1.8x10^6 cells/10 cm dish in fresh PMEF-CFL medium. Inactivated PMEF-CFL were then incubated for one to two days, until they were used.

3.2 Generation and culture of human induced pluripotent stem cells

The production of human iPSCs was achieved through two techniques based on nucleic-acid delivery of the four Yamanaka transcription factors *OCT4*, *KLF4*, *SOX2* and *cMYC*: lentiviral infection using the human STEMCCA (hSTEMCCA) Cre-Excisable Constitutive Polycistronic Lentivirus kit (Millipore) and transient transfection through electroporation of episomal plasmid vectors.

3.2.1 Lentiviral infection

Initially, human primary fibroblasts were reprogrammed using the hSTEMCCA Cre-Excisable Constitutive Polycistronic Lentivirus kit. A Cre-excisable polycistronic lentiviral vector allows for expression of a stem cell cassette, or STEMCCA, comprised of all four transcription factors (*OCT4*, *KLF4*, *SOX2* and *c-MYC*). This enables a reduced number of viral integrations with respect to co-infection of these factors in four separate expression vectors.

On day 0, the fibroblasts to be reprogrammed were seeded in two wells of a 6-well plate at a concentration of $2x10^4$ cells/well in human fibroblast growth medium. Cells were incubated overnight and the following day, before transduction, the number of cells in one well of the 6-well plate were counted in order to calculate the volume of virus needed to achieve a MOI of 50 using the following equation:

$$\text{Virus volume (µl) required} = \frac{\text{Number of cells}}{\text{Virus Titer (IFU/ml)}} \times \frac{\text{Desired MOI}}{1\ \text{ml}} \times 1000\ \mu\text{l}$$

The vial of hSTEMCCA Lentivirus was thawed and kept on ice. The medium from each well was replaced with 1 ml fresh human fibroblast medium and the required volume of virus was added to the wells containing the fibroblasts. The plate was incubated overnight and 24 h later a second virus infection was performed. The following day cells were washed three times with PBS, aspirating after each wash, then 3 ml fresh human fibroblast medium were added to each well and cells were transferred to a 5% O_2 incubator. On days 4 and 5 the medium was replaced. On day 4 the appropriate number of wells of inactivated PMEF-CFL feeder layers was prepared as described in section 3.1 to support the cells being reprogrammed. On day 6, the medium was removed from the 6-well plate containing the feeder layers and, after rinsing with PBS, replaced with human iPSC medium consisting of DMEM/F12 supplemented with 20% KnockOut serum replacement (Life Technologies), 100 units/ml penicillin, 100 µg/ml

streptomycin, 100 µM non-essential amino acids, 2 mM glutamine, 1 mM sodium pyruvate, 100 µM 2-mercaptoethanol and 20 ng/ml bFGF (Peprotech, Rocky Hill, NJ, USA). The virus-infected cells were detached from the wells with trypsin/EDTA solution and, after adding fibroblast medium for trypsin neutralization, were collected in a 15 ml tube and centrifuged at 1200 rpm for 5 min. Cells were resuspended in 2 ml of human iPSC medium, counted, and seeded at a concentration of $3x10^4$ cell/well onto the 6-well plate containing inactivated PMEF-CFL. The next day the medium was not changed, but it was exchanged every other day with fresh human iPSC medium starting on day 8. Fresh inactivated PMEF-CFL were added every 7 days to replenish older feeders during the reprogramming timecourse. Cell growth and morphology was monitored daily. After 20-25 days, human iPSC colonies started to appear and when they reached approximately 200 cells or over in size, they were ready to be picked.

For expansion on a feeder layer, two days prior to picking the human iPSC colonies, fresh wells from a 6-well plate were prepared with inactivated PMEF-CFL. For expansion in feeder-free conditions, fresh wells from a 6-well plate were coated with human ESC-qualified Matrigel (Corning) for 30 min at 37°C. The colonies were manually picked under a tissue culture hood containing a dissecting microscope using a P200 Pipetman and each was transferred into a new well of the previously prepared 6-well plate in human iPSC medium or in Nutristem culture medium (Stemgent, Cambridge, MA, USA) supplemented with 100 units/ml penicillin and 100 µg/ml streptomycin for feeder-free culture.

3.2.2 Transient transfection

In order to obtain integration-free human iPSCs, we performed a transient transfection by electroporating three episomal plasmid vectors carrying genes for the four reprogramming factors *OCT4*, *KLF4*, *SOX2* and *l-MYC* and a p53 short hairpin RNA (shRNA) into the A-T and control primary dermal fibroblasts, adapting the protocol described in Okita et al. (155).

Fibroblasts were electroporated using the Amaxa Nucleofector Technology (Lonza), which allows the transfection of nucleic acids into both the cytoplasm and nucleus of cells and is based on an optimized combination of electrical parameters and cell-type specific solutions, together with the Amaxa Human Dermal Fibroblast Nucleofector Kit (Lonza). The plasmids we employed were the following: pCXLE-hOCT3/4-shp53-F (Addgene plasmid 27077) carrying OCT4 and shp53; pCXLE-hSK (Addgene plasmid 27078) carrying SOX2 and KLF4; and pCXLE-hUL(Addgene plasmid 27080) carrying l-MYC.

Fibroblasts were transfected on day 1 when they reached 60-70% confluency in a T75 flask. For each cell sample to be electroporated, 18 µl Nucleofector Supplement from the Amaxa Human Dermal Fibroblast Nucleofector Kit was added to 82 µl Nucleofector Solution. Moreover, a 10 cm dish was filled with 7 ml of human fibroblast medium without penicillin or streptomycin and equilibrated in the incubator. Fibroblasts were harvested by trypsinization, centrifuged and counted. For each sample, $5x10^5$ cells were transferred to a 15 ml tube and centrifuged at 1300 rpm for 6 min. The cell pellet was resuspended in the previously prepared 100 µl Supplement-Nucleofector Solution mix, and 3 µg DNA (1µg/plasmid) was added to the cell suspension. The suspension was transferred to a cuvette, which was inserted into the Nucleofector device. The program U-023 was selected and applied. Once the program was finished, 500 µl of pre-equilibrated medium was added to the cuvette. The sample was gently transferred into the 10 cm dish and incubated in a 5% O_2 incubator, as mild hypoxia is the optimal condition for both the generation and proliferation of iPSCs (156). The medium was replaced the following day with fresh fibroblast medium and every other day thereafter for 8 days.

Next, the transfected cells were shifted onto a PMEF-CFL feeder layer in a medium appropriate for human iPSCs. To do this, three 10 cm dishes of inactivated PMEF-CFL feeder layers were prepared for each fibroblast line as described in section 3.1 to support the cells

being reprogrammed. The medium was removed from the dishes containing the feeder layers and, after rinsing with PBS, it was replaced with human fibroblast medium. The electroporated fibroblasts were harvested by trypsinization, centrifuged, counted, and $1x10^5$ cells were plated in each 10 cm dish in fibroblast medium. The next day the medium was replaced with 12 ml human iPSC medium, which was changed every other day.

Finally, after about two weeks, human iPSC colonies began to appear and were manually picked under a tissue culture hood containing a dissecting microscope using a P200 Pipetman. Each was transferred into a new well of a human ESC-qualified Matrigel-coated 6 well plate in Nutristem culture medium supplemented with 100 units/ml penicillin, 100 µg/ml streptomycin, 10 ng/ml leukaemia inhibitory factor (LIF, Millipore), which helps maintain cells in a pluripotent state, and 10 µM rho-associated protein kinase (ROCK) inhibitor (Y-27632; Carlo Erba, Milan, Italy), which inhibits apoptosis of non-clustered iPS cells.

3.2.3 Maintenance of human induced pluripotent stem cell cultures

A feeder layer of inactivated PMEF-CFL was employed for the maintenance of human iPSCs until a feeder-free culture condition was optimized. Human iPSCs were passaged when they reached 80% confluence at a split ratio of 1:4 in wells of a 6-well plate. To do this, the medium was removed from the well and cells were incubated with DMEM/F12 containing 1 mg/ml collagenase IV (Sigma) at 37°C for 10 min. When the edges of the colonies began to curl, the wells were scraped with a 1 ml pipette and clumps of cells were collected and transferred to a 15 ml tube. They were centrifuged at 500 rpm for 3 min and seeded in a new plate on inactivated PMEF-CFL in human iPSC medium. For feeder-free culture, human iPSCs were seeded on human ESC-qualified Matrigel-coated plates in Nutristem culture medium supplemented with 100 units/ml penicillin and 100 µg/ml streptomycin.

Alternatively, human iPSCs were harvested using Accutase cell detachment solution (Carlo Erba), which was added to the well after removal of the medium. The plate was incubated for 2-3 min until cells had detached. They were collected in a 15 ml tube and centrifuged at 800 rpm for 3 min. They were then seeded on human ESC-qualified Matrigel-coated plates in Nutristem culture medium supplemented with 100 units/ml penicillin, 100 μg/ml streptomycin and 10 μM ROCK inhibitor. Between passages, the medium was changed every other day.

3.3 In vitro pluripotency assay

For differentiation into derivatives of all three primary germ layers, human iPSCs were collected using 1 mg/ml collagenase IV as previously described, centrifuged and transferred to a 0.1% gelatin-coated plate in PMEF-CFL medium. Medium was changed every other day for 20 days and cells were then analyzed.

3.4 Generation and differentiation of human neural precursor cells

The first step for obtaining neural cells was the generation of human embryoid bodies (EBs). EBs are three-dimensional aggregates which recapitulate many aspects of cell differentiation during early mammalian embryogenesis and give rise to mature cells of all three germ layers (157), and therefore represent the initial step in many neural induction protocols. When human iPSCs reached 80% confluence, the medium was removed from the well and cells were incubated in DMEM/F12 containing 1 mg/ml collagenase IV (Sigma-Aldrich) at 37°C for 10 min. When the edges of the colonies began to curl, the wells were scraped with a 1 ml pipette and clumps of cells were collected and transferred to a 15 ml tube. They were centrifuged at 500

rpm for 3 min, the supernatant was carefully removed and the cells were resuspended in human EB medium, which consisted of human iPSC medium without bFGF. They were then plated in low-attachment dishes (Nunc, Sigma-Aldrich) for human EB formation in suspension culture. The exact amount of human EB medium used varied depending on the number of cells: the cells from one well of a 6-well plate were resuspended in 3 ml and plated in a 35 mm dish. Half of the medium was changed every other day: the dish was laid at a 45° angle to let the human EBs sink, the medium was aspirated without disturbing the aggregates, and fresh medium was added.

The following step consisted in the generation of neural rosettes. Neural rosettes consist of neuroprogenitors and are radial arrangements of columnar cells that express many of the proteins expressed in neuroepithelial cells in the neural tube and differentiate into neurons, oligodendrocytes, and astrocytes (158). After 5 days of suspension culture, human EBs were collected in a 15 ml tube and let sink for 3-5 min. The supernatant was removed and the aggregates were resuspended in human iPSC medium supplemented with 1:100 N2 supplement (Gibco, Life Technologies) and plated into growth factor-reduced Matrigel-coated wells of a 6-well plate. The medium was changed every other day for 7 days as neural rosettes appeared.

Finally, human neural precursor cells (NPCs) were expanded. Neural rosettes were manually picked and collected in a 15 ml tube in 1 ml NPC medium consisting of DMEM/F12 supplemented with 100 units/ml penicillin, 100 µg/ml streptomycin, 2 mM glutamax, 1:500 B27 supplement (Gibco, Life Technologies), 1:100 N2 supplement, 20 ng/ml EGF and 20 ng/ml bFGF (Società Italiana Chimici, Rome, Italy). They were mechanically dissociated using a 1 ml pipette and plated in a growth factor-reduced Matrigel-coated T25 flask in 5 ml NPC medium. Human NPCs were passaged when they reached 80% confluence at a split ratio of 1:4 in T25 or T75 flasks. To do this, the medium was removed and cells were incubated with Accutase cell

detachment solution at 37°C for 2-3 min. They were then collected in a 15 ml tube, centrifuged at 700 rpm for 5 min and seeded in a new growth factor-reduced Matrigel-coated flask in fresh NPC medium.

In order to obtain terminally differentiated neurons, proliferating human NPCs were seeded at a concentration of 3 x 10^4 cells/cm^2 in NPC medium, which was replaced 24 h later with NPC medium without bFGF and EGF. Cells were fed every 2-3 days thereafter. Like human iPSCs, human NPCs and neurons were obtained and maintained in 5% O_2, as mild hypoxia enhances the proliferation and differentiation of human neural stem cells (159).

3.5 Western blot analysis

3.5.1 Whole-cell extracts and protein quantification

For protein expression analysis, cells were harvested, centrifuged, transferred to a 1.5 ml tube, washed once in PBS and finally centrifuged at 3200 rpm for 6 min at 4°C. The pellet was resuspended in two volumes of lysis buffer, composed of 0.125 M Tris–HCl pH 6.8, 5% SDS, and boiled for 7 min. An equal volume of lysis buffer containing 2X phosphatase and protease inhibitors (2 mM phenylmethylsulfonyl fluoride, 20 µg/ml pepstatin, 200 kallikrein-inactivating units/ml aprotinin, 20 µg/ml leupeptin) was then added and lysates were kept on ice from this moment on. Lysates were sonicated at 20% for 20 s for DNA fragmentation and centrifuged at 11000 rpm for 1 min.

The final supernatant, corresponding to the total protein extract, was transferred to a new 1.5 ml tube and quantified using the colorimetric Micro BCA Protein Assay Kit (Thermo Scientific Pierce) as follows: in a 96 well plate, a BSA standard of 2 mg/ml (Thermo Scientific Pierce) was used to create a standard color response curve by diluting growing quantities of BSA in distilled water (from 0 to 15 µg/well) to a final volume of 150 µl/well, and 1 µl of each

sample to be quantified was diluted in 149 µl of distilled water. The appropriate volume of Micro BCA working reagent was prepared by mixing 50% reagent MA with 48% reagent MB and 2% reagent MC and 150 µl were added to each well of the standards and the samples. The plate was incubated in the dark for 45 min at room temperature. Absorbance was measured at 595 nm on a GENios plate reader (Tecan). The absorbance reading of the blank standard was subtracted from the readings of all other individual standards and samples. A standard curve was prepared by plotting the blank-corrected reading for each BSA standard vs. its content in µg and was used to determine the protein concentration of each sample.

3.5.2 SDS page and Western blot

A total of 50 µg of proteins for each sample were brought to a total volume of 15 µl in lysis buffer and 5% β-mercaptoethanol was added. The samples were then boiled for 7 min and size-fractionated by SDS–PAGE on a NuPAGE precast polyacrylamide gel (7%, 3-8% or 4-12% according to the molecular weight of the proteins of interest) in 1X Tris-acetate SDS or 1X MES SDS running buffer (Life Technologies), according to the gel used. Resolved proteins were electroblotted at 35 V for 2 h onto PVDF membranes (Millipore), which were previously activated by incubation in 100% methanol for 1 min and subsequently in transfer buffer (Life Technologies) for 10 min.

The membranes were then incubated overnight with primary antibodies diluted in 4% nonfat dry milk dissolved in PBS containing 0.1% Tween 20 (PBST) in sealed bags using the XBLOT P100 hybridization instrument (Isenet, Milan, Italy). The following primary antibodies were used:

Antibody	Host	Supplier
anti-OCT3/4(Clone C-10)	Mouse	Santa Cruz Biotecnology
anti-p53	Mouse	Santa Cruz Biotecnology
anti-Cdc2 (p34)	Mouse	Santa Cruz Biotecnology
anti-p21waf1	Mouse	Santa Cruz Biotecnology
anti-β-tubulin III (Clone 2G10)	Mouse	Sigma
anti-synaptophysin	Mouse	Sigma
anti-vinculin	Mouse	Sigma
anti-β-actin	Mouse	Sigma
anti-TRA-1-81	Mouse	Gift of Dr. Christian Unger
anti-SOX2	Mouse	Abcam
anti-CDC25A	Mouse	Abcam
anti-cyclin B1 (Clone GNS-1)	Mouse	BD Pharmingen
anti-γH2AX (H2AX-pSer139, clone JBW301)	Mouse	Millipore
anti-PSD95	Mouse	NeuroMab
anti-SCG10	Mouse	NeuroMab
anti-pan-KChIP	Mouse	NeuroMab
anti-synaptophysin	Mouse	NeuroMab
anti-nestin	Mouse	Chemicon
anti-MAP2 (Clone AP20)	Mouse	Chemicon
anti-KAP1 (TIF1β, Clone 4E1)	Mouse	Cell Signaling Technology
anti-CHK2 (Clone DCS270-273)	Mouse	MBL Intl Corp
anti-Top1	Mouse	BD Biosciences
anti-ATM (Clone Y170)	Rabbit	Epitomics
anti-ATM pS1981	Rabbit	Rockland

anti-cleaved PARP	Rabbit	Cell Signaling Technology
anti-caspase 3	Rabbit	Cell Signaling Technology
anti-caspase 9	Rabbit	Cell Signaling Technology
anti-XRCC1	Rabbit	Cell Signaling Technology
anti-KAP1 pS824	Rabbit	Cell Signaling Technology
anti-CHK2 pThr68	Rabbit	Cell Signaling Technology
anti-p53 pSer15	Rabbit	Cell Signaling Technology
anti-GFAP	Rabbit	Millipore
anti-VGAT	Rabbit	Synaptic System
anti-VGLUT	Rabbit	Synaptic System
anti-pol β	Rabbit	Abcam
anti-FEN1	Rabbit	Abcam
anti-APE1	Rabbit	Santa Cruz Biotechnology
anti-SMC1	Rabbit	Bethyl Laboratories
anti-SMC1 pSer966	Rabbit	Bethyl Laboratories
anti-KAP1 pS473	Rabbit	Biolabs

The membranes were washed three times in PBST and incubated for 45 min with peroxidase-conjugated goat anti-mouse or anti-rabbit IgG secondary antibodies (GE Healthcare) diluted in 4% nonfat dry milk dissolved in PBST. Following three washes in PBST, the proteins of interest were detected using and an ECL western blotting detection system (Thermo Scientific Pierce) on autoradiographic films. Bands were acquired with a digital scanner. Vinculin and β-actin were used as loading controls.

3.6 Immunofluorescence

For immunofluorescence analysis, cells were grown on glass coverslips, fixed in 4% buffered paraformaldehyde for 10 min at room temperature, washed in PBS and permeabilized with 0.1% Triton X-100 in PBS for 10 min. They were then blocked in PBS containing 10% normal goat serum (Life Technologies) for 30 min and incubated overnight at 4°C with primary antibodies diluted in blocking solution. The following primary antibodies were used:

Antibody	Host	Supplier
anti-OCT 3/4 (Clone C-10)	Mouse	Santa Cruz Biotecnology
anti-SSEA4	Mouse	Gift of Dr. Christian Unger
anti-TRA-1-81	Mouse	Gift of Dr. Christian Unger
anti-α-SMA (Clone 1A4)	Mouse	Sigma
anti-SOX17 (Clone 245013)	Mouse	R&D System
anti-β-tubulin III (Clone TUJ1)	Mouse	Covance
anti-Nestin	Mouse	Chemicon
anti-MAP2 (Clone AP20)	Mouse	Chemicon
anti-Vimentin	Mouse	DAKO
anti-GFAP	Rabbit	Millipore
anti- GABA	Rabbit	Sigma
anti-Ki67	Rabbit	Thermo Scientific

Following three washes with PBS, cells were incubated with Alexa fluor green-emitting 488- or red-emitting 555-conjugated goat anti-mouse IgG or anti-rabbit IgG (Life Technologies) for 45 min at room temperature. Cells were washed three times in PBS, counterstained with 1 μg/ml DAPI for 10 min and mounted on glass slides with Prolong Gold Antifade mounting

solution (Life Technologies). Fluorescent signals were detected using a fluorescence microscope equipped with a CCD camera.

3.7 Electrophysiological recordings and analysis

Cells were used for electrophysiological recordings with the whole-cell configuration of the patch-clamp technique 60 days after plating. Recordings were performed at room temperature using a Multiclamp 700A patch-clamp amplifier and pClamp 10.2 software (Molecular Devices). Recordings were usually started 5 min after the rupture of the membrane patch, to allow intracellular dialysis with the pipette solution. External bath solution contained 129 mM NaCl, 1.25 mM NaH2PO4, 35 mM glucose, 1.8 mM MgSO2, 1.6 mM CaCl2, 3 mM KCl and 10 mM HEPES, pH 7.4 with NaOH; internal pipette solution contained 120 mM K gluconate, 15 mM KCl, 2 mM MgCl2, 0.2 mM EGTA, 10 mM HEPES, 20 mM P-creatine, 2 mM ATP-Na2, 0.2 mM GTP-Na2 and 0.1 mM Leupeptine, pH 7.2 with KOH. Cell capacitance and series resistance errors were carefully compensated (~85%) throughout the experiment. The remaining linear capacity and leakage currents were eliminated online using a P/4 subtraction paradigm. Pipette resistance was between 2.6 and 3.0 MΩ. For the recordings of total voltage-gated ion currents, signals were filtered at 10 kHz and sampled at 100 kHz. For the recordings of postsynaptic currents signals were filtered at 3 kHz and sampled at 10 kHz. When we switched the amplifier to current-clamp mode, we applied the bridge balance compensation and held the resting potential at -70 mV by injecting the appropriate holding current. Neuronal firing was recorded injecting depolarizing current pulses of increasing amplitude. The neurons with unstable resting potential and/or unstable firing were discarded. In current clamp mode signals were filtered at 10 kHz and sampled at 20 kHz.

3.8 Comet assay

The comet assay, or single cell gel electrophoresis, is a method for measuring DNA damage in eukaryotic cells. The assay depends on the relaxation of supercoiled DNA in agarose-embedded cells after lysis: DNA containing a break loses its supercoiling and becomes free to extend toward the anode under electrophoresis, forming comet-like images detectable under fluorescence microscopy following staining of DNA. The intensity of the comet tail relative to the head reflects the number of DNA breaks and the extent of DNA damage can be calculated automatically by imaging softwares.

To prepare comet slides, the day before analysis microscope glass slides were washed with methanol, air dried and immersed in molten 1% normal-gelling-temperature agarose to obtain the first agarose layer, before being stored overnight at 4°C. To evaluate DNA strand breaks, terminally differentiated neuronal cells were incubated with 20 µM H_2O_2 (Sigma) for 20 min or irradiated with 5 Gy. After treatment, cells were collected with Accutase, reduced to a single cell suspension and resuspended in ice cold Ca^{2+}- and Mg^{2+}-free PBS to a concentration of $1x10^6$ cells/ml. An aliquot of 20 µl of cells (2×10^4 cells) was added to 180 µl of molten 0.7% low-gelling-temperature agarose kept at 37 °C, and was immediately spread onto the comet slides, covered with a coverslip and stored at 4°C in the dark to accelerate gelling of the agarose. After 25 min, the coverslip was gently removed and a second low-gelling-temperature agarose layer was spread onto the slides. The slides were then transferred to a pre-chilled lysis solution composed of 2.5 M NaCl, 100 mM EDTA, 10 mM Tris-base, 300 mM NaOH, pH 10, and 1% Triton X-100 (added just before using) for 2 h at 4°C in the dark then processed as follows.

3.8.1 Neutral comet assay

The neutral comet assay was emplyed for the detection of DSBs as described in Calini et al. (160). After the lysis step the slides were washed twice with 1X Tris-borate EDTA buffer solution (TBE), pH 8.3, for 10 min. The slides were placed in a horizontal electrophoresis chamber and covered with TBE buffer. Electrophoresis was carried out at the rate of 1.0 V/cm for 20 min. The slides were then removed from the electrophoresis chamber and washed in deionized water for 5 min. After washing, the slides were immersed in prechilled methanol for 10 min for cell fixation and air dried overnight. DNA was stained with 90 µl of 0.1 mg/ml ethidium bromide for 10 min, then comet slides were observed under the microscope. Fluorescent signals were detected using a fluorescence microscope equipped with a CCD camera and comet images were analyzed with the Comet Score software (v1.5; TriTek Corporation).

3.8.2 Alkaline comet assay

The neutral comet assay was emplyed for the detection of single strand breaks (SSBs) as described in Calini et al. (160). The slides were placed in a horizontal electrophoresis chamber and a denaturation step was performed in pre-chilled alkaline electrophoresis solution (300 mM NaOH, 1 mM EDTA), pH > 13, at 4°C in the dark. After 20 min the slides were subjected to electrophoresis at 1 V/cm, 300 mA for 20 min. Following electrophoresis, slides were washed for 10 min with cold neutralization buffer (0.4 M Tris-HCl, pH 7.4). After washing, the slides were immersed in prechilled methanol for 10 min for cell fixation and air dried overnight. DNA was stained with 90 µl of 0.1 mg/ml ethidium bromide for 10 min, then comet slides were observed under the microscope. Fluorescent signals were detected using a fluorescence microscope equipped with a CCD camera and comet images were analyzed with the Comet Score software (v1.5; TriTek Corporation).

3.8.3 Modified alkaline comet assay

A modified alkaline comet assay was employed for the indirect detection of Top1ccs as described in Alagoz et al. (161). Terminally differentiated human NPCs were incubated with 30 µM CPT (Sigma) for 45 min. Cells were washed three times with PBS supplemented with 50 mM CPT at room temperature. Cells were finally suspended in PBS containing 100 mM CPT supplemented with 800 mg/ml proteinase K (Sigma) and kept at room temperature. Cell suspension was mixed with an equal volume of 1.2% low-gelling-temperature agarose (Sigma) maintained at 42°C to bring the final CPT concentration to 50 mM. Cell suspension was immediately layered onto frosted glass slides pre-coated with 0.6% agarose, covered with a coverslip and maintained in the dark at room temperature for 15 min. The coverslip was then gently removed and slides were immersed in lysis solution, composed of 400 mg/ml proteinase K, 50 mM CPT, 10 mM Tris-HCl, 100 mM EDTA pH 8.0, 1% Triton X-100, 1% DMSO, pH 10, for 1 h at 40°C. Lysis solution was then supplemented with 2.5 M NaCl for additional 3 h at 40°C. Cells were immediately immersed in alkaline electrophoresis buffer, composed of 50 mM NaOH, 1 mM EDTA, 1% DMSO, and electrophoresis was conducted at 1 V/cm for 25 min, followed by neutralization in 400 mM Tris-HCl pH 7.0 for 1 h. The slides were then immersed in prechilled methanol for 10 min for cell fixation and air dried overnight. DNA was stained with 90 µl of 0.1 mg/ml ethidium bromide for 10 min, then comet slides were observed under the microscope. Fluorescent signals were detected using a fluorescence microscope equipped with a CCD camera and comet images were analyzed with the Comet Score software (v1.5; TriTek Corporation).

3.9 Detection of γH2AX and 53BP1 nuclear foci

For the assessment of nuclear foci, 30-day terminally differentiated neurons on coverslips were irradiated with 0.5 Gy. After 15 min, 6 h and 24 h cells were washed with a 0.9% NaCl solution to remove the medium, air dried overnight, fixed in 3% buffered paraformaldehyde and permeabilized for 5 min at 4°C in a solution composed of 20 mM Hepes pH 7.4, 50 mM NaCl, 3 mM $MgCl_2$, 300 mM sucrose and 0.5% Triton. Cells were then blocked in PBS containing 5% BSA and 0.2% Tween20 for 30 min and labeled with a mouse anti-γH2AX antibody (clone JBW301, Upstate Biotechnology, NY, USA) or a rabbit anti-53BP1 antibody (NB100-304; Novus Biologicals, Cambridge, UK) overnight at 4°C. Following three washes in PBS, cells were incubated with Alexa Fluor green-emitting 488-conjugated goat anti-mouse or anti-rabbit IgG secondary antibodies (Life Technologies) for 45 min at room temperature. Cells were washed three times in PBS, counterstained with 1 ug/ml DAPI for 10 min and mounted on glass-slides with Prolong Gold Antifade mounting. Fluorescent signals were detected using a fluorescence microscope equipped with a CCD camera.

3.10 In vitro base excision repair assay

The *in vitro* BER assay was employed for measuring BER efficiency and mode in human NPCs and terminally differentiated neurons. First, whole-cell extracts were prepared. Approximately $15x10^6$ exponentially growing cells were harvested and gently resuspended in buffer I (10 mM Tris pH 7.8, 200 mM KCl) at a concentration of $50x10^6$ cells/ml. An equal volume of buffer II (10 mM Tris pH 7.8, 200 mM KCl, 2 mM EDTA, 40% glycerol, 0.2% Nonidet-P40, 2 mM DTT and protease inhibitors)was added. The cell suspension was stirred by rocking for 1 h at 4°C. Following centrifugation at 14000 rpm for 10 min at 4°C, the supernatant was dispensed into aliquots and stored at -80°C.

DNA substrates were then prepared. Closed circular DNA molecules containing a single lesion were constructed (162) by priming single-stranded pGem-3Zf(+) DNA (Promega) with the oligonucleotides containing the modified base of interest (uracile and tetrahydrofuran (THF) (163). These oligonucleotides were [γ-32P]ATP 5′ end labelled. The *in vitro* DNA synthesis was performed by using T4 DNA polymerase holoenzyme, single-stranded DNA binding protein, dNTPs and T4 DNA ligase. The plasmid DNA containing a single uracil residue was digested with UDG to produce a single abasic site.

Finally, repair of the plasmid DNA containing the lesions (pGEM-AP/THF) was conducted as described in Frosina et al. (162). Reaction mixtures (50 µl) contained 40 mM HEPES/KOH (pH 7.9), 75 mM KCl, 5 mM MgCl2, 0.5 mM dithiothreitol, 50 uM of each dNTP, 2 mM ATP, 40 mM phosphocreatine, 2.5 µg of creatine phosphokinase type I (Sigma), 3.4% glycerol, 18 µg of bovine serum albumin and 50 µg cell extracts. After incubation at 30°C for increasing periods of time, the plasmid DNA was recovered and digested with restriction enzymes. The digestion products were electrophoresed on a denaturing 15% polyacrylamide gel. The repair products were visualized and quantified by autoradiography (Istant Imager, Packard) and the relative yield of the different plasmid forms was measured.

3.11 Rapid approach to DNA adduct recovery assay

The rapid approach to DNA adduct recovery (RADAR) assay allows the immunodetection of protein-DNA adducts. First of all, cells were lysed and DNA-protein covalent complexes (DPCCs) were isolated as follows. Neurons terminally differentiated for 30 days in 6-well plates were incubated with 30 µM CPT for 1 h. Following treatment, part of the cells was immediately lysed, while part was washed with PBS and incubated in fresh medium for 3 h before lysis. For the isolation of DPCCs, cells were lysed in the plate by addition of 2 ml lysis reagent composed of 6M GTC, 10 mM Tris-HCl pH 6.5, 20 mM EDTA, 4% Triton X100,

1% Sarkosyl and 1% dithiothreitol, and processed as follows (164). Each lysate was collected in two 1.5 ml tubes (containing 1 ml each) and nucleic acids and DPCCs were precipitated by addition of 500 µl of 100% ethanol and incubation at -20°C for 5 min. The solutions were then sonicated at 20% for 20 s and centrifuged at 13000 rpm for 15 min. The supernatant was discarded and the precipitate was washed twice in 75% ethanol and immediately resuspended in 200 µl freshly prepared 8 mM NaOH. For complete solubilization, it was essential not to allow the pellet to dry. Recovered DNA was quantified by measuring the absorbance at 260 nm using a NanoDrop 2000c spectrophotometer (Thermo Scientific). Samples were stored at -20°C.

Next, DPCCs were immunodetected. The desired quantity of purified DNA from each sample was diluted in PBS to a final volume of 100 µl and applied to a nitrocellulose membrane (Bio-Rad) using a vacuum slot-blot manifold (Bio-Rad). The membrane was then blocked for 1 h in 4% nonfat dry milk dissolved PBST and incubated with a mouse monoclonal anti-human Top1 primary antibody (BD Biosciences) diluted in 4% nonfat dry milk overnight at 4°C in a sealed bag using the XBLOT P100 hybridization instrument. The membrane was washed three times in PBST and incubated for 45 min with a goat anti-mouse peroxidase-conjugated IgG secondary antibody (GE Healthcare) diluted in 4% nonfat dry milk. Following three washes in PBST, Top1 was detected using and an ECL detection system (Thermo Scientific Pierce) on autoradiographic films. Signals were acquired with a digital scanner and signal intensity was quantified using the ImageQuant software. Sample loading was normalized based on DNA content as determined by DAPI fluorescence. The presence of contaminant non-covalently bound proteins was excluded by incubation with an anti-β-actin antibody.

3.12 Neuronal viability assay

Neuronal viability was evaluated using the Cell Titer-Glo luminescent cell viability assay (Promega), which allows to determine the number of viable cells in culture based on

quantitation of the ATP present, an indicator of metabolically active cells directly proportional to the number of cells present in culture. Neurons terminally differentiated for 30 days in 96-well plates were treated with increasing doses of CPT, trabectedin, H_2O_2 or Paraquat (all from Sigma) for 72 h (H_2O_2 was removed after 20 min). Three wells were employed for each concentration. After treatment, a volume of CellTiter-Glo Reagent equal to the volume of cell culture medium present was added to each well. The contents were then mixed in the dark at room temperature for 15 min on a shaker to induce cell lysis. Cellular luminescence was recorded using a GENios plate reader (Tecan).

3.13 Cell cycle phase analysis

Primary fibroblasts, human iPSCs and proliferating and differentiated human NPCs grown in a 6-well plate were irradiated at 5 Gy when they reached 70% confluence. After 24 h, cells were harvested and gently triturated to obtain single cell suspensions, washed with cold PBS, centrifuged and finally fixed with 1.5 ml 70% cold ethanol added dropwise. Cells were stored at 4°C and before analysis they were centrifuged at 3000 rpm for 5 min, resuspended in 1.5 ml of 50 µg/ml PBS-RNAse A, incubated at 37°C for 30 min and then stained with 30 µg/ml propidium iodide. Radiation-induced cell cycle phase modifications were examined by flow cytofluorimetry using a FACSCalibur instrument fitted with a Cell Quest software package (Becton Dickinson).

4. Results

4.1 Generation and characterization of human induced pluripotent stem cells derived from ataxia-telangiectasia and control fibroblasts

Human iPSC lines were established from primary dermal fibroblasts of two unrelated A-T patients and a healthy control. Colonies with embryonic stem cell-like morphology were expanded on a PMEF-CFL feeder layer (Figure 5A, left). Western blot analysis revealed, as expected, a positive signal for ATM in fibroblasts and human iPSCs from control but not from A-T cases (Figure 5A, right). No ATM protein was detectable in PMEF-CFL as the antibody used was human-specific. Furthermore, only control and A-T human iPSC lines expressed the pluripotency marker OCT3/4, but not fibroblasts or PMEF-CFL (Figure 5A, right). Immunofluorescence analysis attested the pluripotency of the human iPSCs, being positive for OCT3/4, stage-specific embryonic antigen 4 (SSEA4) and TRA-1-81 (Figure 5B).

Moreover, the human iPSCs gave rise to the embryonic derivatives ectoderm, endoderm and mesoderm, labeled positive for β-tubulin III, SOX17 and alpha-smooth muscle actin (α-SMA), respectively (Figure 5C). Also, through EB generation, neural rosette formation and subsequent culture in a mitogen-free medium containing N2 supplement, human iPSCs differentiated into microtubule-associated protein 2+ (MAP2+) neurons (Figure 5D).

Figure 5

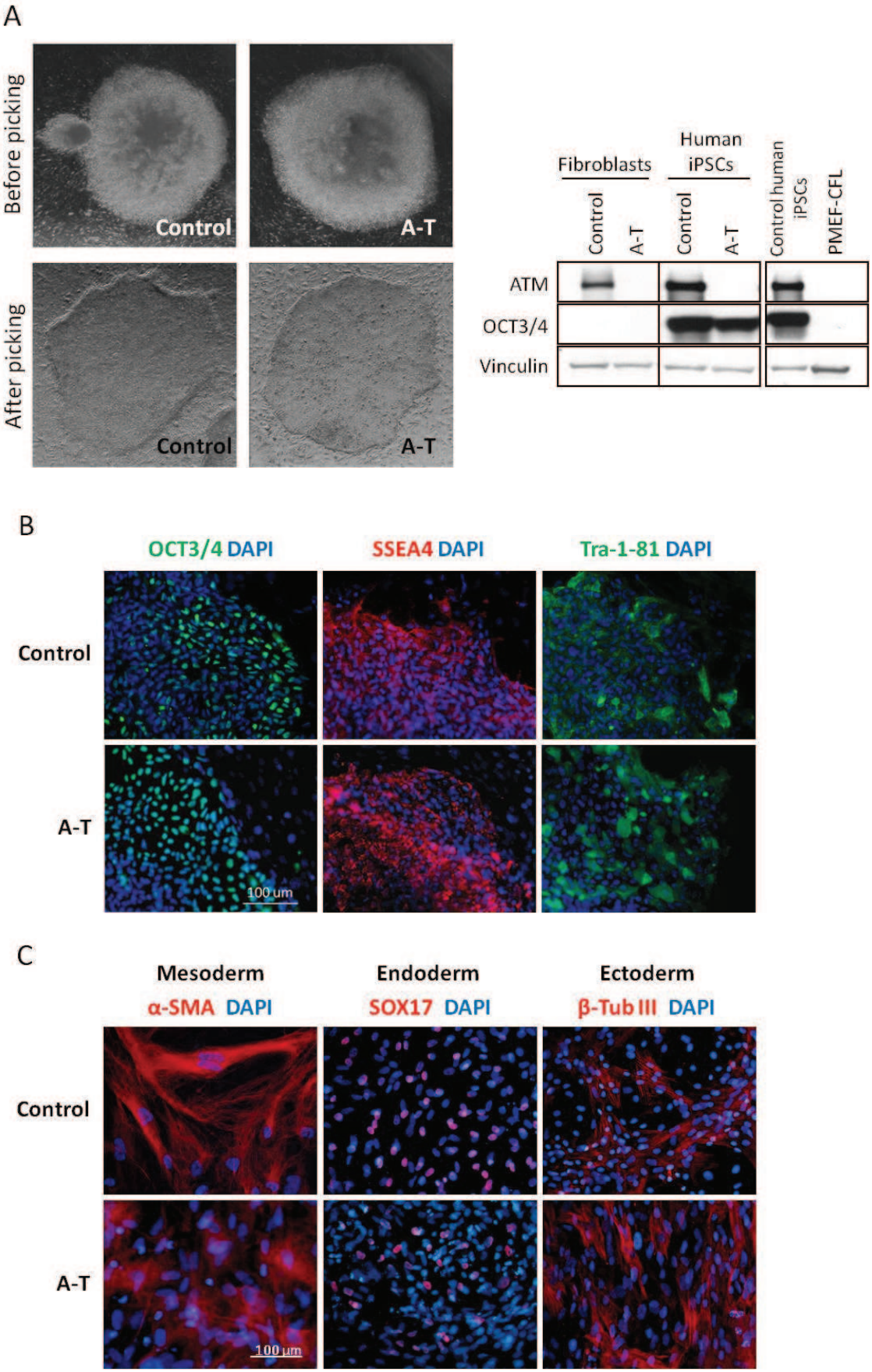
A
Before picking
After picking
Control
A-T
Control
A-T
Fibroblasts
Human iPSCs
Control
A-T
Control
A-T
Control human iPSCs
PMEF-CFL
ATM
OCT3/4
Vinculin
B
OCT3/4 DAPI
SSEA4 DAPI
Tra-1-81 DAPI
Control
A-T
100 um
C
Mesoderm
Endoderm
Ectoderm
α-SMA DAPI
SOX17 DAPI
β-Tub III DAPI
Control
A-T
100 um

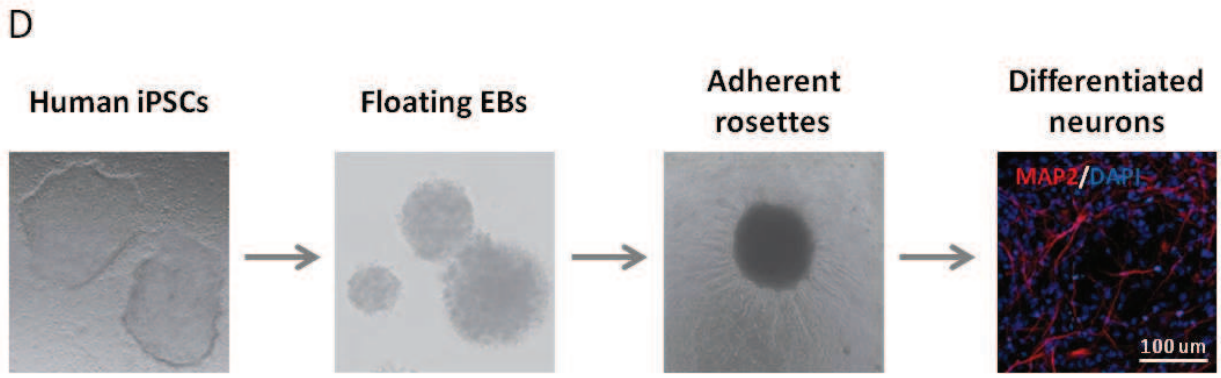

Fig. 5 : Generation, characterization, pluripotency validation and neuronal differentiation of human iPSC colonies from control and A-T patients. In A, representative images of newly formed human iPSC colonies before picking (upper panel) and after picking (bottom panel). The human iPSC colonies were characterized by Western blot (right) to evaluate the expression of the ATM protein and of the pluripotency marker OCT3/4, and were compared with primary fibroblasts and PMEF-CFL feeders. Vinculin was used as a loading control. In B, human iPSC colonies were labeled to visualize the expression of the pluripotency markers OCT3/4, SSEA4 and TRA-1-81. Nuclei were counterstained with DAPI (blue). In C, control and A-T human iPSCs were differentiated *in vitro* into the three germ layers for 20 days. Cells were labeled with antibodies specific for α-SMA (mesoderm marker), SOX17 (endoderm marker) and β-tubulin III (ectoderm marker). Nuclei were counterstained with DAPI (blue). The ability of human iPSCs to generate neuronal cells was confirmed through the formation of floating EBs and rosettes, and representative images for each differentiation step are shown in D.

4.2 Generation of neural precursor cells and neurons from ataxia-telangiectasia and control human induced pluripotent stem cells

To generate proliferating NPCs, human iPSC-derived rosettes were cultured in a medium containing B27, N2, EGF and bFGF, as depicted in Figure 6A. Phenotypically, both control and A-T human NPCs were negative for the pluripotency markers TRA-1-81 and OCT3/4 (Figure 6B, left) and positive for the neural precursor markers SOX2, nestin and vimentin, and for the proliferation marker Ki67 (Figure 6B, right). On Western blots, human NPCs showed lower expression of TRA-1-81 and OCT3/4 than human iPSCs, and higher levels

of SOX2 and nestin, which then decreased during terminal neuronal differentiation obtained by withdrawal of the growth factors for at least 15 days (Figure 6B, bottom left).

To determine the capacity of human NPCs to activate the DNA damage response, we investigated the time-dependent response of control and A-T NPCs to IR, which induces DSBs and ATM signalling (32). Using phospho-specific antibodies for the ATM substrates SMC1-pS66, KAP1-pS824, CHK2-pT68, p53-pS15 and γH2AX, and for the CHK2 substrate KAP1-pS473, we found that after 15-60 min of IR these target molecules were strongly phosphorylated in control but not in A-T NPCs (Figure 6C). Interestingly, after IR an accumulation of cleaved poly (ADP ribose) polymerase (PARP), a marker of apoptosis, was detected in control but not in A-T human NPCs, suggesting that ATM deficiency confers radioresistance in proliferative NPCs (Figure 6C).

When human NPCs were induced to differentiate, they acquired a neuronal-like morphology and at day 15 of differentiation (D15) were positive for β-tubulin III and MAP2, with a fraction of cells also expressing the marker of inhibitory neurons γ-aminobutyric acid (GABA; Figure 6D), which we were no longer able to detect at day 50 of differentiation (D50) in mature neuronal cells (165) expressing β-tubulin III or MAP2 (Figure 6E).

Western blot analysis confirmed the downregulation of the stem cell marker nestin and the upregulation of the neuronal marker β-tubulin III at day 30 of differentiation (D30) (Figure 6F, left) and at D15 and D50 (Figure 6F, right), and the expression of the postsynaptic marker postsynaptic density protein 95 (PSD95), of the inhibitory synapse marker vesicular GABA transporter (VGAT), of the neuronal growth-associated protein SCG10 and of potassium channel-interacting proteins (KChIPs). At D30 and D50, but not D15, cells also expressed the presynaptic marker synaptophysin (SYP). We detected no obvious differences between control and A-T human NPCs concerning the generation of neuronal cells, but A-T neurons displayed

deficits in the expression of SYP and PSD95 as well as of SCG10 and KChIP, and higher amounts of glial fibrillary acidic protein (GFAP; Figure 6F).

The post-mitotic status of the differentiated cells was confirmed by the downregulation in D15, D50 (Figure 6G) and D30 samples (Figure 6H) of CDC2 and cyclin B1, which are proteins involved in the G2 cell cycle phase. To note, the expression of the apoptosis marker cleaved PARP was consistently higher in control than in A-T neuronal cells and γH2AX was also highly expressed at D50, and its levels were lower in A-T than in control cells (Figure 6G).

Figure 6

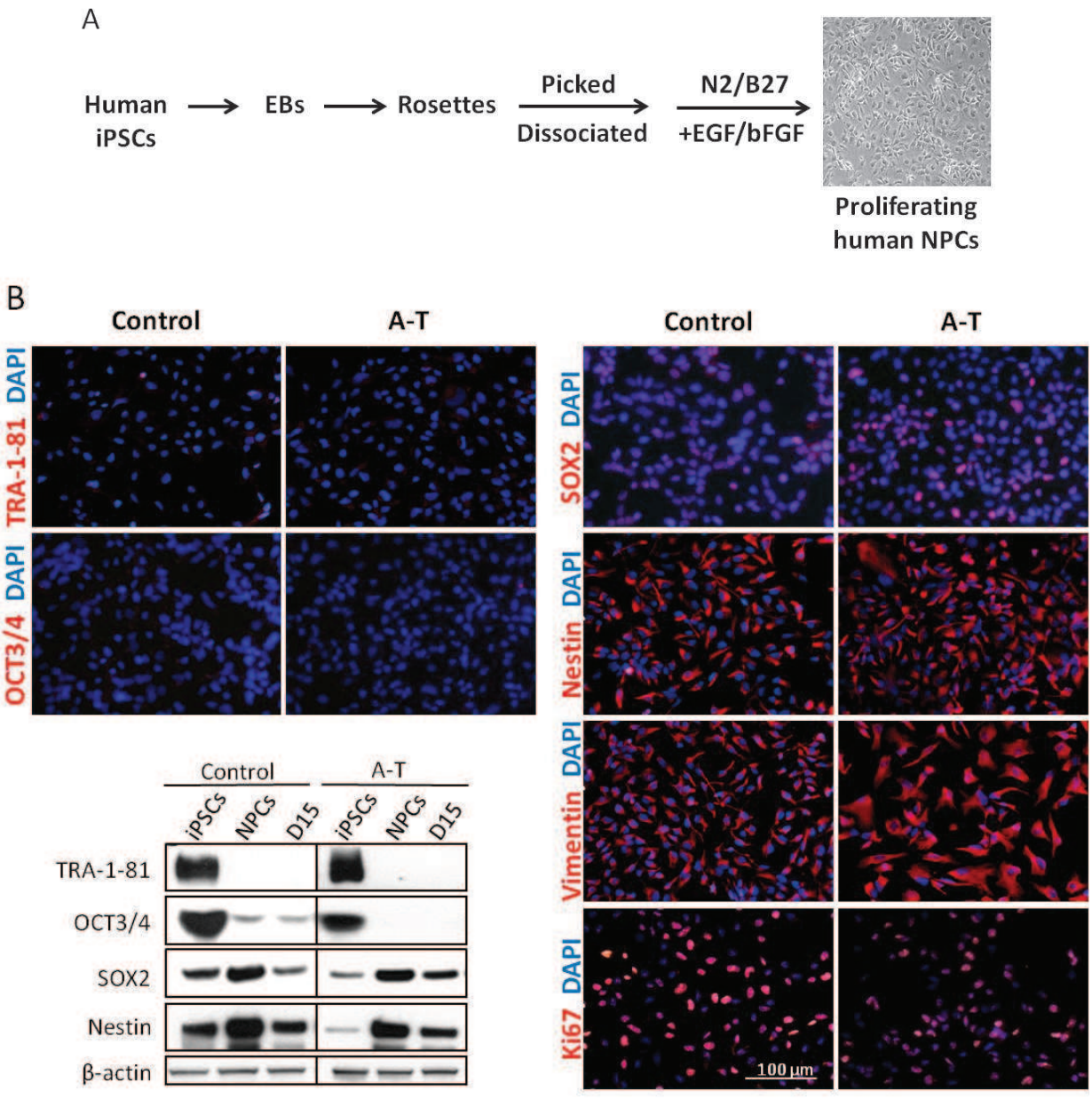

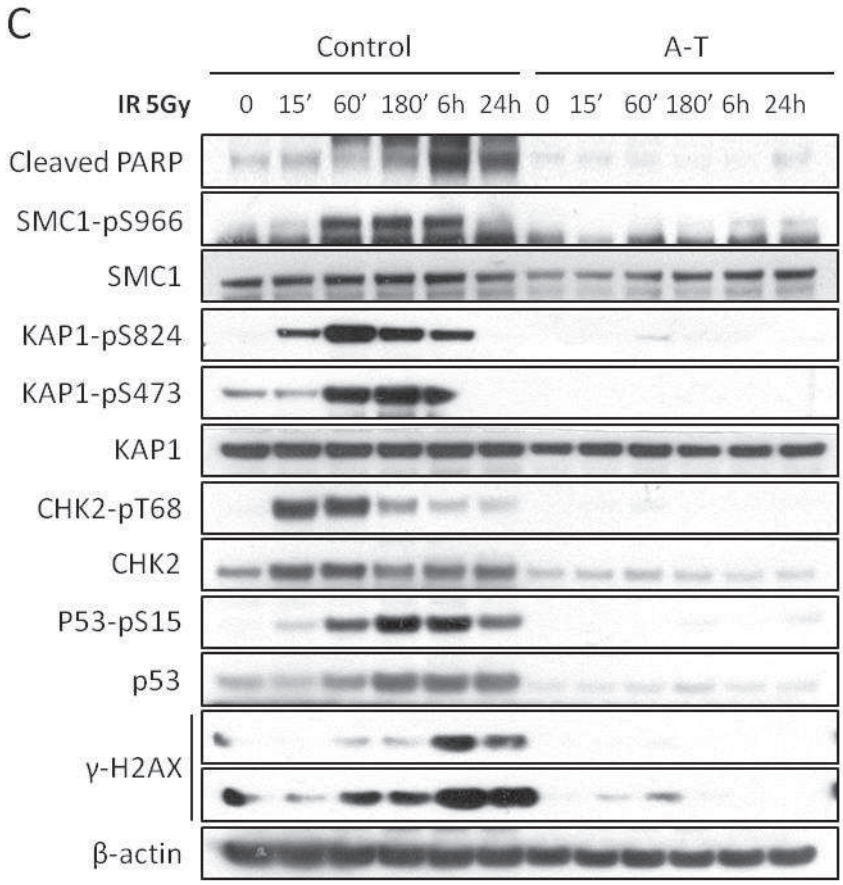
C
Control
A-T
IR 5Gy
0 15' 60' 180' 6h 24h 0 15' 60' 180' 6h 24h
Cleaved PARP
SMC1-pS966
SMC1
KAP1-pS824
KAP1-pS473
KAP1
CHK2-pT68
CHK2
P53-pS15
p53
γ-H2AX
β-actin

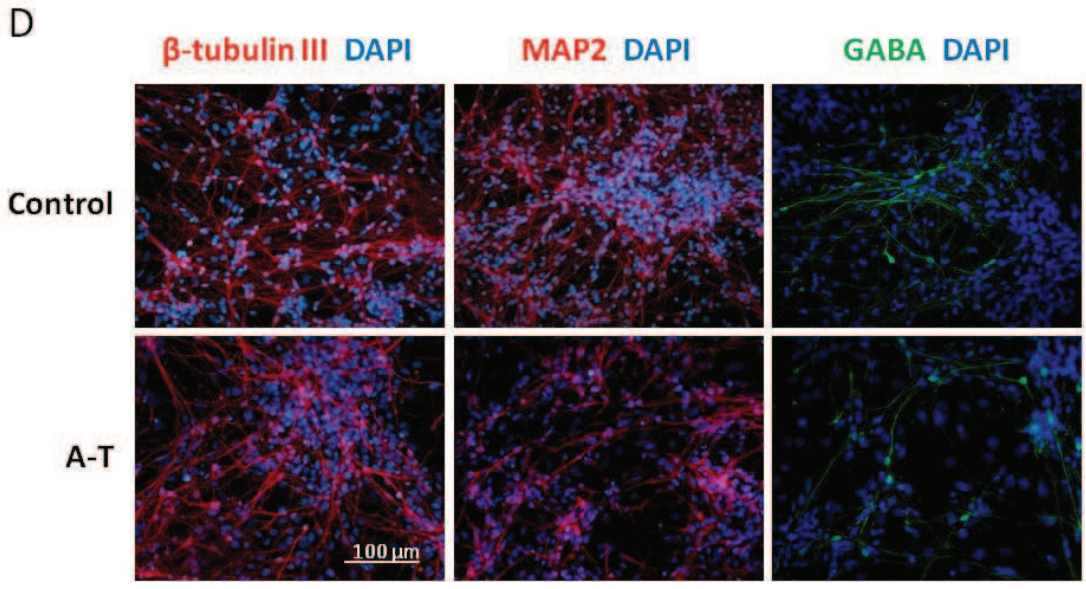
D
β-tubulin III DAPI
MAP2 DAPI
GABA DAPI
Control
A-T
100 µm

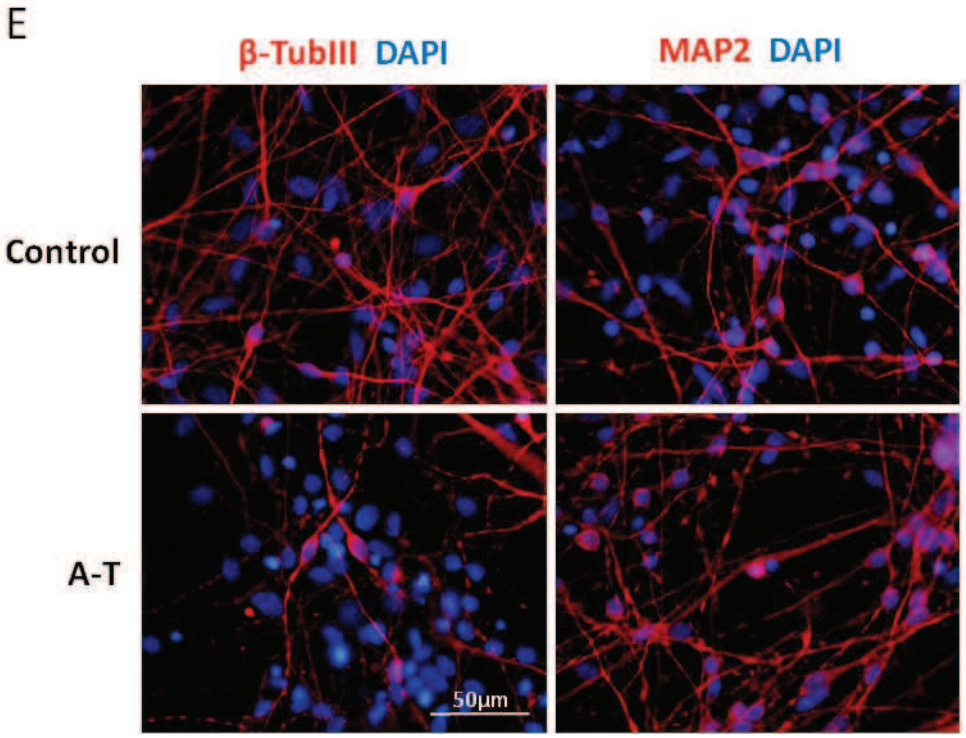
E
β-TubIII DAPI
MAP2 DAPI
Control
A-T
50μm

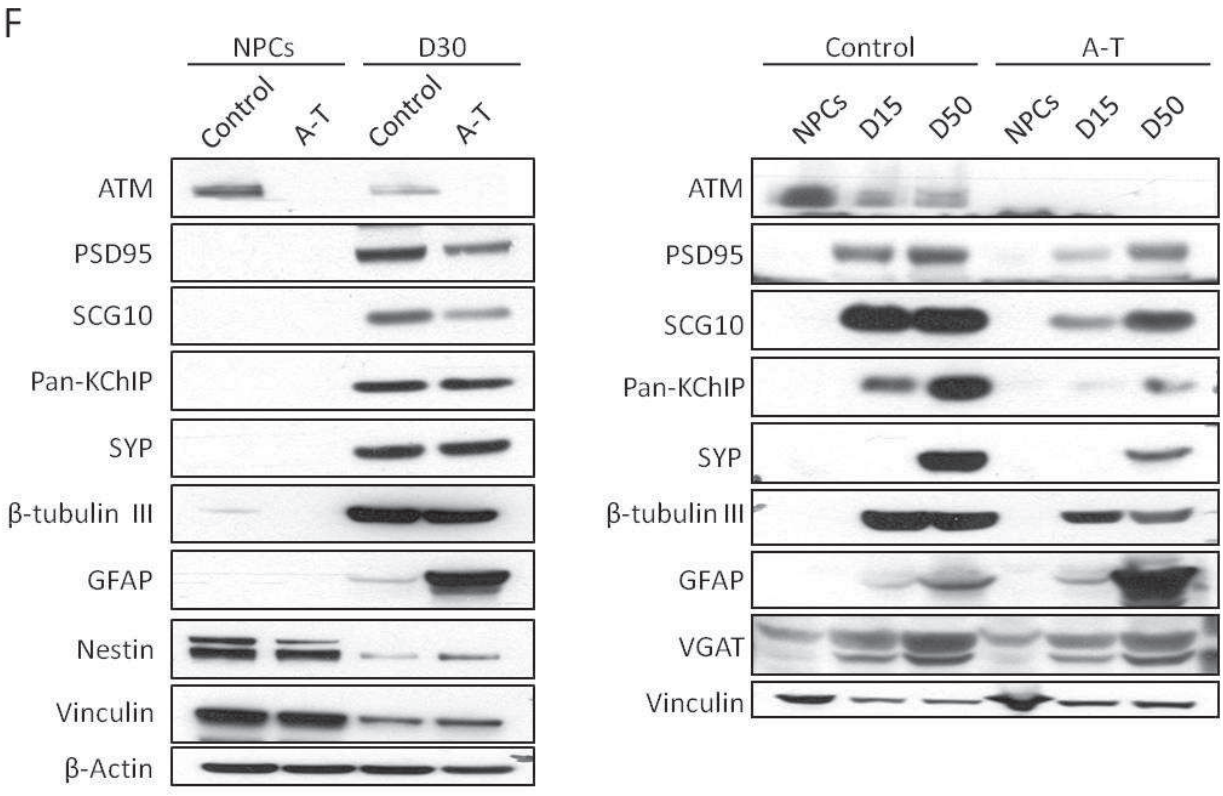
F
NPCs
D30
Control
A-T
Control
A-T
ATM
PSD95
SCG10
Pan-KChIP
SYP
β-tubulin III
GFAP
Nestin
Vinculin
β-Actin
Control
A-T
NPCs
D15
D50
NPCs
D15
D50
ATM
PSD95
SCG10
Pan-KChIP
SYP
β-tubulin III
GFAP
VGAT
Vinculin

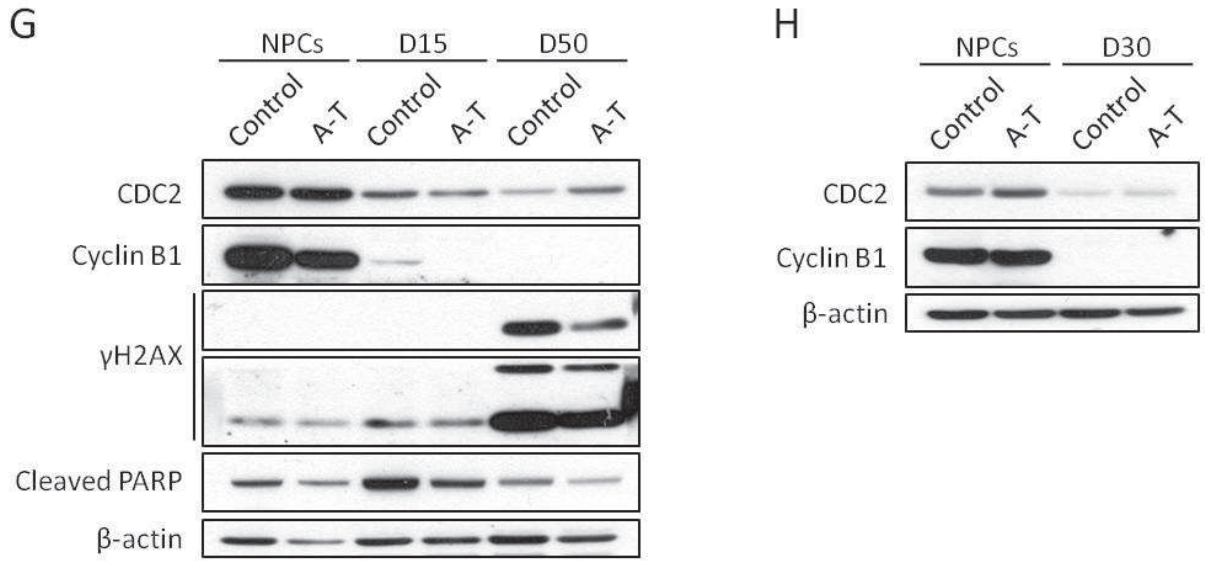

Fig. 6: Generation of human NPCs from control and A-T human iPSCs. In A, the protocol we followed to obtain stable and proliferating human NPCs is depicted and a representative image of the cell culture obtained is shown. In B, the characterization of human NPCs by immunofluorescence demonstrates loss of the pluripotency markers TRA-1-81 and OCT3/4, expression of the neural markers SOX2, nestin and vimentin and proliferation ability (Ki67). A comparative analysis between human iPSCs, proliferating human NPCs and differentiated (D15) human NPCs was performed by Western blot. In C, proliferating human NPCs were exposed to ionizing radiation (5 Gy), and the time-dependent activation of the DNA damage response was evaluated by analyzing the phosphorylation of the indicated ATM substrates. The expression of cleaved PARP was also analyzed. β-actin was used as a loading control. In D, the real capacity of human NPCs to differentiate into neurons is shown, where a high number of MAP2+, β-tubulin III+ and GABA+ cells are detected at 15 and, in E, at 50 days of differentiation. In F, human NPCs and neurons at 15, 30 or 50 days of differentiation were collected and analyzed by Western blot for the expression of differentiation and maturation markers and, in G and H, for the indicated proteins.

4.3 Electrophysiological characterization

Control and A-T neurons at D53±6 were analyzed by whole-cell patch clamp recordings in order to verify their functional maturation. Voltage clamp experiments showed similar voltage-gated potassium currents (Figure 7A) and, most importantly, voltage-gated sodium currents, selectively blocked by tetrodotoxin (TTX), which is a specific feature of mature

neurons (Figure 7A, right panel). Transient peak sodium inward currents had similar amplitude in control and A-T neurons: maximal peak current density was 84.9±19.6 pA/pF, n¼10 in control neurons and 82.7±13.5 pA/pF, n¼13 in A-T neurons (Figure 7B). Moreover, current clamp experiments showed that both control and A-T neurons could generate discharges of action potentials in response to injection of depolarizing current steps (Figure 7C).

Finally, to determine whether neurons developed functional synapses, we performed voltage clamp experiments for recording spontaneous excitatory and inhibitory postsynaptic currents (sEPSCs and sIPSCs). Both control and A-T neurons exhibited sEPSCs (Figure 7D) with similar frequencies (0.02±0.01 Hz, n¼4 cells and 0.03±0.02 Hz, n¼4 cells, respectively), which were blocked by application of kynurenic acid (3 mM; data not shown), but no sIPSCs (Figure 7E).

Figure 7

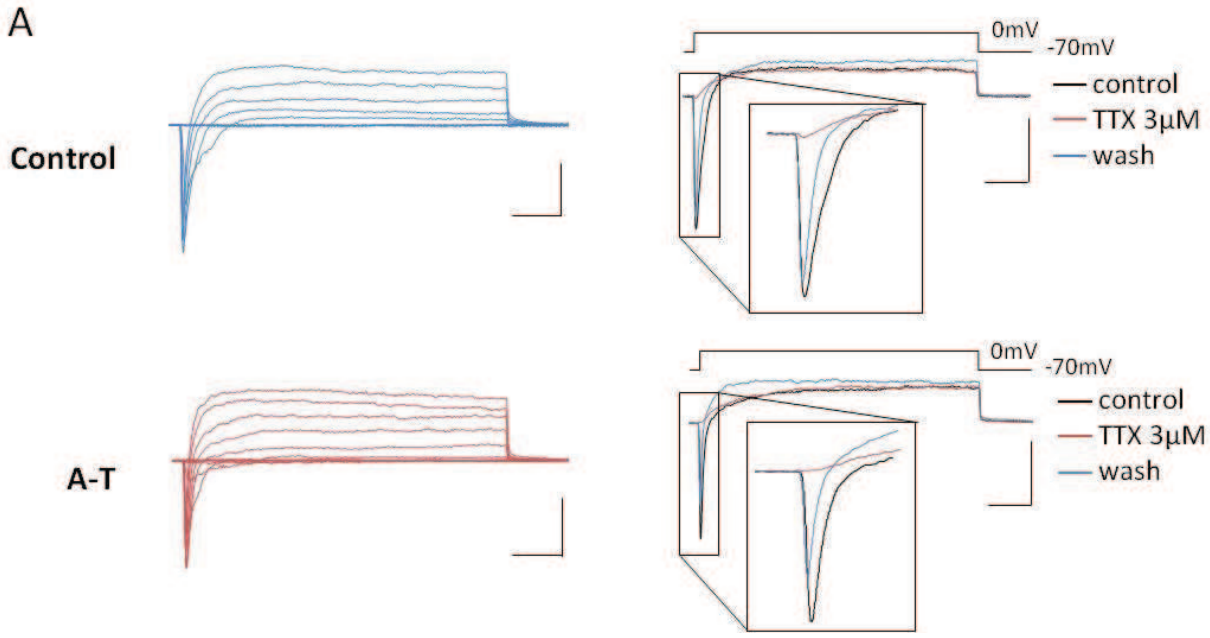

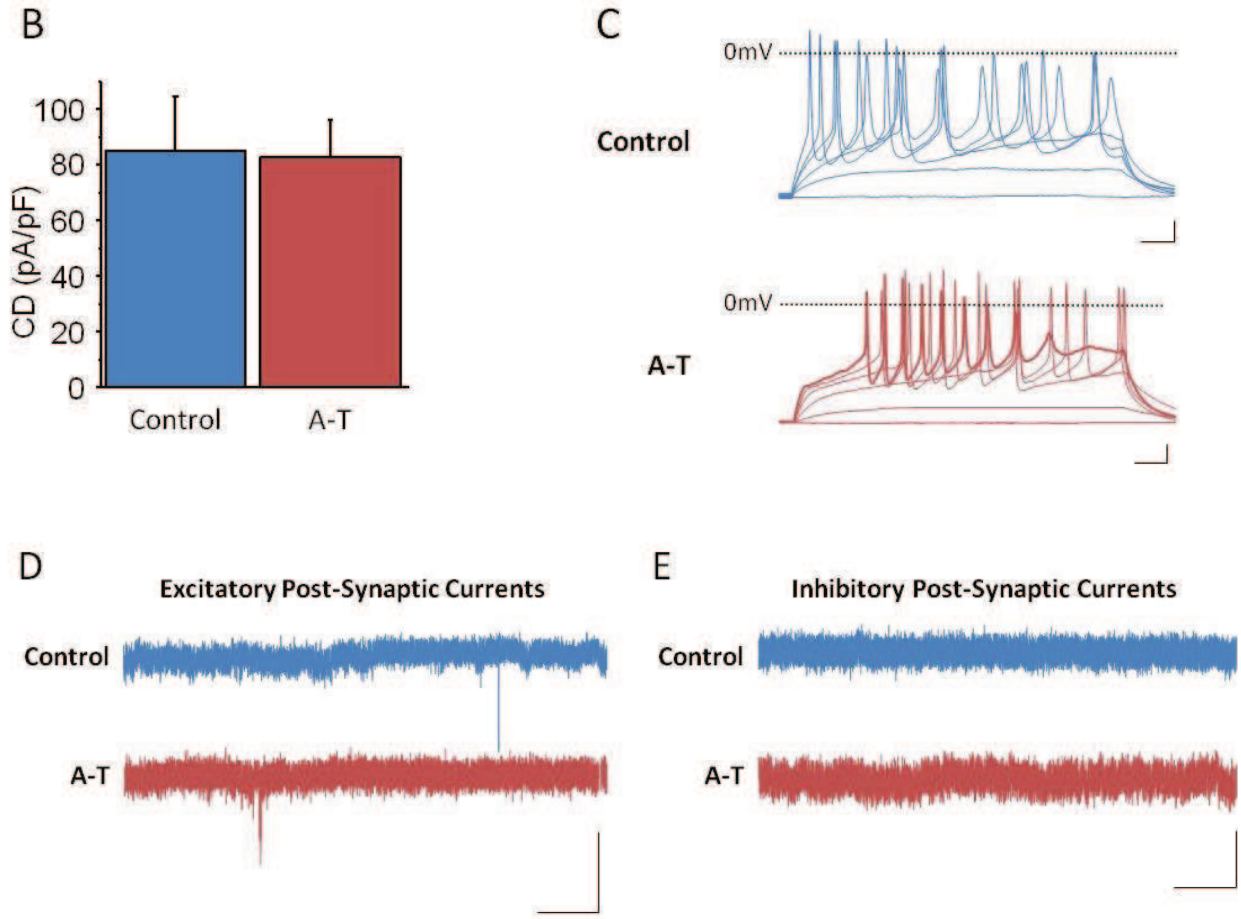

Fig. 7: Functional characterization of control and A-T neurons after 50 days of differentiation. In A, left, patch clamp whole-cell recordings of representative total ionic currents elicited with depolarizing voltage steps between –70 and +10 mV (10 mV increments from a holding potential of –70 mV) in control and A-T human NPC-derived neurons; scale bar: 500 pA, 10 ms. In A, right, representative currents elicited with a depolarizing voltage step to -10 mV in control (black), during perfusion with TTX 3 mM (red) and after washout (blue) in control (upper panels) and A-T (lower panels) human NPC-derived neurons; scale bar: 500 pA, 10 ms. In B, bar graph of maximum sodium current densities (CD) in control and A-T human NPC-derived neurons (no statistically significant difference: Student's T-test). In C, representative action potential discharges recorded in current clamp during injections of 1-s long depolarizing current steps from a holding potential of -70 mV; scale bar: 10 mV, 100 ms. In D, traces showing spontaneous excitatory postsynaptic currents, recorded at the holding potential of -70 mV, while in E traces showing the absence of spontaneous inhibitory postsynaptic currents, recorded at the holding potential of +30 mV; scale bar: 10 mV, 1 s.

4.4 DNA damage response and repair in postmitotic ataxia-telangiectasia neurons

We investigated the ATM-dependent DNA damage response of human NPC-derived terminally differentiated neurons through Western blotting using phospho-specific antibodies for ATM substrates. IR time course analysis of control neurons at D30 showed a vigorous ATM-dependent phosphorylation of SMC1-S966, KAP1-S824, CHK2-T68, p53-S15 and γH2AX, while this response was repressed in A-T neurons (Figure 8A). Similarly, the phosphorylation of the CHK2 substrate KAP1-S473 was abrogated in A-T neurons. Interestingly, as previously described for proliferating human NPCs (Figure 6C), 24 h after IR an accumulation of cleaved PARP was detected in control but not in A-T neurons, suggesting that ATM deficiency confers short-term radioresistance also in terminally differentiated cells (Figure 8A, upper panel). Altogether, these results indicate that normal postmitotic neurons activate the DNA damage response as efficiently as their proliferating precursors, and that ATM deficiency ablates this response.

The ability of postmitotic neurons to repair DSBs induced by IR was investigated with the neutral comet assay (166) and appeared defective in A-T neurons, which displayed 30% more unrepaired lesions than control cells (Figure 8B). This finding is consistent with a defective ATM-dependent DNA damage response pathway activation in response to DSBs, as shown in Figure 8A.

To investigate the role of ATM in the resolution of IR-induced DSBs in D30 postmitotic neurons, we scored the time-dependent formation and clearance of γH2AX and 53BP1 nuclear foci by immunofluorescence (167). Unirradiated control D30 neurons showed a basal number of γH2AX and 53BP1 foci per cell (1.4±1.2 and 0.9±1), which increased to 13.3±3.3 and 10.1±2.4, respectively, after IR, to decline after 6 h and even further after 24 h (Figures 8C and D).

Untreated A-T cells showed a number of foci per cell comparable to control cells, which increased more modestly, 5.6±2.6 for γH2AX and 5.6±2.1 for 53BP1 after 15 min, and persisted after 24 h (Figures 8C and D). These findings indicate that A-T postmitotic neurons show slower kinetics of DSB repair than control neurons.

The apoptotic effect of radiation on control and A-T neurons 24 h after 5 Gy IR was assessed by flow cytometry analysis of the subdiploid DNA peak on DNA histograms (Figure 8E). Fewer apoptotic cells were detected in IR-treated A-T cells (22.2%) than in control cells (32.3%), suggesting that ATM deficiency attenuates short-term apoptosis, concordant with the findings on cleaved PARP (Figure 8A, upper panel).

Figure 8

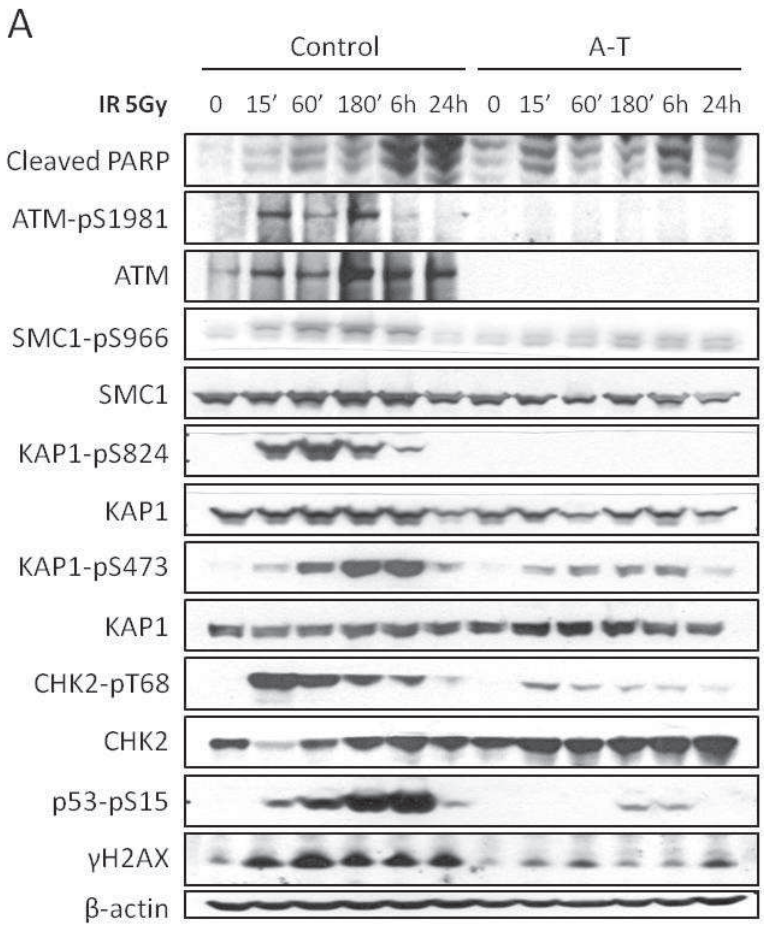

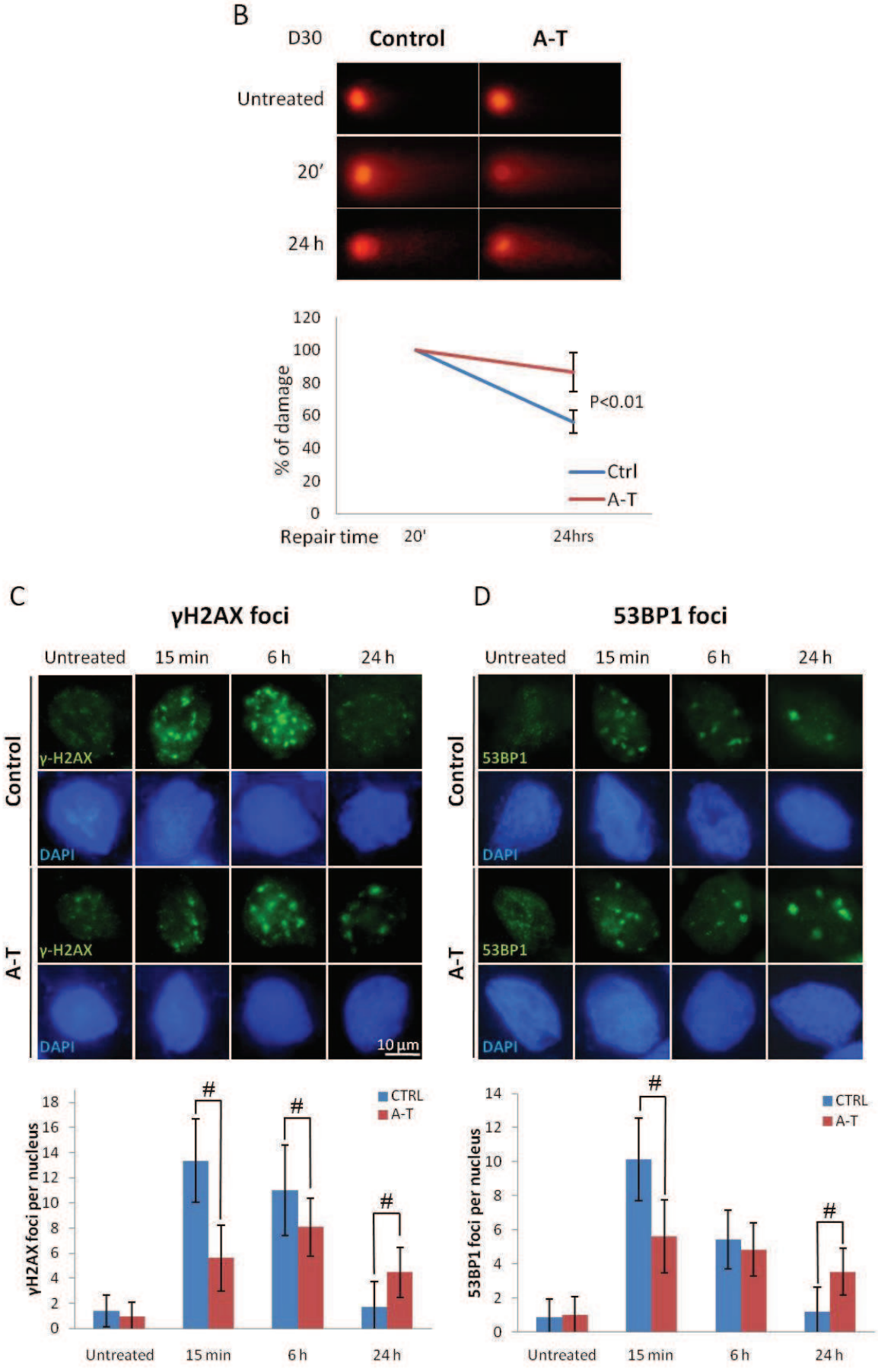
B
D30
Control
A-T
Untreated
20'
24 h
120
100
80
60
40
20
0
% of damage
P<0.01
Ctrl
A-T
Repair time
20'
24hrs
C
γH2AX foci
Untreated
15 min
6 h
24 h
Control
A-T
γ-H2AX
DAPI
10 µm
γH2AX foci per nucleus
CTRL
A-T
#
Untreated
15 min
6 h
24 h
D
53BP1 foci
53BP1
53BP1 foci per nucleus

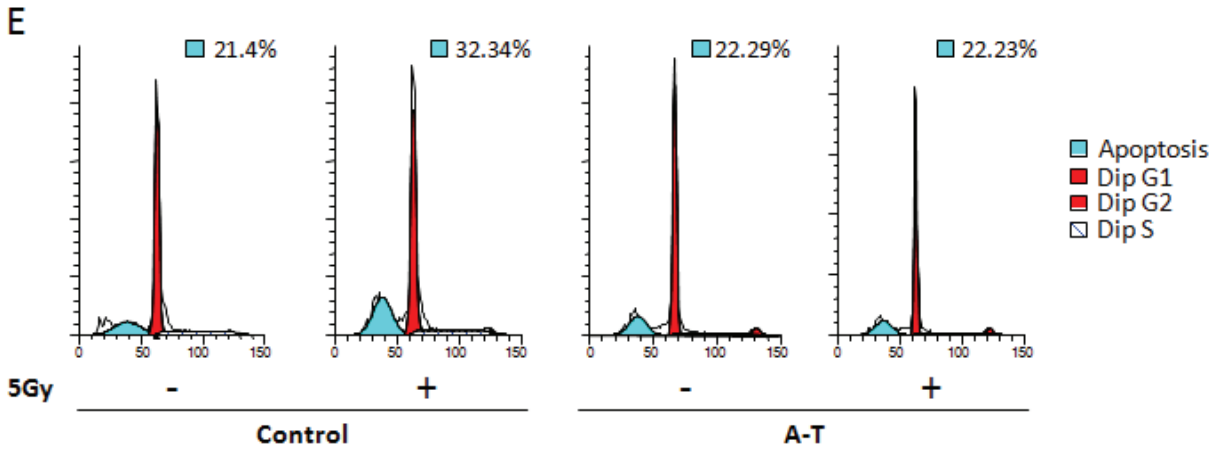

Fig. 8: A-T postmitotic neurons are defective in DNA damage response. In A, postmitotic neurons (D30) were tested by Western blot with antibodies specific for the various ATM phospho-substrates and cleaved PARP at various times after treatment with 5 Gy ionizing radiation. β-actin was used as a loading control. In B, DNA DSBs were analyzed in D30 neurons by neutral comet assay at two different times after treatment. Representative photos of comets from untreated cells and at different time points following treatment are shown. The time point with the maximum DNA damage was considered 20 min after ionizing radiation treatment. The ratio between treated and untreated tail moments of at least 50–70 cells per experimental point is shown in the graphs (values in %). One representative experiment out of three is shown. In C and D, formation and resolution of ionizing radiation-induced nuclear foci. D30 neurons were irradiated with 0.5 Gy, collected at the indicated times and labeled for γH2AX (C) and 53BP1 (D). For each marker, the number of foci was scored from 100 cell nuclei per duplicate preparations and from three independent experiments (mean ± S.D.). Where indicated, the difference between control and A-T was statistically significant (#P=0.01: Student's T-test). In E, D30 postmitotic control and A-T cells were treated with 5 Gy ionizing radiation, collected after 24 h and analyzed for DNA content by flow cytometry. The percentage of sub-diploid apoptotic cells is indicated.

4.5 Base excision repair capacity in undifferentiated and differentiated neural precursor cells and repair of single strand breaks in postmitotic neurons

In neurons, the BER pathway is essential to remove oxidative DNA damage and SSBs generated by high levels of ROS, and defects in BER contribute to neurodegeneration (168-170).

To determine how BER is regulated in pre- and postmitotic neurons, we analyzed the efficiency of the short-patch (SP) and long-patch (LP) BER subpathways. Analysis of SP-BER revealed no significant differences between control and A-T human NPCs both in the proliferation and postmitotic (D15) stage (Figure 9A). To better understand this result, we analyzed the levels of the SP-BER proteins apurinic/apyridinic endonuclease 1 (APE1), DNA polymerase β (pol β) and XRCC1. After 15 days of differentiation (D15) only the levels of XRCC1 were reduced (Figure 9C). Similar findings were seen in D30 neurons.

Next, we analyzed LP-BER activity, which appeared markedly lower in both control and A-T postmitotic neurons than in their respective proliferating human NPCs (Figure 9B). This finding is concordant with the reduced expression of flap endonuclease 1 (FEN1), a protein involved in LP-BER in non-replicating cells (Figure 9C). Overall, these results point out differences that depend on different levels of expression or differential activation of BER enzymes in undifferentiated and differentiated cells, but appear independent of ATM.

Moreover, we investigated the ability of postmitotic neurons to repair SSBs induced by H_2O_2 with the alkaline comet assay (166). Consistent with the results on BER efficiency, we found that control and A-T neurons displayed no significant differences in the repair kinetics of this type of damage (Figure 9D).

Figure 9

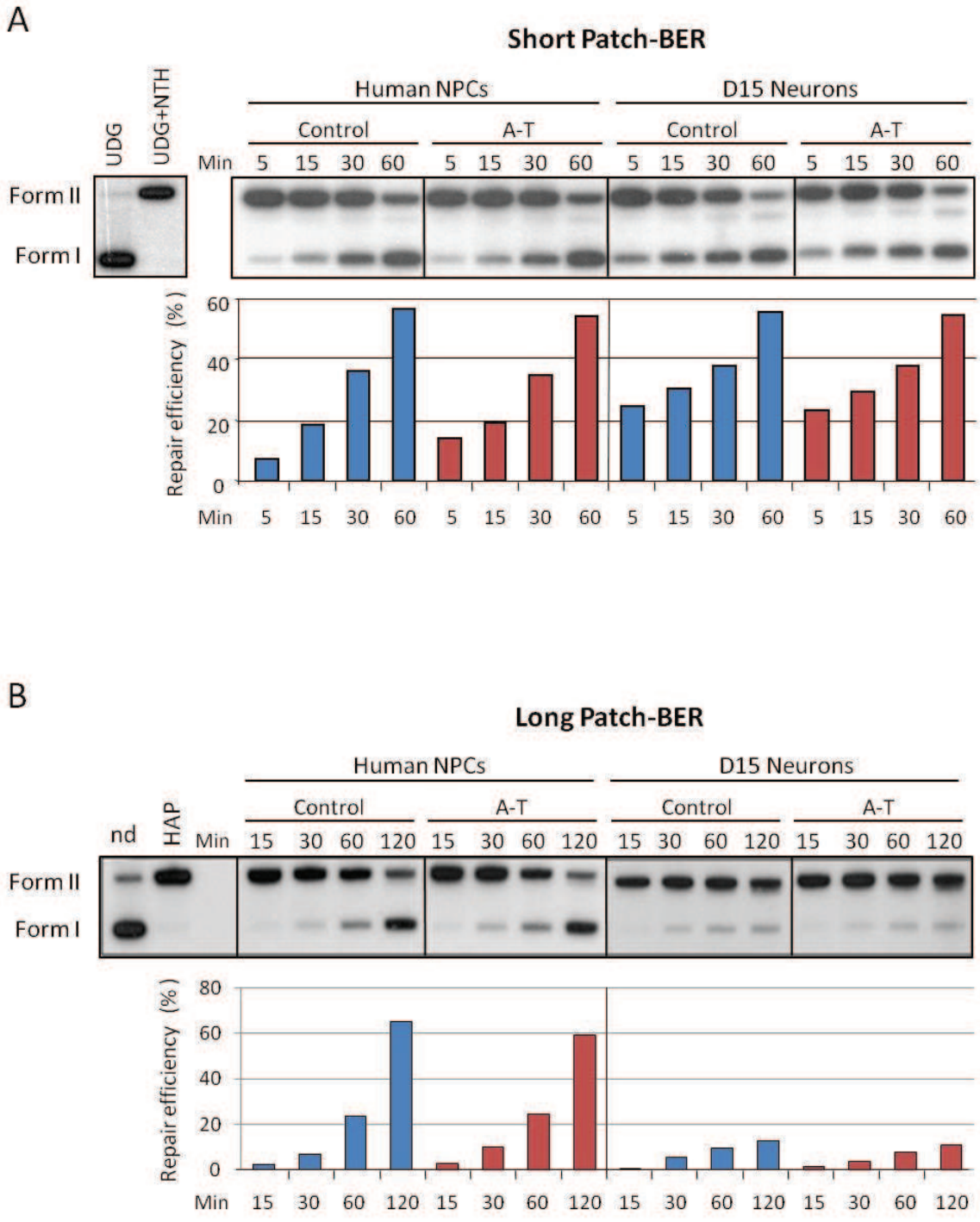
A
Short Patch-BER
UDG
UDG+NTH
Form II
Form I
Human NPCs
D15 Neurons
Control
A-T
Min
5 15 30 60
Repair efficiency (%)
60
40
20
0
B
Long Patch-BER
nd
HAP
15 30 60 120
80
60
40
20
0

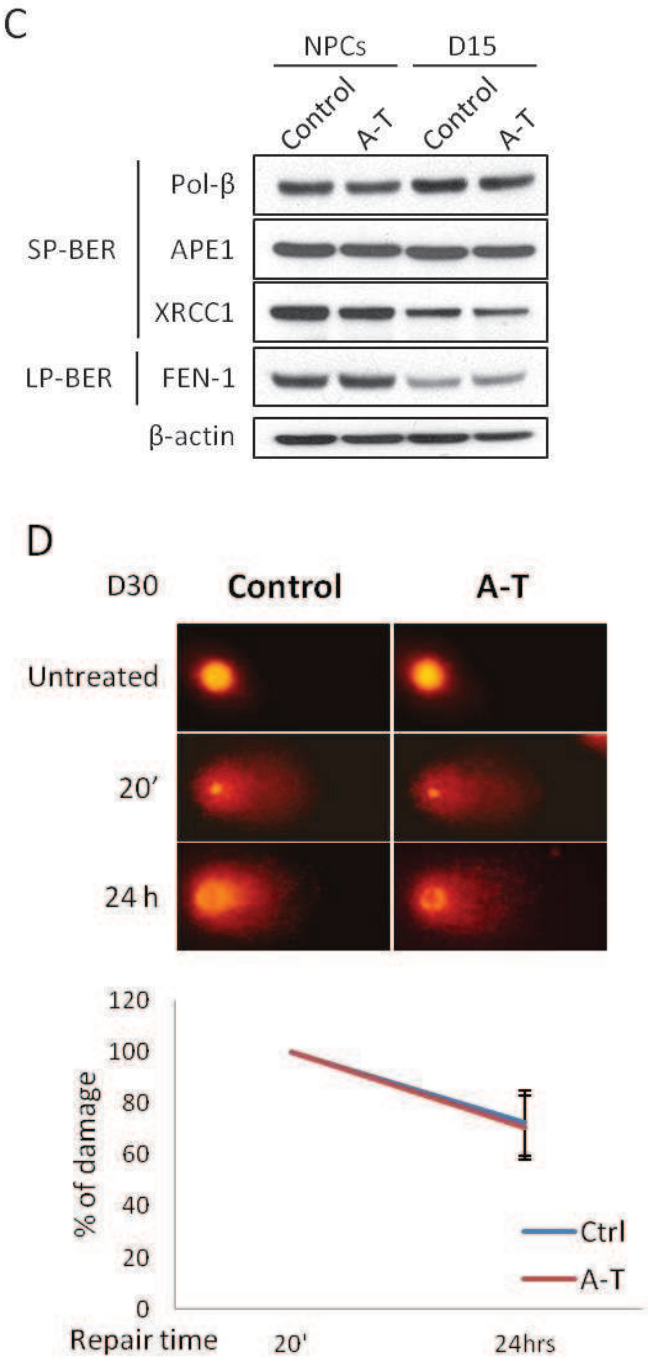

Fig. 9: Base excision repair (BER) activities in proliferating and postmitotic control and A-T neuronal cells. In A and B, *in vitro* repair reactions were performed by using whole-cell extracts and as substrate a 32P-labeled circular plasmid containing a single AP site (pGEM-AP) to measure short patch-BER (A) or a THF residue (pGEM-THF) for long patch-BER (B). The correct insertion of a single lesion in the plasmid molecules was checked by digestion with uracil DNA glycosylase (UDG) followed by endonuclease III (NTH) for pGEM-AP (A), and by AP endonuclease (HAP1) for pGEM-THF (B). Repair kinetics of the AP site (A) or THF residue (B) by proliferating

human NPCs and postmitotic neurons (D15) were measured following incubation of the single lesion-containing plasmids with extracts from control or A-T defective neuronal cells for increasing periods of time. Repair products were analyzed by agarose gel electrophoresis and the radioactivity of the bands corresponding to nicked (form II) and supercoiled (form I) plasmids was quantified. Repair efficiency is expressed as relative amount of Form I over total radioactivity in each lane. In C, the expression level of short patch-BER and long patch-BER proteins was evaluated by Western blot in proliferating and postmitotic NPCs. β-actin was used as a loading control. In D, DNA SSBs were analyzed in D30 neurons by alkaline comet assay at two different times after treatment. Representative photos of comets from untreated cells and at different time points following treatment are shown. The time point with the maximum DNA damage was considered 20 min after H_2O_2 treatment. The ratio between treated and untreated tail moments of at least 50–70 cells per experimental point is shown in the graphs (values in %). One representative experiment out of three is shown.

4.6 Treatment of ataxia-telangiectasia and control neuronal cells with genotoxic and oxidative agents

As genotoxic agents and oxidative stress may similarly affect ATM-deficient neurons, we investigated the viability of control and A-T D30 postmitotic neurons upon treatment with compounds that work through different mechanisms: CPT, which inhibits Top1 and traps Top1ccs; trabectedin, which blocks transcription factor activity (171); Paraquat, which induces ROS through depolarization of the inner mitochondrial membrane (172), and H_2O_2. Control and A-T postmitotic neurons were equally sensitive to the cytotoxic effects of H_2O_2 and Paraquat (Figures 10A and B), a finding concordant with the results in Figure 9D showing that these cells have the same ability to resolve SSBs. By contrast, A-T neurons were significantly more resistant than control neurons to CPT and trabectedin by about 40% and 30%, respectively (Figures 10C and D).

Figure 10

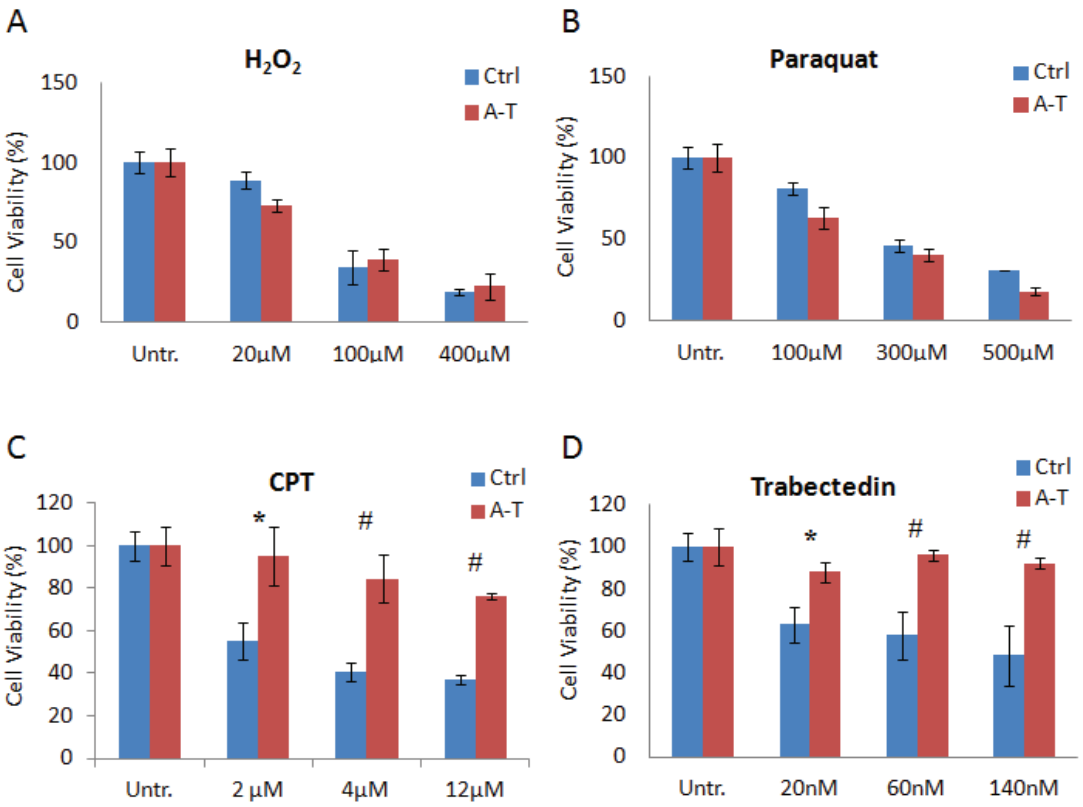

Fig. 10: A-T post-mitotic cells are resistant to CPT and trabectedin treatment. D30 neurons grown in 96-well plates were assessed for cell viability by CellTiter-Glo 72 h after exposure to H_2O_2 for 20 min (A), or continuous treatment with Paraquat (B), CPT (C) or trabectedin (D) at the indicated doses. All treatments were performed in triplicate wells. The graphs show mean ± S.D. and, where indicated, the difference between control and A-T was statistically significant (*P=0.05; #P=0.01: Student's T-test).

4.7 Accumulation of topoisomerase 1-DNA cleavage complexes in ataxia-telangiectasia postmitotic neurons

As in murine neural cells ATM deficiency results in accumulation of Top1ccs and failure to recover global transcription after Top1cc trapping (163), we used a modified alkaline comet assay, which indirectly quantifies Top1ccs, to analyze human NPC-derived D30 neurons untreated or treated for 45 min with 30 mM CPT (Figure 11A, left). The accumulation of

Top1ccs was much greater in A-T than in control neurons, both before and after CPT treatment. Of note, the overall levels of Top1 in proliferating and postmitotic neurons were similar (Figure 11A, right).

To further confirm these findings, we applied the RADAR assay, which allows to directly detect Top1ccs bound to genomic DNA. D30 neurons, incubated for 1 h with 30 mM CPT, were harvested immediately or 3 h after washout of the drug to analyze the recovery of the damage. The levels of Top1ccs (Figure 11B, left panel) were then normalized with the total amount of DNA, revealed by DAPI (Figure 11B, middle panel). β-actin was used to verify that the DNA samples were free of non-covalently bound contaminating proteins (Figure 11B, right panel). As expected, untreated A-T neurons displayed higher accumulation of Top1ccs than control cells, and also appeared defective in Top1cc recovery after CPT removal (Figure 11B, graph).

Figure 11

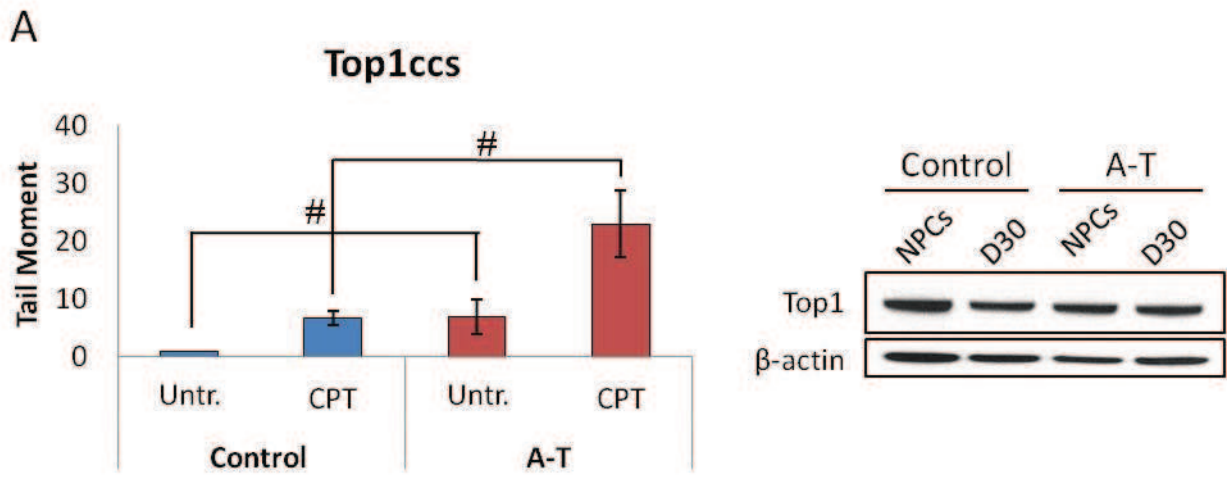

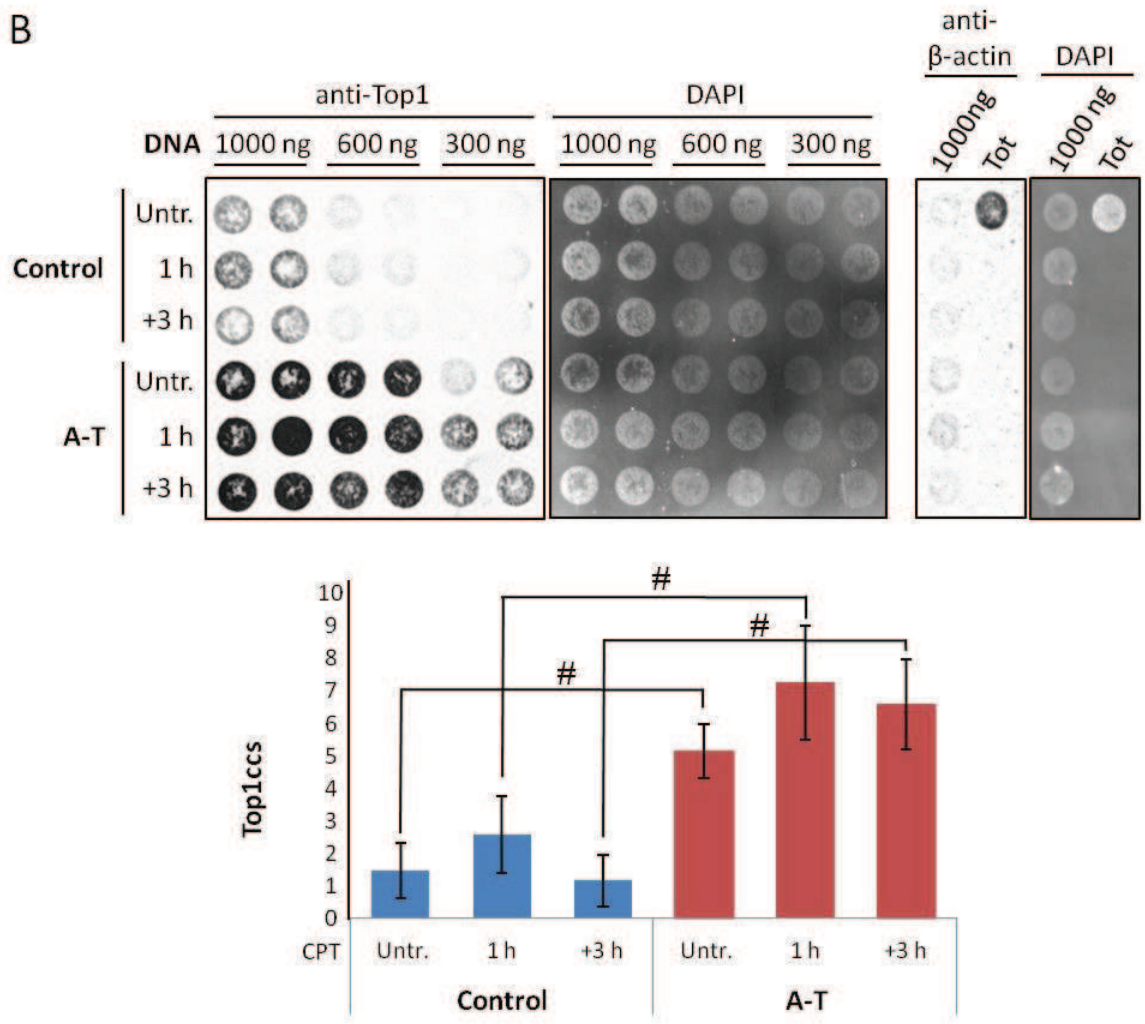

Fig. 11: A-T postmitotic neurons accumulate abnormal levels of topoisomerase 1-DNA cleavage complexes (Top1ccs). In A, the levels of endogenous Top1ccs were quantified in control and A-T D30 postmitotic neurons treated with 30 mM CPT for 40 min by modified alkaline comet assay (A, left). Fifty cells per sample per experiment were analyzed. Data are the average of three independent experiments (mean ± S.D.). The difference between control and A-T was statistically significant (#P=0.01). Total intracellular levels of Top1 protein were analyzed by Western blot in proliferating human NPCs and postmitotic neurons (A, right). In B, control and A-T D30 postmitotic neuronal cells were untreated or treated with 30 mM CPT for 60 min or incubated and harvested 3 h after washing. DNA was purified from the cells after lysis with a denaturing buffer. The indicated amount of DNA was vacuum blotted on a nitrocellulose membrane, which was then tested with an anti-Top1 antibody and ECL (left) and with DAPI (middle). β-actin (right) represents the control for non-covalently bound contaminant proteins. The densitometric analysis of Top1cc signals after normalization for blotted DNA (using DAPI) from three biological replicates (mean ± S.D.) is reported in the graph. Y axis represents the relative signal intensity. Where indicated, the difference between control and A-T was statistically significant (#P=0.01: Student's T-test).

4.8 DNA damage-induced G1/S checkpoint in relation to development stage

In somatic cells ATM mediates the G1/S cell cycle checkpoint arrest to prevents cells with damaged DNA from entering the S phase, thereby protecting genomic integrity (173). However, the G1/S checkpoint seems to be developmentally regulated, and is inactive in ESCs and iPSCs (174,175). Given the role of the G1/S checkpoint in genomic stability, its absence in pluripotent stem cells underlies fundamental differences in the way these cells preserve genome integrity, relative to somatic cells. To further delineate this activity in relation to developmental stage, we analyzed the cell cycle profile of primary fibroblast, human iPSCs, human NPCs and terminally differentiated neurons by flow cytometry before and 24 h after IR treatment. Primary control fibroblasts displayed a normal G1/S checkpoint arrest, as evident from the small redistribution of the cell cycle phases after IR, in marked contrast to A-T fibroblasts, in which this checkpoint defect resulted in a significant drop in the percentage of G1 and concomitant increase in G2 phase cells (Figure 12A). Notably, not only A-T human iPSCs, but also control human iPSCs lacked the G1/S checkpoint. Interestingly, control NPCs regained the capacity to activate the checkpoint after IR, whereas A-T NPCs maintained this defect. The analysis of neurons at D30 revealed that all cells were in the G0/G1 phase and this condition was not perturbed 24 h after IR. The distribution of cells in the different cell cycle phases is summarized in Figure 12B.

To better understand the implication of DNA damage response proteins in the regulation of cell cycle arrest in fibroblasts, iPSCs and NPCs, control cells were harvested at the indicated time points after treatment with 5 Gy IR and the expression of ATM-pS1981, p53-pS15, CDC25A and p21waf1 was analyzed (Figure 12C). Interestingly, although all cell types proficiently activated ATM and induced the accumulation of p53, human iPSCs were unable to

induce p21waf1, and did not express CDC25A. This could explain the incapacity of iPSCs to regulate the cell cycle after DNA damage. We also investigated the expression of other DNA damage response proteins such as RAD51, the MRN complex and X-ray repair cross-complementing 1 (XRCC1), and found changes in protein expression during the different differentiation steps, suggesting a different ability to repair DNA damage in the different cell types (Figure 12D).

Figure 12

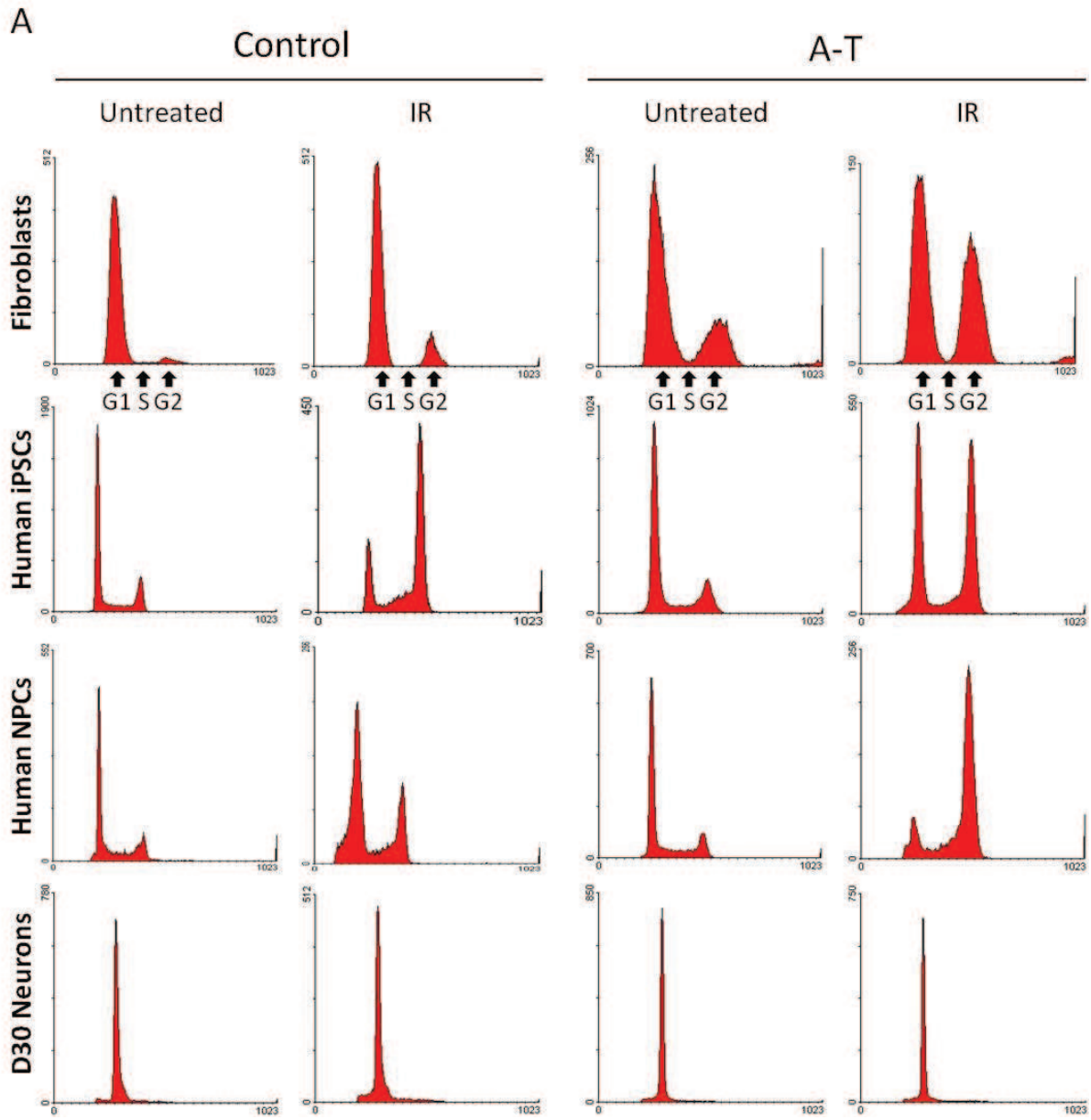

B

	Control		A-T	
	G1/G2-M Untreated	G1/G2-M (5 Gy, 24 h)	G1/G2-M Untreated	G1/G2-M (5 Gy, 24 h)
Fibroblast	16.4	7	3.7	1.5
Human iPSCs	2.7	0.3	3.2	0.76
Human NPCs	4.1	1.7	3.4	0.07
Post-Mitotic (D30)	29.1	23.64	14.4	16.2

C

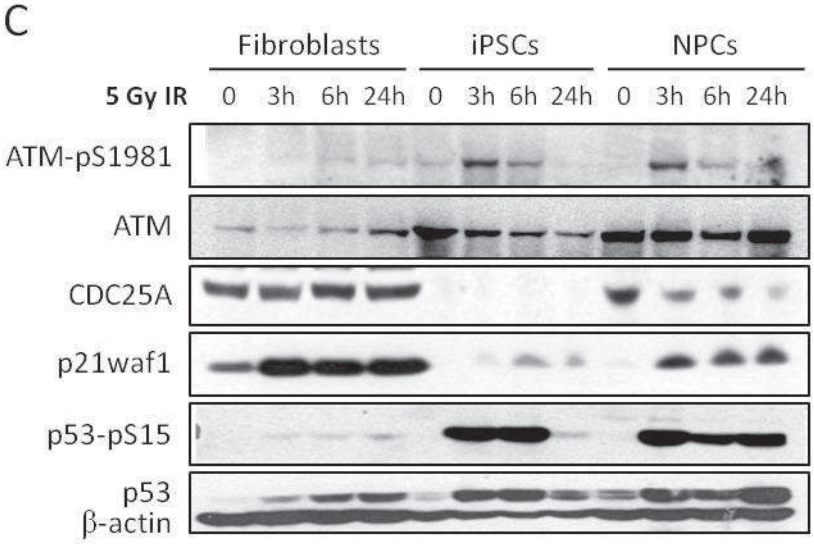

D

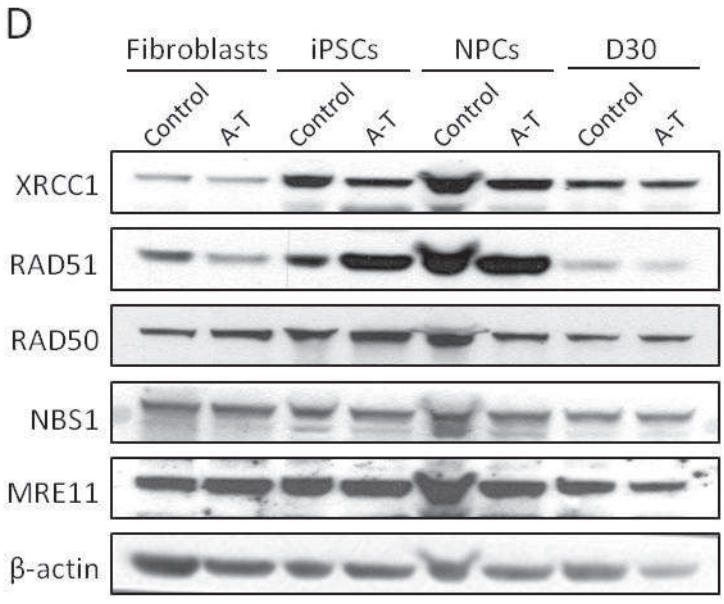

Fig. 12: Cell cycle phase distribution changes after ionizing radiation treatment. In A, control and A-T cells at various developmental stages (primary fibroblasts, human iPSCs, human NPCs, D30 postmitotic neurons) were treated with 5 Gy ionizing radiation, collected after 24 h, and analyzed for DNA content by flow cytometry. In B, the G1/G2-M ratio before and 24 h after ionizing radiation treatment for each cell type was determined from the DNA histograms depicted in A. In C, control fibroblasts, iPSCs and NPCs were treated with 5 Gy ionizing radiation, collected at the indicated times and analyzed by Western blot for the expression of the indicated proteins. β-actin was used as a loading control. In D, primary fibroblasts, human iPSCs, proliferating human NPCs and postmitotic neurons at 30 days of differentiation (D30) were compared by Western blot for the expression of the indicated DNA damage response proteins. β-actin was used as a loading control.

5. Discussion

The mechanisms underlying neurodegeneration in A-T still remain elusive. Up to the present, ATM knockout and knockin mice and *in vitro* ATM-deficient human cellular models have been useful for elucidating many aspects of the neuropathology, but the first do not recapitulate the central nervous system disease (118), while the latter cannot fully mirror the effects of A-T-causing mutations (135,136).

In order to obtain human A-T neurons *in vitro*, in this study we produced proliferating self-renewing human NPCs through the reprogramming of A-T fibroblasts into human iPSCs. These NPCs can be differentiated into neurons but also expanded, frozen and thawed. Consequently, *in vitro* analysis of the mechanisms leading to neurodegeneration in A-T can be investigated in both self-renewing neural precursors and mature neurons, without having to constantly undertake the laborious and time-consuming neuronal differentiation of human iPSCs. This technique has proven to be a powerful tool for modeling neurological diseases and indeed it has been useful for studying the pathological mechanisms underlying many neurodegenerative disorders (176). The generation of human iPSC-derived neural cells has previously been described for A-T patients (153,154), but a functional analysis of the neuronal cells harboring patient-specific mutations in ATM has not yet been reported. Thus, we performed a thorough examination of our human iPSC-derived A-T NPCs and terminally differentiated neurons in culture.

We found that A-T human proliferating NPCs displayed a strongly attenuated response to DSBs with respect to control human NPCs, which is concordant with a previous study on human NSCs (134). Moreover, although electrophysiological properties were similar in control and A-T cells, terminally differentiated A-T neurons exhibited decreased expression of SYP and PSD95. This is concordant with previous works showing pre- and postsynaptic degeneration in ATM knockout mice (117), the requirement of cytoplasmic ATM for phosphorylation of the synaptic vesicle proteins VAMP2 and synapsin 1, and that ATM deficiency affects spontaneous

vesicle release and establishment of long-term potentiation (96). We also showed that A-T neurons are defective in the expression of SCG10 and KChIP, altogether underpinning defects in neuronal maturation.

It has been previously reported that fetal brain-derived human NSC exhibit a normal response to IR, which is attenuated by ablation or inhibition of ATM (134). Subsequently Nayler (153) demonstrated that A-T iPSCs display defective IR-induced signaling, radiosensitivity, and cell cycle checkpoint defects. In accordance with these results, here we found that the DNA damage response was vigorously activated in postmitotic control neurons, as evident from the strong phosphorylation of ATM substrates, whereas in A-T postmitotic neurons this response was almost ablated, demonstrating that normal human iPSCs-derived neurons maintain the ability to activate the ATM-dependent DNA damage response. Through the neutral comet assay and the assessment of γH2AX and 53BP1 foci we also highlighted relevant DSB repair defects in A-T neurons, which indicates that ATM deficiency delays the repair of DSBs, in accordance with previous reports (128,134) and with the observation that ATM is required for the repair of heterochromatic DSBs (177). Furthermore, we demonstrated that A-T neurons show less apoptosis-related sub-diploid DNA content and a lower cleaved PARP induction after IR-treatment than control neurons. Indeed, ATM deficiency has been found to attenuate the apoptotic response to IR in A-T lymphoblastoid cells and in human NSCs (90,134) and studies using ATM-deficient mice have shown that ATM is required for the p53-mediated apoptosis of developing postmitotic neurons exposed to IR (114,178).

Oxidative stress and ensuing oxidative DNA damage can contribute to neural cell death. BER is the major pathway for the repair of oxidatively damaged DNA and various SSB intermediates (168), and previous findings demonstrate that ATM and CHK2 facilitate the recruitment of downstream BER proteins during the initial damage recognition and excision step to promote BER (179). Here, we found no significant differences in SP-BER activity

between control and A-T proliferative human NPCs and postmitotic neurons, while conversely, LP-BER activity was reduced in postmitotic neurons. When we analyzed the expression of SP-BER proteins after differentiation, we found that the levels of XRCC1 were downregulated, and the same was true for the LP-BER-associated FEN1 protein. It should be noted that both SP-BER and LP-BER enzymatic efficiencies have been found to decrease, along with the respective protein components, in a neuroblastoma cell line upon differentiation (170), and while our data on LP-BER concord with these results, those on SP-BER are clearly at variance. This could be because the expression of the SP-BER component XRCC1 is totally ablated in differentiated neuroblastoma cells (170), while being only partially downregulated in our neurons. Regardless of this discrepancy, the variations in LP-BER activity between postmitotic neurons and proliferative human NPCs were totally independent of ATM expression. Moreover, although ATM appears involved in sensing and modulating the cellular response to ROS (68), alkaline comet assays showed that A-T and control neurons equally repaired SSBs.

Consistent with these results, in our study A-T post-mitotic neurons were as sensitive to oxidative agents as control postmitotic neurons, in agreement with results obtained with A-T lymphoblastoid cells (180). By contrast, A-T postmitotic neurons were significantly more resistant than control neurons to the genotoxic agents CPT and trabectedin, probably because, in the absence of ATM, drug-induced DSBs in transcribed genes fail to activate a p53-dependent apoptotic response. This finding is concordant with results showing that ATM inhibition suppresses the genotoxic response in rat cerebellar granule neurons (181).

It has been recently shown that postmitotic neural cells from ATM-deficient mice accumulate Top1ccs and fail to recover global transcription after Top1cc trapping by CPT (163). Given that Top1ccs can promote transcription elongation arrest and decay (182) and consequent transcriptional decline, a phenomenon underlying neurodegeneration (183-185), we analyzed Top1ccs by two different assays and found greater levels of these intermediates in A-T than in

control neurons. This finding, which to our knowledge has never been reported in human A-T neurons, warrants further studies to determine the impact of Top1ccs on genome-wide global transcription.

Finally, in order to delineate the activity of the G1/S checkpoint in relation to developmental stage, we analyzed the cell cycle profile of primary fibroblast, human iPSCs, human NPCs and terminally differentiated neurons. In agreement with the role of ATM in establishing the G1/S checkpoint arrest to prevent cells with damaged DNA from entering the S phase (32), primary control fibroblasts effectively arrested at the G1/S boundary after IR, but once reprogrammed into human iPSCs they lost this G1/S checkpoint arrest to regain it at the stage of human NPCs. Instead, A-T cells showed a disrupted G1/S checkpoint whatever the developmental stage. Notably, the absence of the G1/S checkpoint arrest in control human iPSCs is a characteristic of ESCs, where cells subjected to DNA damage in G1 enter the S phase to be eliminated by apoptosis, thus avoiding the propagation of mutations which would be detrimental for the whole organism (186-187). Accordingly, human iPSCs showed a great accumulation of p53-pS15 and faint induction of p21waf1, compatible with a p53-dependent apoptotic response rather than with a G1/S checkpoint activation. Moreover, we found that control human iPSCs upregulate HR components such as RAD51, concordant with the fact that ESCs predominantly use this high fidelity pathway to avoid the accumulation of mutations, in contrast to somatic cells, which rely on the error-prone NHEJ to repair DNA damage occurring in G1 (188).

Importantly, although human A-T neuronal cells represent an attractive *in vitro* model for the study of the neurodegenerative processes in A-T, the cell type which is specifically lost in patients, i.e. human Purkinje neurons, cannot yet be generated from fibroblast-derived pluripotent stem cells due to the lack of optimized protocols. Indeed, the efficient generation of human iPSC-derived neural subtypes with correct phenotypes remains a challenge (189).

Moreover, our *in vitro* model does not take into account possible non-cell autonomous effects that the ubiquitous lack of ATM could exert on neurons in the complex context of the central nervous system (190). Therefore, although this model may be useful for unraveling the mechanisms of ATM functions in neurons, these limitations must be kept into account.

To summarize, we have shown that human A-T iPSC-derived postmitotic neurons display normal electrophysiological activity, defective expression of maturation markers, attenuated response to and repair of DSBs, but normal capacity to repair SSBs and normal BER activities. Strikingly, A-T neurons exhibit elevated levels of Top1ccs, which may potentially impair transcriptional fidelity, a possibility that requires further investigation. Finally, we have shown that human iPSCs, like ESCs, provide a unique *in vitro* model to study the details of the G1/S cell cycle checkpoint in a developmental context.

In conclusion, the generation of A-T patient-derived neuronal cells allows overcoming the obstacle posed by the inadequacy of ATM-deficient animals and cell lines. This model represents a powerful tool for exploring the mechanisms that cause degeneration of patient ATM-deficient neurons and it may be exploited for identifying therapeutic targets and for screening molecules with potential neuroprotective properties. Our previously undocumented functional and molecular characterization of patient-derived neuronal cells represents the first step in the employment of these cells as the most informative *in vitro* model to investigate neurodegeneration in A-T.

6. Future perspectives

Severe cerebellar atrophy and less pronounced degeneration in the brainstem and spinal cord tracts characterize A-T, but the selectivity of these cellular targets of degeneration is still undetermined. In the brain, high oxygen consumption and metabolic activity expose neurons to elevated ROS levels that can induce abundant SSBs. These lesions can also arise indirectly during BER, or as the result of aborted Top1 activity, and if unresolved undermine global transcription and viability. One distinctive feature of Purkinje cells, relative to other neurons, is their intrinsically heightened transcriptional rate, as inferred from the large and almost entirely euchromatic nuclei characterized by epigenetic marks for active chromatin (191,192). Based on these observations, we hypothesize that in postmitotic A-T neurons two combined effects of ATM loss, increased levels of endogenous ROS and of transcription-blocking Top1ccs, drive the accumulation of SSBs, promoting gene transcription/elongation decline and ultimately cell death. This phenomenon in A-T Purkinje neurons could be further exacerbated by their excessive transcriptional demand, likely to increase the rate of chemical and genotoxic modifications on the exposed DNA template (193,194), and to overwhelm the capabilities of the transcriptional machinery (195). To address this possibility, we will assess genome-wide transcription and RNA splicing in human iPSC-derived neurons with normal or inactive ATM activity using RNA-seq, and analyze by Top1cc-IP-seq the occupancy of Top1cc across the genome and gene bodies and match this information with gene expression data obtained by RNA-seq.

The activation of ionotropic glutamate receptors induces membrane depolarization, Ca^{2+} influx, and a signaling cascade culminating in transcriptional induction of immediate/early genes. Yet, prolonged exposure to glutamate leads to excitotoxicity, characterized by delayed deregulation of cellular Ca^{2+} homeostasis, dramatic increase in ROS and collapse of mitochondrial membrane potential (196). Since A-T cells present an impaired ROS regulation (197) and defective mobilization of intracellular Ca^{2+} (198), conceivably these dysfunctions

might favor excitotoxicity, especially in the case of Purkinje cells which, unlike other neurons, are normally highly susceptible to AMPA-mediated excitotoxicity owing also to poor handling of Ca^{2+} load leading to calpain activation (199). We will therefore assess the excitotoxic response of normal and A-T human iPSC-derived neurons to ligands for ionotropic glutamate receptors.

Human iPSCs allow to model genetic diseases *in vitro* and to elucidate their underlying mechanisms. Yet, in the case of A-T, a current drawback is the lack of a protocol to differentiate human iPSCs into Purkinje neurons. Albeit these neurons can be generated *in vitro* from mouse ESCs using an established protocol (200-202), it is unknown whether it would work with human iPSCs, but if successful this would far advance the knowledge of Purkinje cell biology in A-T. Here, two experimental approaches will be undertaken. One, *in vitro*, aimed at generating Purkinje neurons from normal and A-T human iPSCs adapting protocols developed for mouse ESCs. The other, *in vivo*, involving the orthotopic transplantion in utero into the cerebellar plate of rat embryos (203) of human iPSC-derived neural precursors fated with caudalizing and dorsalizing factors, to find out if the system is permissive for the development of human Purkinje cells, and if so to investigate their properties in organotypic cultures.

7. References

1. Ambrose M, Gatti RA. Pathogenesis of ataxia-telangiectasia: the next generation of ATM functions. Blood. 2013; 121(20): 4036-45.

2. Syllaba L, Henner K. *Contribution a l'independence de l'athetose double idiopathique et congenitale.* Rev Neurol. 1926; 1:541-562.

3. Louis Barr D. Sur un syndrome progressif comprenent des telangiectasies capillaires cutanees et conjonctivales symetriques, a disposition naevoide et des troubles cerebelleux. Confin Neurol. 1941; 4: 32-42.

4. Boder E, Sedgwick RP. Ataxia-telangiectasia. A familial syndrome of progressive cerebellar ataxia, oculocutaneous telangiectasia and frequent pulmonary infection. A preliminary report on 7 children, an autopsy, and a case history. Univ S Calif Med Bull. 1957; 9:15–28.

5. Swift M, Morrell D, Cromartie E, Chamberlin AR, Skolnick MH, Bishop DT. The incidence and gene frequency of ataxia-telangiectasia in the United States. Am J Hum Genet. 1986; 39(5):573-83.

6. Savitsky K, Bar-Shira A, Gilad S, Rotman G, Ziv Y, Vanagaite L, et al. A single ataxia-telangiectasia gene with a product similar to PI-3 kinase. Science. 1995; 268(5218): 1749-53.

7. Boder E, Sedgwick RP. Ataxia-telangiectasia; a familial syndrome of progressive cerebellar ataxia, oculocutaneous telangiectasia and frequent pulmonary infection. Pediatrics. 1958; 21(4):526-54.

8. Hoche F, Seidel K, Theis M, Vlaho S, Schubert R, Zielen S, et al. Neurodegeneration in ataxia telangiectasia: what is new? What is evident? Neuropediatrics. 2012; 43(3):119-29.

9. Verhagen MM, Martin JJ, van Deuren M, Ceuterick-de Groote C, Weemaes CM, Kremer BH, et al. Neuropathology in classical and variant ataxia-telangiectasia. Neuropathology. 2012 Jun;32(3):234-44.

10. Bottini AR, Gatti RA, Wirenfeldt M, Vinters HV. Heterotopic Purkinje cells in ataxia-telangiectasia. Neuropathology. 2012; 32(1):23-9.
11. Vinters HV, Gatti RA, Rakic P. Sequence of cellular events in cerebellar ontogeny relevant to expression of neuronal abnormalities in ataxia-telangiectasia. Kroc Found Ser. 1985; 19:233-55.
12. Chun HH, Gatti RA. Ataxia-telangiectasia, an evolving phenotype. DNA Repair. 2004; 3(8-9):1187-96.
13. Tavani F, Zimmerman RA, Berry GT, Sullivan K, Gatti R, Bingham P. Ataxia-telangiectasia: the pattern of cerebellar atrophy on MRI. Neuroradiology. 2003; 45(5):315-9.
14. Aguilar MJ, Kamoshita S, Landing BH, Boder E, Sedgwick RP. Pathological observations in ataxia-telangiectasia. A report of five cases. J Neuropathol Exp Neurol. 1968; 27:659–676.
15. Goodman WN, Cooper WC, Kessler GB, Fischer MS, Gardner MB. Ataxia-telangiectasia. A report of two cases in siblings presenting a picture of progressive spinal muscular atrophy. Bull Los Angeles Neurol Soc. 1969; 34:1–22.
16. De Leon GA, Grover WD, Huff DS. Neuropathologic changes in ataxia-telangiectasia. Neurology. 1976; 26:947–951.
17. Koepp M, Schelosky L, Cordes I, Cordes M, Poewe W. Dystonia in ataxia telangiectasia: report of a case with putaminal lesions and decreased striatal [123I]iodobenzamide binding. Mov Disord. 1994; 9(4):455–459.
18. Opeskin K, Waterston J, Nirenberg A, Hare WS. Ataxia telangiectasia with long survival. J Clin Neurosci. 1998; 5:471–473.
19. Peterson RD, Funkhouser JD, Tuck-Muller CM, Gatti RA. Cancer susceptibility in ataxia-telangiectasia. Leukemia. 1992; 6 (Suppl. 1): 8–13.
20. Ahmed M, Rahman N. ATM and breast cancer susceptibility. Oncogene. 2006; 25(43):5906-11.

21. Lavin MF, Gueven N, Bottle S, Gatti RA. Current and potential therapeutic strategies for the treatment of ataxia-telangiectasia. Br Med Bull. 2007; 81-82:129-47.

22. van Deuren M, Verhagen M, Weemeas C. Hereditary persistence of alpha-fetoprotein. Neth J Med. 2011; 69(2):96.

23. Aurias A, Dutrillaux B, Buriot D, Lejeune J. High frequencies of inversions and translocations of chromosomes 7 and 14 in ataxia telangiectasia. Mutat Res. 1980; 69(2):369-74.

24. Bar RS, Levis WR, Rechler MM, Harrison LC, Siebert C, Podskalny J, et al. Extreme insulin resistance in ataxia telangiectasia: defect in affinity of insulin receptors. N Engl J Med. 1978; 298(21):1164-71.

25. Crawford TO, Skolasky RL, Fernandez R, Rosquist KJ, Lederman HM. Survival probability in ataxia telangiectasia. Arch Dis Child. 2006; 91(7):610-1.

26. Cabana MD, Crawford TO, Winkelstein JA, Christensen JR, Lederman HM. Consequences of the delayed diagnosis of ataxia-telangiectasia. Pediatrics. 1998; 102(1 Pt 1):98-100.

27. Perlman S, Becker-Catania S, Gatti RA. Ataxia-telangiectasia: diagnosis and treatment. Semin Pediatr Neurol. 2003; 10:173-82.

28. Gatti RA, Berkel I, Boder E, Braedt G, Charmley P, Concannon P, et al. Localization of an ataxia-telangiectasia gene to chromosome 11q22-23. Nature. 1988; 336(6199):577-80.

29. Savitsky K, Sfez S, Tagle DA, Ziv Y, Sartiel A, Collins FS, et al. The complete sequence of the coding region of the ATM gene reveals similarity to cell cycle regulators in different species. Hum Mol Genet. 1995; 4(11):2025-32.

30. McConville CM, Stankovic T, Byrd PJ, McGuire GM, Yao QY, Lennox GG, et al. Mutations associated with variant phenotypes in ataxia-telangiectasia. Am J Hum Genet. 1996; 59(2):320-30.

31. Concannon P, Gatti RA. Diversity of ATM gene mutations detected in patients with ataxia-telangiectasia. Hum Mutat. 1997; 10(2):100-7.

32. Shiloh Y, Ziv Y. The ATM protein kinase: regulating the cellular response to genotoxic stress, and more. Nat. Rev. Mol. Cell Biol. 2013; 14(4): 197-210.

33. Lempiäinen H, Halazonetis TD. Emerging common themes in regulation of PIKKs and PI3Ks. EMBO J. 2009; 28(20):3067-73.

34. Kim ST, Lim DS, Canman CE, Kastan MB. Substrate specificities and identification of putative substrates of ATM kinase family members. J Biol Chem. 1999; 274(53):37538-43.

35. Lavin MF. Ataxia-telangiectasia: from a rare disorder to a paradigm for cell signalling and cancer. Nat Rev Mol Cell Biol. 2008; 9(10):759-69.

36. Polo SE, Jackson SP. Dynamics of DNA damage response proteins at DNA breaks: a focus on protein modifications. Genes Dev. 2011; 25(5):409-33.

37. Iyama T, Wilson DM 3rd. DNA repair mechanisms in dividing and non-dividing cells. DNA Repair. 2013; 12(8):620-36.

38. Metzger L, Iliakis G. Kinetics of DNA double-strand break repair throughout the cell cycle as assayed by pulsed field gel electrophoresis in CHO cells. Int J Radiat Biol. 1991; 59:1325-1339.

39. Goodarzi AA, Jeggo P, Lobrich M. The influence of heterochromatin on DNA double strand break repair: Getting the strong, silent type to relax. DNA Repair. 2010; 9(12):1273-82.

40. Bakkenist CJ, Kastan MB. DNA damage activates ATM through intermolecular autophosphorylation and dimer dissociation. Nature. 2003; 421(6922):499-506.

41. Lee JH, Paull TT. ATM activation by DNA double-strand breaks through the Mre11-Rad50-Nbs1 complex. Science. 2005; 308(5721):551-4.

42. Kozlov SV, Graham ME, Jakob B, Tobias F, Kijas AW, Tanuji M, et al. Autophosphorylation and ATM activation: additional sites add to the complexity. J Biol Chem. 2011 Mar 18;286(11):9107-19.

43. Sun Y, Xu Y, Roy K, Price BD. DNA damage-induced acetylation of lysine 3016 of ATM activates ATM kinase activity. Mol Cell Biol. 2007; 27(24):8502-9.

44. Ali A, Zhang J, Bao S, Liu I, Otterness D, Dean NM, et al. Requirement of protein phosphatase 5 in DNA-damage-induced ATM activation. Genes Dev. 2004; 18(3):249-54.

45. Lamarche BJ, Orazio NI, Weitzman MD. The MRN complex in double-strand break repair and telomere maintenance. FEBS Lett. 2010; 584(17):3682-95.

46. Burma S, Chen BP, Murphy M, Kurimasa A, Chen DJ. ATM phosphorylates histone H2AX in response to DNA double-strand breaks. J Biol Chem. 2001; 276(45):42462-7.

47. Lou Z, Minter-Dykhouse K, Franco S, Gostissa M, Rivera MA, Celeste A, et al. MDC1 maintains genomic stability by participating in the amplification of ATM-dependent DNA damage signals. Mol Cell. 2006; 21(2):187-200.

48. Ward IM, Minn K, Jorda KG, Chen J. Accumulation of checkpoint protein 53BP1 at DNA breaks involves its binding to phosphorylated histone H2AX. J Biol Chem. 2003 May 30;278(22):19579-82.

49. Paull TT, Rogakou EP, Yamazaki V, Kirchgessner CU, Gellert M, Bonner WM. A critical role for histone H2AX in recruitment of repair factors to nuclear foci after DNA damage. Curr Biol. 2000; 10(15):886-95.

50. Shiloh Y. The ATM-mediated DNA-damage response: taking shape. Trends Biochem Sci. 2006; 31(7):402-10.

51. Stiff T, O'Driscoll M, Rief N, Iwabuchi K, Löbrich M, Jeggo PA. ATM and DNA-PK function redundantly to phosphorylate H2AX after exposure to ionizing radiation. Cancer Res. 2004; 64(7):2390-6.

52. Noon AT, Shibata A, Rief N, Löbrich M, Stewart GS, Jeggo PA, et al. 53BP1-dependent robust localized KAP-1 phosphorylation is essential for heterochromatic DNA double-strand break repair. Nat Cell Biol. 2010; 12(2):177-84.

53. Riballo E, Kühne M, Rief N, Doherty A, Smith GC, Recio MJ, et al. A pathway of double-strand break rejoining dependent upon ATM, Artemis, and proteins locating to gamma-H2AX foci. Mol Cell. 2004; 16(5):715-24.

54. Smith J, Tho LM, Xu N, Gillespie DA. The ATM-Chk2 and ATR-Chk1 pathways in DNA damage signaling and cancer. Adv Cancer Res. 2010; 108:73-112.

55. Finn K, Lowndes NF, Grenon M. Eukaryotic DNA damage checkpoint activation in response to double-strand breaks. Cell Mol Life Sci. 2012; 69(9):1447-73.

56. McKinnon PJ. ATM and the molecular pathogenesis of ataxia telangiectasia. Annu Rev Pathol. 2012; 7:303-21.

57. Herrup K. Post-mitotic role of the cell cycle machinery. Curr Opin Cell Biol. 2013; 25(6):711-6.

58. Valko M, Leibfritz D, Moncol J, Cronin MT, Mazur M, Telser J. Free radicals and antioxidants in normal physiological functions and human disease. Int J Biochem Cell Biol. 2007; 39(1):44-84.

59. Yi M, Rosin MP, Anderson CK. Response of fibroblast cultures from ataxia-telangiectasia patients to oxidative stress. Cancer Lett. 1990; 54(1-2):43-50.

60. Ward AJ, Olive PL, Burr AH, Rosin MP. Response of fibroblast cultures from ataxia-telangiectasia patients to reactive oxygen species generated during inflammatory reactions. Environ Mol Mutagen. 1994; 24(2):103-111.

61. Shackelford RE, Manuszak RP, Johnson CD, Hellrung DJ, Link CJ, Wang S. Iron chelators increase the resistance of Ataxia telangiectasia cells to oxidative stress. DNA Repair. 2004; 3(10):1263-1272.

62. Taylor A, Shang F, Nowell T, Galanty Y, Shiloh Y. Ubiquitination capabilities in response to neocarzinostatin and H_2O_2 stress in cell lines from patients with ataxia-telangiectasia. Oncogene. 2002; 21(28):4363-4373.

63. Canman CE, Wolff AC, Chen CY, Fornace AJ Jr, Kastan MB. The p53-dependent G1 cell cycle checkpoint pathway and ataxia-telangiectasia. Cancer Res. 1994; 54(19):5054-8.

64. Jung M, Zhang Y, Lee S, Dritschilo A. Correction of radiation sensitivity in ataxia telangiectasia cells by a truncated I kappa B-alpha. Science. 1995; 268(5217):1619-1621.

65. Beamish H, Williams R, Chen P, Lavin MF. Defect in multiple cell cycle checkpoints in ataxia-telangiectasia post-irradiation. J Biol Chem. 1996; 271(34):20486-20493.

66. Barlow C, Dennery PA, Shigenaga MK, Smith MA, Morrow JD, Roberts LJ 2nd, et al. Loss of the ataxia-telangiectasia gene product causes oxidative damage in target organs. Proc Natl Acad Sci USA. 1999; 96(17):9915-9919.

67. Meredith MJ, Dodson ML. Impaired glutathione biosynthesis in cultured human ataxia-telangiectasia cells. Cancer Res. 1987; 47(17): 4576-4581.

68. Guo Z, Kozlov S, Lavin MF, Person MD, Paull TT. ATM activation by oxidative stress. Science. 2010; 330(6003):517-521.

69. Cosentino C, Grieco D, Costanzo V. ATM activates the pentose phosphate pathway promoting anti-oxidant defence and DNA repair. EMBO J. 2011 ;30(3):546-555.

70. Li J, O W, Li W, Jiang ZG, Ghanbari HA. Oxidative stress and neurodegenerative disorders. Int J Mol Sci. 2013; 14(12):24438-75.

71. Devin A, Rigoulet M. Mechanisms of mitochondrial response to variations in energy demand in eukaryotic cells. Am J Physiol Cell Physiol. 2007;292(1):C52-8.

72. Kamsler A, Daily D, Hochman A, Stern N, Shiloh Y, Rotman G et al. Increased oxidative stress in ataxia telangiectasia evidenced by alterations in redox state of brains from Atmdeficient mice. Cancer Res. 2001; 61(5):1849-1854.

73. Ambrose M, Goldstine JV, Gatti RA. Intrinsic mitochondrial dysfunction in ATM-deficient lymphoblastoid cells. Hum Mol Genet. 2007; 16(18):2154-2164.

74. Valentin-Vega YA, Maclean KH, Tait-Mulder J, Milasta S, Steeves M, Dorsey FC, et al. Mitochondrial dysfunction in ataxia-telangiectasia. Blood. 2012; 119(6):1490-500.

75. Sharma NK, Lebedeva M, Thomas T, Kovalenko OA, Stumpf JD, Shadel GS, et al. Intrinsic mitochondrial DNA repair defects in Ataxia Telangiectasia. DNA Repair. 2014; 13:22-31.

76. Pessin JE, Saltiel AR. Signaling pathways in insulin action: molecular targets of insulin resistance. J Clin Invest. 2000; 106(2):165-9.

77. Yang DQ, Kastan MB. Participation of ATM in insulin signalling through phosphorylation of eIF-4E-binding protein 1. Nat Cell Biol. 2000; 2(12):893-8.

78. Viniegra JG, Martínez N, Modirassari P, Hernández Losa J, Parada Cobo C, Sánchez-Arévalo Lobo VJ, et al. Full activation of PKB/Akt in response to insulin or ionizing radiation is mediated through ATM. J Biol Chem. 2005; 280(6):4029-36.

79. Halaby MJ, Hibma JC, He J, Yang DQ. ATM protein kinase mediates full activation of Akt and regulates glucose transporter 4 translocation by insulin in muscle cells. Cell Signal. 2008; 20(8):1555-63.

80. Armata HL, Golebiowski D, Jung DY, Ko HJ, Kim JK, Sluss HK. Requirement of the ATM/p53 tumor suppressor pathway for glucose homeostasis. Mol Cell Biol. 2010; 30(24):5787-94.

81. Peretz S, Jensen R, Baserga R, Glazer PM. ATM-dependent expression of the insulin-like growth factor-I receptor in a pathway regulating radiation response. Proc Natl Acad Sci USA. 2001; 98(4):1676-81.

82. Foley EA, Kapoor TM. Microtubule attachment and spindle assembly checkpoint signalling at the kinetochore. Nat Rev Mol Cell Biol. 2013; 14:25‐37.

83. Stolz A, Ertych N, Kienitz A, Vogel C, Schneider V, Fritz B, et al. The CHK2-BRCA1 tumour suppressor pathway ensures chromosomal stability in human somatic cells. Nat Cell Biol. 2010; 12(5):492-9.

84. Xiong B, Li S, Ai JS, Yin S, Ouyang YC, Sun SC, et al. BRCA1 is required for meiotic spindle assembly and spindle assembly checkpoint activation in mouse oocytes. Biol Reprod. 2008; 79(4):718-26.

85. Zachos G, Black EJ, Walker M, Scott MT, Vagnarelli P, Earnshaw WC, et al. Chk1 is required for spindle checkpoint function. Dev Cell. 2007; 12(2):247-60.

86. Oricchio E, Saladino C, Iacovelli S, Soddu S, Cundari E. ATM is activated by default in mitosis, localizes at centrosomes and monitors mitotic spindle integrity. Cell Cycle. 2006; 5(1):88-92.

87. Yang C, Tang X, Guo X, Niikura Y, Kitagawa K, Cui K, et al. Aurora-B mediated ATM serine 1403 phosphorylation is required for mitotic ATM activation and the spindle checkpoint. Mol Cell. 2011; 44(4):597-608.

88. Yang C, Hao J, Kong D, Cui X, Zhang W, Wang H, et al. ATM-mediated Mad1 Serine 214 phosphorylation regulates Mad1 dimerization and the spindle assembly checkpoint. Carcinogenesis. 2014; 35(9):2007-13.

89. Shigeta T, Takagi M, Delia D, Chessa L, Iwata S, Kanke Y, et al. Defective control of apoptosis and mitotic spindle checkpoint in heterozygous carriers of ATM mutations. Cancer Res. 1999; 59:2602‐7.

90. Takagi M, Delia D, Chessa L, Iwata S, Shigeta T, Kanke Y, et al. Defective control of apoptosis, radiosensitivity, and spindle checkpoint in ataxia telangiectasia. Cancer Res. 1998; 58:4923‐9.

91. Shen KC, Heng H, Wang Y, Lu S, Liu G, Deng CX, et al. ATM and p21 cooperate to suppress aneuploidy and subsequent tumor development. Cancer Res. 2005; 65:8747‐53.

92. Katyal S, Lee Y, Nitiss KC, Downing SM, Li Y, Shimada M, et al. Aberrant topoisomerase-1 DNA lesions are pathogenic in neurodegenerative genome instability syndromes. Nat Neurosci. 2014; 17(6):813-21.

93. Sordet O, Redon CE, Guirouilh-Barbat J, Smith S, Solier S, Douarre C, et al. Ataxia telangiectasia mutated activation by transcription- and topoisomerase I-induced DNA double-strand breaks. EMBO Rep. 2009; 10(8):887-93.

94. Pommier Y. Topoisomerase I inhibitors: camptothecins and beyond. Nat Rev Cancer. 2006; 6(10):789-802.

95. Herrup K, Li J, Chen J. The role of ATM and DNA damage in neurons: upstream and downstream connections. DNA Repair. 2013; 12(8):600-4.

96. Li J, Han YR, Plummer MR, Herrup K. Cytoplasmic ATM in neurons modulates synaptic function. Curr Biol. 2009; 19(24):2091-6.

97. Schweizer FE, Ryan TA. The synaptic vesicle: cycle of exocytosis and endocytosis. Curr Opin Neurobiol. 2006; 16(3):298-304.

98. Siddoway B, Hou H, Yang H, Petralia R, Xia H. Synaptic activity bidirectionally regulates a novel sequence-specific S-Q phosphoproteome in neurons. J Neurochem. 2014; 128(6):841-51.

99. Kim TS, Kawaguchi M, Suzuki M, Jung CG, Asai K, Shibamoto Y, et al. The ZFHX3 (ATBF1) transcription factor induces PDGFRB, which activates ATM in the cytoplasm to protect cerebellar neurons from oxidative stress. Dis Model Mech. 2010; 3(11-12):752-762.

100. Lau A, Tymianski M. Glutamate receptors, neurotoxicity and neurodegeneration. Pflugers Arch. 2010; 460(2):525-42.

101. Ishii Y, Oya T, Zheng L, Gao Z, Kawaguchi M, Sabit H, et al. Mouse brains deficient in neuronal PDGF receptor-beta develop normally but are vulnerable to injury. J Neurochem. 2006; 98(2):588-600.

102. Sweatt JD. The emerging field of neuroepigenetics. Neuron. 2013; 80(3):624-32.

103. Li J, Chen J, Ricupero CL, Hart RP, Schwartz MS, Kusnecov A, et al. Nuclear accumulation of HDAC4 in ATM deficiency promotes neurodegeneration in ataxia telangiectasia. Nat. Med. 2012; 18(5): 783-790.

104. Li J, Hart RP, Mallimo EM, Swerdel MR, Kusnecov AW, Herrup K. EZH2-mediated H3K27 trimethylation mediates neurodegeneration in ataxia-telangiectasia. Nat. Neurosci. 2013; 16(12): 1745-1753.

105. Ribeiro FM, Camargos ER, de Souza LC, Teixeira AL. Animal models of neurodegenerative diseases. Rev Bras Psiquiatr. 2013; 35 Suppl 2:S82-91.

106. Lenz S, Karsten P, Schulz JB, Voigt A. Drosophila as a screening tool to study human neurodegenerative diseases. J Neurochem. 2013; 127(4):453-60.

107. Rimkus SA, Katzenberger RJ, Trinh AT, Dodson GE, Tibbetts RS, Wassarman DA. Mutations in String/CDC25 inhibit cell cycle re-entry and neurodegeneration in a Drosophila model of Ataxia telangiectasia. Genes Dev. 2008; 22(9):1205-20.

108. Petersen AJ, Wassarman DA. Drosophila innate immune response pathways moonlight in neurodegeneration. Fly (Austin). 2012; 6(3):169-72.

109. Petersen AJ, Katzenberger RJ, Wassarman DA. The innate immune response transcription factor relish is necessary for neurodegeneration in a Drosophila model of ataxia-telangiectasia. Genetics. 2013; 194(1):133-42.

110. Nguyen D, Xu T. The expanding role of mouse genetics for understanding human biology and disease. Dis Model Mech. 2008; 1(1):56-66.

111. Barlow C, Hirotsune S, Paylor R, Liyanage M, Eckhaus M, Collins F, et al. Atm-deficient mice: a paradigm of ataxia telangiectasia. Cell. 1996; 86(1):159-71.

112. Elson A, Wang Y, Daugherty CJ, Morton CC, Zhou F, Campos-Torres J, et al. Pleiotropic defects in ataxia-telangiectasia protein-deficient mice. Proc Natl Acad Sci U S A. 1996; 93(23):13084-9.

113. Xu Y, Baltimore D. Dual roles of ATM in the cellular response to radiation and in cell growth control. Genes Dev. 1996; 10(19):2401-10.

114. Herzog KH, Chong MJ, Kapsetaki M, Morgan JI, McKinnon PJ. Requirement for Atm in ionizing radiation-induced cell death in the developing central nervous system. Science. 1998; 280(5366):1089-91.

115. Spring K, Cross S, Li C, Watters D, Ben-Senior L, Waring P, et al. Atm knock-in mice harboring an in-frame deletion corresponding to the human ATM 7636del9 common mutation exhibit a variant phenotype. Cancer Res. 2001; 61(11):4561-8.

116. Borghesani PR, Alt FW, Bottaro A, Davidson L, Aksoy S, Rathbun GA, et al. Abnormal development of Purkinje cells and lymphocytes in Atm mutant mice. Proc Natl Acad Sci U S A. 2000; 97(7):3336-41.

117. Kuljis RO, Xu Y, Aguila MC, Baltimore D. Degeneration of neurons, synapses, and neuropil and glial activation in a murine Atm knockout model of ataxia-telangiectasia. Proc Natl Acad Sci U S A. 1997; 94(23):12688-93.

118. Lavin MF. The appropriateness of the mouse model for ataxia-telangiectasia: neurological defects but no neurodegeneration. DNA Repair. 2013; 12(8):612-9.

119. Biton S, Barzilai A, Shiloh Y. The neurological phenotype of ataxia-telangiectasia: solving a persistent puzzle. DNA Repair. 2008; 7(7):1028-38.

120. Chiesa N, Barlow C, Wynshaw-Boris A, Strata P, Tempia F. Atm-deficient mice Purkinje cells show age-dependent defects in calcium spike bursts and calcium currents. Neuroscience. 2000; 96(3):575-83.

121. Eilam R, Peter Y, Groner Y, Segal M. Late degeneration of nigro-striatal neurons in ATM-/- mice. Neuroscience. 2003; 121(1):83-98.

122. Carlessi L, Fusar Poli E, De Filippis L, Delia D. ATM-deficient human neural stem cells as an in vitro model system to study neurodegeneration. DNA Repair. 2013; 12(8):605-11.

123. Boehrs JK, He J, Halaby MJ, Yang DQ. Constitutive expression and cytoplasmic compartmentalization of ATM protein in differentiated human neuron-like SH-SY5Y cells. J Neurochem. 2007; 100(2):337-45.

124. Biton S, Dar I, Mittelman L, Pereg Y, Barzilai A, Shiloh Y. Nuclear ataxia-telangiectasia mutated (ATM) mediates the cellular response to DNA double strand breaks in human neuron-like cells. J Biol Chem. 2006; 281(25):17482-91.

125. Li Y, Xiong H, Yang DQ. Functional switching of ATM: sensor of DNA damage in proliferating cells and mediator of Akt survival signal in post-mitotic human neuron-like cells. Chin J Cancer. 2012; 31(8):364-72.

126. Agholme L, Lindström T, Kågedal K, Marcusson J, Hallbeck M. An in vitro model for neuroscience: differentiation of SH-SY5Y cells into cells with morphological and biochemical characteristics of mature neurons. J Alzheimers Dis. 2010; 20(4):1069-82.

127. Biton S, Gropp M, Itsykson P, Pereg Y, Mittelman L, Johe K, et al. ATM-mediated response to DNA double strand breaks in human neurons derived from stem cells. DNA Repair. 2007; 6(1):128-34.

128. Adams BR, Golding SE, Rao RR, Valerie K. Dynamic dependence on ATR and ATM for double-strand break repair in human embryonic stem cells and neural descendants. PLoS One. 2010; 5(4):e10001.

129. Broccoli V, Giannelli SG, Mazzara PG. Modeling physiological and pathological human neurogenesis in the dish. Front Neurosci. 2014; 8:183.

130. Baldwin T. Morality and human embryo research. Introduction to the Talking Point on morality and human embryo research. EMBO Rep. 2009; 10(4):299-300.

131. De Filippis L, Binda E. Concise review: self-renewal in the central nervous system: neural stem cells from embryo to adult. Stem Cells Transl Med. 2012; 1(4):298-308.

132. Jakel RJ, Schneider BL, Svendsen CN. Using human neural stem cells to model neurological disease. Nat Rev Genet. 2004; 5(2):136-44.

133. Hickson I, Zhao Y, Richardson CJ, Green SJ, Martin NM, Orr AI, Reaper PM, et al. Identification and characterization of a novel and specific inhibitor of the ataxia-telangiectasia mutated kinase ATM. Cancer Res. 2004; 64(24):9152-9.

134. Carlessi L, De Filippis L, Lecis D, Vescovi A, Delia D. DNA-damage response, survival and differentiation in vitro of a human neural stem cell line in relation to ATM expression. Cell Death Differ. 2009; 16(6):795-806.

135. Gilad S, Chessa L, Khosravi R, Russell P, Galanty Y, Piane M, et al. Genotype-phenotype relationships in ataxia-telangiectasia and variants. Am J Hum Genet. 1998; 62(3):551-61.

136. Daniel JA, Pellegrini M, Lee BS, Guo Z, Filsuf D, Belkina NV, et al. Loss of ATM kinase activity leads to embryonic lethality in mice. J Cell Biol. 2012; 198(3):295-304.

137. Stewart R, Kozlov S, Matigian N, Wali G, Gatei M, Sutharsan R, et al. A patient-derived olfactory stem cell disease model for ataxia-telangiectasia. Hum Mol Genet. 2013; 22(12):2495-509.

138. Takahashi K, Yamanaka S. Induction of pluripotent stem cells from mouse embryonic and adult fibroblast cultures by defined factors. Cell. 2006; 126(4):663-76.

139. Takahashi K, Tanabe K, Ohnuki M, Narita M, Ichisaka T, Tomoda K, et al. Induction of pluripotent stem cells from adult human fibroblasts by defined factors. Cell 2007; 131(5): 861-872.

140. Zhou YY, Zeng F. Integration-free methods for generating induced pluripotent stem cells. Genomics Proteomics Bioinformatics. 2013; 11(5):284-7.

141. Okano H, Yamanaka S. iPS cell technologies: significance and applications to CNS regeneration and disease. Mol Brain. 2014; 7:22.

142. Israel MA, Yuan SH, Bardy C, Reyna SM, Mu Y, Herrera C, et al. Probing sporadic and familial Alzheimer's disease using induced pluripotent stem cells. Nature. 2012; 482(7384):216-20.

143. Kondo T, Asai M, Tsukita K, Kutoku Y, Ohsawa Y, Sunada Y, et al. Modeling Alzheimer's disease with iPSCs reveals stress phenotypes associated with intracellular Aβ and differential drug responsiveness. Cell Stem Cell. 2013; 12(4):487-96.

144. Imaizumi Y, Okada Y, Akamatsu W, Koike M, Kuzumaki N, Hayakawa H, et al. Mitochondrial dysfunction associated with increased oxidative stress and alpha-synuclein accumulation in PARK2 iPSC-derived neurons and postmortem brain tissue. Mol Brain 2012, 5:35.

145. Reinhardt P, Schmid B, Burbulla LF, Schöndorf DC, Wagner L, Glatza M, et al. Genetic correction of a LRRK2 mutation in human iPSCs links parkinsonian neurodegeneration to ERK-dependent changes in gene expression. Cell Stem Cell. 201; 12(3):354-67.

146. Dimos JT, Rodolfa KT, Niakan KK, Weisenthal LM, Mitsumoto H, Chung W, et al. Induced pluripotent stem cells generated from patients with ALS can be differentiated into motor neurons. Science 2008; 321(5893):1218–1221.

147. Egawa N, Kitaoka S, Tsukita K, Naitoh M, Takahashi K, Yamamoto T, et al. Drug screening for ALS using patient-specific induced pluripotent stem cells. Sci Transl Med. 2012; 4 (145):145ra104.

148. Jeon I, Lee N, Li JY, Park IH, Park KS, Moon J, et al. Neuronal properties, in vivo effects, and pathology of a Huntington's disease patient-derived induced pluripotent stem cells. Stem Cells. 2012; 30(9):2054-62.

149. Juopperi TA, Kim WR, Chiang CH, Yu H, Margolis RL, Ross CA, et al. Astrocytes generated from patient induced pluripotent stem cells recapitulate features of Huntington's disease patient cells. Mol Brain. 2012; 5:17.

150. Chang T, Zheng W, Tsark W, Bates S, Huang H, Lin RJ, et al. Brief report: phenotypic rescue of induced pluripotent stem cell-derived motoneurons of a spinal muscular atrophy patient. Stem Cells. 2011; 29(12):2090-3.

151. Ricciardi S, Ungaro F, Hambrock M, Rademacher N, Stefanelli G, Brambilla D, et al. CDKL5 ensures excitatory synapse stability by reinforcing NGL-1-PSD95 interaction in the postsynaptic compartment and is impaired in patient iPSC-derived neurons. Nat Cell Biol. 2012; 14(9):911-23.

152. Ananiev G, Williams EC, Li H, Chang Q. Isogenic pairs of wild type and mutant induced pluripotent stem cell (iPSC) lines from Rett syndrome patients as in vitro disease model. PLoS One. 2011; 6(9):e25255.

153. Nayler S, Gatei M, Kozlov S, Gatti RA, Mar JC, Wells CA, et al. Induced pluripotent stem cells from ataxia-telangiectasia recapitulate the cellular phenotype. Stem Cells Transl Med. 2012; 1(7):523-35.

154. Lee P, Martin NT, Nakamura K, Azghadi S, Amiri M, Ben-David U, et al. SMRT compounds abrogate cellular phenotypes of ataxia telangiectasia in neural derivatives of patient-specific hiPSCs. Nat Commun. 2013; 4:1824.

155. Okita K, Matsumura Y, Sato Y, Okada A, Morizane A, Okamoto S, et al. A more efficient method to generate integration-free human iPS cells. Nat Methods. 2011; 8(5):409-12.

156. Yoshida Y, Takahashi K, Okita K, Ichisaka T, Yamanaka S. Hypoxia enhances the generation of induced pluripotent stem cells. Cell Stem Cell. 2009; 5(3):237-41.

157. Itskovitz-Eldor J, Schuldiner M, Karsenti D, Eden A, Yanuka O, Amit M, et al. Differentiation of human embryonic stem cells into embryoid bodies compromising the three embryonic germ layers. Mol Med. 2000; 6(2):88-95.

158. Wilson PG, Stice SS. Development and differentiation of neural rosettes derived from human embryonic stem cells. Stem Cell Rev. 2006; 2(1):67-77.

159. Santilli G, Lamorte G, Carlessi L, Ferrari D, Rota Nodari L, Binda E, et al. Mild hypoxia enhances proliferation and multipotency of human neural stem cells. PLoS One. 2010; 5(1):e8575.

160. Calini V, Urani C, Camatini M. Comet assay evaluation of DNA single- and double-strand breaks induction and repair in C3H10T1/2 cells. Cell Biol Toxicol. 2002;18(6):369-79.

161. Alagoz M, Chiang SC, Sharma A, El-Khamisy SF. ATM deficiency results in accumulation of DNA-topoisomerase I covalent intermediates in neural cells. PLoS One. 2013; 8(4):e58239.

162. Frosina G, Cappelli E, Ropolo M, Fortini P, Pascucci B, Dogliotti E. In vitro base excision repair assay using mammalian cell extracts. Methods Mol Biol. 2006; 314:377-96.

163. Matsumoto Y, Kim K, Bogenhagen DF. Proliferating cell nuclear antigen-dependent abasic site repair in Xenopus laevis oocytes: an alternative pathway of base excision DNA repair. Mol Cell Biol. 1994; 14(9):6187-97.

164. Kiianitsa K, Maizels N. A rapid and sensitive assay for DNA-protein covalent complexes in living cells. Nucleic Acids Res. 2013; 41(9):e104.

165. Verpelli C, Carlessi L, Bechi G, Fusar Poli E, Orellana D, Heise C et al. Comparative neuronal differentiation of self-renewing neural progenitor cell lines obtained from human induced pluripotent stem cells. Front Cell Neurosci 2013; 7: 175.

166. Benitez-Bribiescal L, Sanchez-Suarez P. Oxidative damage, bleomycin, and gamma radiation induce different types of DNA strand breaks in normal lymphocytes and thymocytes: a comet assay study. Ann. N Y Acad Sci. 1999; 887: 133–149.

167. Löbrich M, Shibata A, Beucher A, Fisher A, Ensminger M, Goodarzi AA, et al. GammaH2AX foci analysis for monitoring DNA double-strand break repair: strengths, limitations and optimization. Cell Cycle. 2010; 9(4):662-9.

168. Xu G, Herzig M, Rotrekl V, Walter CA. Base excision repair, aging and health span. Mech Ageing Dev. 2008; 129: 366–382.

169. Hegde ML, Hegde PM, Rao KS, Mitra S. Oxidative genome damage and its repair in neurodegenerative diseases: function of transition metals as a double-edged sword. J Alzheimers Dis. 2011; 24(Suppl 2): 183–198.

170. Sykora P, Yang JL, Ferrarelli LK, Tian J, Tadokoro T, Kulkarni A et al. Modulation of DNA base excision repair during neuronal differentiation. Neurobiol Aging. 2013; 34: 1717–1727.

171. Minuzzo M, Marchini S, Broggini M, Faircloth G, D'Incalci M, Mantovani R. Interference of transcriptional activation by the antineoplastic drug ecteinascidin-743. Proc Natl Acad Sci USA. 2000; 97: 6780–6784.

172. McCarthy S, Somayajulu M, Sikorska M, Borowy-Borowski H, Pandey S. Paraquat induces oxidative stress and neuronal cell death; neuroprotection by water-soluble coenzyme Q10. Toxicol Appl Pharmacol. 2004; 201: 21–31.

173. Shiloh Y. ATM and related protein kinases: safeguarding genome integrity. Nat Rev Cancer. 2003; 3(3):155-68.

174. Momcilović O, Choi S, Varum S, Bakkenist C, Schatten G, Navara C. Ionizing radiation induces ataxia telangiectasia mutated-dependent checkpoint signaling and G(2) but not G(1) cell cycle arrest in pluripotent human embryonic stem cells. Stem Cells. 2009; 27(8):1822-35.

175. Momcilović O, Knobloch L, Fornsaglio J, Varum S, Easley C, Schatten G. DNA damage responses in human induced pluripotent stem cells and embryonic stem cells. PLoS One 2010; 5: e13410.

176. Qiang L, Fujita R, Abeliovich A. Remodeling neurodegeneration: somatic cell reprogramming-based models of adult neurological disorders. Neuron. 2013; 78(6): 957-69.

177. Woodbine L, Brunton H, Goodarzi AA, Shibata A, Jeggo PA. Endogenously induced DNA double strand breaks arise in heterochromatic DNA regions and require ataxia telangiectasia mutated and Artemis for their repair. Nucleic Acids Res. 2011; 39: 6986–6997.

178. Lee Y, Chong MJ, McKinnon PJ. Ataxia telangiectasia mutated-dependent apoptosis after genotoxic stress in the developing nervous system is determined by cellular differentiation status. J Neurosci. 2001; 21: 6687–6693.

179. Chou WC, Wang HC, Wong FH, Ding SL, Wu PE, Shieh SY et al. Chk2-dependent phosphorylation of XRCC1 in the DNA damage response promotes base excision repair. EMBO J. 2008; 27: 3140–3150.

180. Suraweera A, Becherel OJ, Chen P, Rundle N, Woods R, Nakamura J et al. Senataxin, defective in ataxia oculomotor apraxia type 2, is involved in the defense against oxidative DNA damage. J Cell Biol. 2007; 177: 969–979.

181. Tian B, Yang Q, Mao Z. Phosphorylation of ATM by Cdk5 mediates DNA damage signalling and regulates neuronal death. Nat Cell Biol. 2009; 11: 211–218.

182. Solier S, Ryan MC, Martin SE, Varma S, Kohn KW, Liu H et al. Transcription poisoning by Topoisomerase I is controlled by gene length, splice sites, and miR-142-3p. Cancer Res. 2013; 73: 4830–4839.

183. Glass D, Vinuela A, Davies MN, Ramasamy A, Parts L, Knowles D et al. Gene expression changes with age in skin, adipose tissue, blood and brain. Genome Biol. 2013; 14: R75.

184. Berchtold NC, Coleman PD, Cribbs DH, Rogers J, Gillen DL, Cotman CW. Synaptic genes are extensively downregulated across multiple brain regions in normal human aging and Alzheimer's disease. Neurobiol Aging. 2013; 34: 1653–1661.

185. Lu T, Pan Y, Kao SY, Li C, Kohane I, Chan J et al. Gene regulation and DNA damage in the ageing human brain. Nature. 2004; 429: 883–891.

186. Abdelalim EM. Molecular mechanisms controlling the cell cycle in embryonic stem cells. Stem Cell Rev. 2013; 9: 764–773.

187. Momcilović O, Navara C, Schatten G. Cell cycle adaptations and maintenance of genomic integrity in embryonic stem cells and induced pluripotent stem cells. Results Probl Cell Differ 2011; 53: 415–458.

188. Tichy ED, Pillai R, Deng L, Liang L, Tischfield J, Schwemberger SJ et al. Mouse embryonic stem cells, but not somatic cells, predominantly use homologous recombination to repair double-strand DNA breaks. Stem Cells Dev. 2010; 19: 1699–1711.

189. Jongkamonwiwat N, Noisa P. Biomedical and clinical promises of human pluripotent stem cells for neurological disorders. Biomed Res Int. 2013; 2013:656531.

190. Barzilai A. The neuro-glial-vascular interrelations in genomic instability symptoms. Mech. Ageing Dev. 2011; 132(8): 395-404.

191. Baltanás FC, Casafont I, Lafarga V, Weruaga E, Alonso JR, Berciano MT, et al. Purkinje cell degeneration in pcd mice reveals large scale chromatin reorganization and gene silencing linked to defective DNA repair. J Biol Chem. 2011; 286:28287-302.

192. Tzur-Gilat A, Ziv Y, Mittelman L, Barzilai A, Shiloh Y. Studying the cerebellar DNA damage response in the tissue culture dish. Mech Ageing Dev. 2013; 134:496-505.

193. Takahashi T, Burguiere-Slezak G, Van der Kemp PA, Boiteux S. Topoisomerase 1 provokes the formation of short deletions in repeated sequences upon high transcription in Saccharomyces cerevisiae. Proc Natl Acad Sci U S A. 2011; 108:692-7.

194. Fong YW, Cattoglio C, Tjian R. The intertwined roles of transcription and repair proteins. Mol Cell. 2013; 52:291-302.

195. Depken M, Parrondo JM, Grill SW. Intermittent transcription dynamics for the rapid production of long transcripts of high fidelity. Cell Rep. 2013; 5:521-30.

196. Duchen MR. Mitochondria, calcium-dependent neuronal death and neurodegenerative disease. Pflugers Arch. 2012; 464:111-21.

197. Chen P, Peng C, Luff J, Spring K, Watters D, Bottle S, et al. Oxidative stress is responsible for deficient survival and dendritogenesis in Purkinje neurons from ataxia-telangiectasia mutated mutant mice. J Neurosci. 2003; 23:11453-60.

198. Yan J, Khanna KK, Lavin MF. Defective radiation signal transduction in ataxia-telangiectasia cells. Int J Radiat Biol. 2000; 76:1025-35.

199. Gugger OS, Kapfhammer JP. Reduced size of the dendritic tree does not protect Purkinje cells from excitotoxic death. J Neurosci Res. 2010; 88:774-83.

200. Muguruma K, Nishiyama A, Ono Y, Miyawaki H, Mizuhara E, Hori S, et al. Ontogeny-recapitulating generation and tissue integration of ES cell-derived Purkinje cells. Nat Neurosci. 2010; 13:1171-80.

201. Leto K, Rolando C, Rossi F. The genesis of cerebellar GABAergic neurons: fate potential and specification mechanisms. Front Neuroanat. 2012; 6:6.

202. Muguruma K, Sasai Y. In vitro recapitulation of neural development using embryonic stem cells: from neurogenesis to histogenesis. Dev Growth Differ. 2012; 54:349-57.

203. Magrassi L. Vision-guided technique for cell transplantation and injection of active molecules into rat and mouse embryos. Methods Mol Biol. 2002; 198: 327-40.

Publications in International ISI Journals

Related to the project:

Carlessi L, Fusar Poli E, Bechi G, Mantegazza M, Pascucci B, Narciso L, Dogliotti E, Sala C, Verpelli C, Lecis D, Delia D. Functional and molecular defects of hiPSC-derived neurons from patients with ATM deficiency. Cell Death Dis. 2014; 5:e1342.

Carlessi L, Fusar Poli E, Delia D. Brain and induced pluripotent stem cell-derived neural stem cells as an in vitro model of neurodegeneration in ataxia-telangiectasia. Exp Biol Med (Maywood). 2013; 238(3):301-7.

Carlessi L, Fusar Poli E, De Filippis L, Delia D. ATM-deficient human neural stem cells as an in vitro model system to study neurodegeneration. DNA Repair. 2013; 12(8):605-11.

Verpelli C, Carlessi L, Bechi G, Fusar Poli E, Orellana D, Heise C, Franceschetti S, Mantegazza R, Mantegazza M, Delia D, Sala C. Comparative neuronal differentiation of self-renewing neural progenitor cell lines obtained from human induced pluripotent stem cells. Front Cell Neurosci. 2013; 7:175.

Non-related to the project:

Fusar Poli E, Zalfa C, D'Avanzo F, Tomanin R, Carlessi L, Bossi M, Nodari LR, Binda E, Marmiroli P, Scarpa M, Delia D, Vescovi AL, De Filippis L. Murine neural stem cells model Hunter disease in vitro: glial cell-mediated neurodegeneration as a possible mechanism involved. Cell Death Dis. 2013; 4:e906.

OPEN

Citation: Cell Death and Disease (2014) 5, e1342; doi:10.1038/cddis.2014.310

www.nature.com/cddis

Functional and molecular defects of hiPSC-derived neurons from patients with ATM deficiency

L Carlessi[1], E Fusar Poli[1], G Bechi[2], M Mantegazza[2,3], B Pascucci[4], L Narciso[5], E Dogliotti[6], C Sala[7], C Verpelli[7], D Lecis[1] and D Delia*[,1]

Loss of ataxia telangiectasia mutated (ATM) kinase, a key factor of the DNA damage response (DDR) pathway, causes the cancer predisposing and neurodegenerative syndrome ataxia-telangiectasia (A-T). To investigate the mechanisms of neurodegeneration, we have reprogrammed fibroblasts from ATM-null A-T patients and normal controls to pluripotency (human-induced pluripotent stem cells), and derived from these neural precursor cells able to terminally differentiate into post-mitotic neurons positive to $>90\%$ for β-tubulin III$+$/microtubule-associated protein 2$+$. We show that A-T neurons display similar voltage-gated potassium and sodium currents and discharges of action potentials as control neurons, but defective expression of the maturation and synaptic markers SCG10, SYP and PSD95 (postsynaptic density protein 95). A-T neurons exhibited defective repair of DNA double-strand breaks (DSBs) and repressed phosphorylation of ATM substrates (e.g., γH2AX, Smc1-S966, Kap1-S824, Chk2-T68, p53-S15), but normal repair of single-strand breaks, and normal short- and long-patch base excision repair activities. Moreover, A-T neurons were resistant to apoptosis induced by the genotoxic agents camptothecin and trabectedin, but as sensitive as controls to the oxidative agents. Most notably, A-T neurons exhibited abnormal accumulation of topoisomerase 1-DNA covalent complexes (Top1-ccs). These findings reveal that ATM deficiency impairs neuronal maturation, suppresses the response and repair of DNA DSBs, and enhances Top1-cc accumulation. Top1-cc could be a risk factor for neurodegeneration as they may interfere with transcription elongation and promote transcriptional decline.
Cell Death and Disease (2014) **5,** e1342; doi:10.1038/cddis.2014.310; published online 17 July 2014

Ataxia-telangiectasia (A-T) is a pleiotropic disorder with predisposition to cancer and early onset neurodegeneration as key features.[1–3] The neuropathological abnormalities in A-T include progressive loss of cerebellar Purkinje and granule neurons, less pronounced degeneration of the bulbar olivae in the brainstem and mild loss of myelinated fibers in corticospinal and spinocerebellar tracts.[4] A-T is caused by germline mutations inactivating the ataxia telangiectasia mutated (ATM) protein kinase, which has an apical role in the DNA damage response (DDR) to double-strand breaks (DSBs). Upon activation by DSBs, ATM phosphorylates a plethora of substrates implicated in cell cycle arrest, DNA processing and repair, chromatin remodeling, transcription and apoptosis.[1] Concordant with the role of ATM in the DDR, the neurodegenerative phenotype in A-T has been attributed to a defective DDR in pre- and post-mitotic neurons and ensuing accumulation of genotoxic lesions. However, the fact that cells from A-T patients and specimens from ATM knock-out mice exhibit increased signatures of oxidative stress,[5,6] together with the discovery that ATM senses and responds to reactive oxygen species (ROS) through formation of active, disulfide-cross-linked ATM dimers[7] suggest that the loss of redox balance may contribute to neurodegeneration in A-T.

In neurons, a fraction of ATM is localized in the cytoplasm where it phosphorylates the synaptic proteins VAMP2 and synapsin-1.[8] Recently, ATM has been detected in dendrites and dendritic spines, and its activation by neuronal firing and synaptic activity induces the phosphorylation of proteins essential for neuronal function.[9]

Neurodegeneration in A-T has additionally been linked to epigenetic modifications associated with deregulation of class II histone deacetylase HDAC4[10] and hyperexpression of the histone-lysine *N*-methyltransferase EZH2,[11] altogether inducing transcriptional repression of multiple neuronal genes and cell death.

[1]Department of Experimental Oncology, Fondazione IRCCS Istituto Nazionale dei Tumori, Via Amadeo 42, 20133 Milano, Italy; [2]Department of Neurophysiopathology, Fondazione IRCCS Istituto Neurologico Carlo Besta, Via Amadeo 42, 20133 Milano, Italy; [3]Institute of Molecular and Cellular Pharmacology (IPMC) CNRS UMR7275 and University of Nice-Sophia Antipolis, 660 Route des Lucioles, 06560 Valbonne, France; [4]CNR Institute of Crystallography, Via Salaria, Km. 29.300, 00016 Monterotondo Scalo, Roma, Italy; [5]Department of Food Safety and Veterinary Public Health, Istituto Superiore di Sanità, Viale Regina Elena 299, 00161 Roma, Italy; [6]Department of Environment and Primary Prevention, Istituto Superiore di Sanità, Viale Regina Elena 299, 00161 Roma, Italy and [7]CNR Institute of Neuroscience and Department of Biotechnology and Translational Medicine, Via Vanvitelli 32, 20129 Milano, Italy

*Corresponding author: D Delia, Department of Experimental Oncology, Fondazione IRCCS Istituto Nazionale dei Tumori, Via Amadeo 42, Milano 20133, Italy. Tel: +39 02 23902641; Fax: +39 02 23902764; E-mail: domenico.delia@istitutotumori.mi.it

Abbreviations: ATM, ataxia telangiectasia mutated; Chk2, checkpoint kinase 2; SSEA4, stage-specific embryonic antigen 4; α-SMA, α-smooth muscle actin; MAP2, microtubule-associated protein 2; PARP, poly (ADP ribose) polymerase; GABA, γ-aminobutyric acid; PSD95, discs large homolog 4; VGAT, vesicular GABA transporter; KChIP, Kv channel-interacting protein 1; GFAP, glial fibrillary acidic protein; XRCC1, X-ray repair cross-complementing 1; CPT, camptothecin; DAPI, 4′,6-diamidin-2-fenilindolo; APE1, apurinic/apyridinic endonuclease 1; Pol-β, DNA polymerase β; bFGF, basic fibroblast growth factor; EGF, epidermal growth factor; NPCs, neural precursor cells; hiPSCs, human-induced pluripotent stem cells; DDR, DNA damage response; DSBs, double-strand breaks; Top1-cc, topoisomerase 1-DNA covalent complexes; IR, ionizing radiation

Received 24.3.14; revised 30.5.14; accepted 16.6.14; Edited by A Verkhratsky

It should be noted that germline mutations in *ATM* severely impair glial cell functionality and vascular integrity, suggesting that Purkinje cell death and cerebellar degeneration in A-T may result from a dysfunctional neuro-astro-vascular unit.[12]

In summary, several factors are implicated in the neurodegenerative phenotype of A-T, but which of them has the most crucial role is still unresolved, primarily because of the unavailability of model systems able to recapitulate the neurological disease. In this regard, ATM knockout mice do not manifest the progressive ataxia seen in A-T nor the loss of cerebellar Purkinje cells.[13]

The reprogramming of human somatic cells into induced pluripotent stem cells (human-induced pluripotent stem cell (hiPSCs)) by the introduction of pluripotency factors (Oct4/Klf4/Sox2/cMyc) represents a prominent advance in stem cell biology, owing to the capacity of these cells to differentiate to virtually any cell type of the human body, and the possibility to model patient- and allele-specific genetic diseases.[14] In the case of A-T, the establishment of hiPSCs and conversion to functional neurons has been recently reported.[15–17]

In this study, we performed a previously undocumented functional and molecular analysis of hiPSC-derived A-T neuronal cells harboring patient-specific mutations, in order to shed light on the causes of the neuropathology in A-T.

Results

Generation and characterization of hiPSCs derived from A-T and Ctrl fibroblasts. The hiPSC lines were established from primary fibroblasts of two unrelated A-T patients and a healthy control (Ctrl), as detailed in Materials and methods section. Colonies with embryonic stem cell-like morphology were expanded on a mouse embryonic fibroblast (MEF) feeder layer (Figure 1a, left). Western blot analysis revealed, as expected, a positive signal for ATM in fibroblasts and hiPSCs from Ctrl but not from A-T cases (Figure 1a, right). No ATM protein was detectable in MEFs as the antibody used was human specific. Furthermore, only Ctrl and A-T hiPSC lines expressed the pluripotency marker Oct3/4, but not fibroblasts or MEFs (Figure 1a, right). Immunofluorescence analysis attested the pluripotency of the hiPSCs, being positive for Oct3/4, stage-specific embryonic antigen 4 (SSEA4) and Tra-1-81 (Figure 1b). Moreover, the hiPSCs gave rise to the embryonic derivatives ectoderm, endoderm and mesoderm, labeled positive for β-tubulin III, Sox17 and alpha-smooth muscle actin (α-SMA), respectively (Figure 1c). Also, through embryoid body (EB) and neural rosette formation and subsequent culture in a mitogen-free medium, hiPSCs differentiated into β-tubulin III+ and

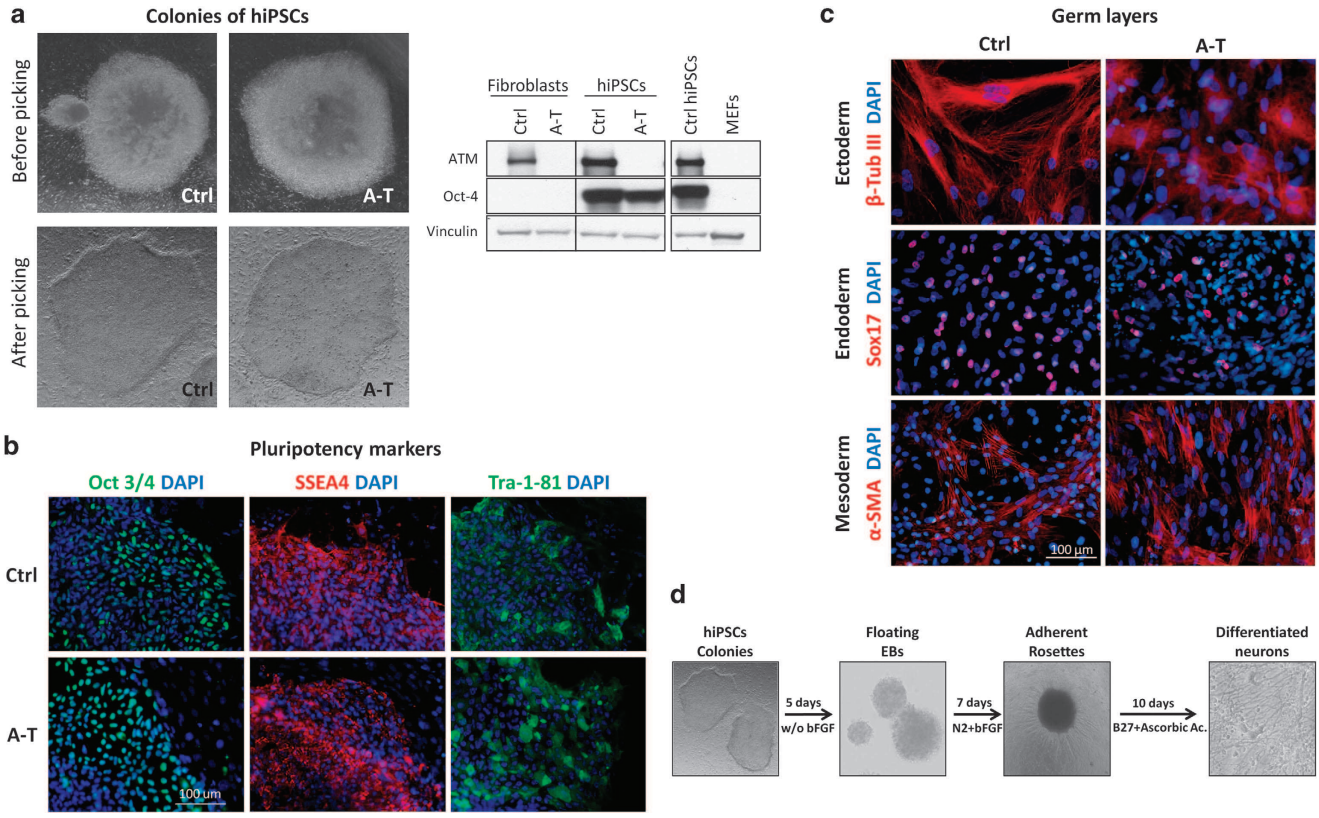

Figure 1 Generation, characterization, pluripotency validation and neuronal differentiation of hiPSC colonies from Ctrl and A-T patients. Representative images of newly formed hiPSC colonies before picking (**a,** upper panel) and after picking (**a,** bottom panel). The hiPSC colonies were characterized by western blot (**a,** right) to evaluate the expression of ATM protein and the pluripotency marker Oct 3/4 and were compared with primary fibroblasts and MEF feeders. Vinculin was used as a loading control. In **b**, hiPSC colonies were labeled to visualize the expression of the pluripotency markers Oct 3/4, SSEA4 and TRA-1-81. Nuclei were counterstained with DAPI (blue). In **c**, Ctrl and A-T hiPSCs were differentiated *in vitro* into the three germ layers. After 20 days of differentiation, cells were labeled with antibodies specific for α-SMA (mesoderm marker), Sox17 (endoderm marker) and β-tubulin III (ectoderm marker). Nuclei were counterstained with DAPI (blue). The ability of hiPSCs to generate neuronal cells was confirmed through the formation of floating EBs and rosette formation. Representative images for each differentiation step are shown in **d**

microtubule-associated protein 2+ (MAP2+) neurons (Figure 1d and Supplementary Figure 1).

Generation of hNPCs and neurons from A-T and Ctrl hiPSCs. Proliferating human neural precursor cells (hNPCs) were generated as depicted in Figure 2a. Both Ctrl and A-T hNPCs were negative for the pluripotency markers Tra-1-81 and Oct3/4 (Figure 2b, left) but positive for the neural precursor markers Sox2, Nestin and Vimentin, and for the proliferation marker Ki67 (Figure 2b, right). On western blots, hNPCs showed lower expression of Tra-1-81 and Oct3/4 than hiPSCs, and higher levels of Sox2 and Nestin, which then decreased during neuronal differentiation (Figure 2b, bottom left).

The capacity of hNPCs to activate the DDR was investigated in response to ionizing radiation (IR), which induces DSBs and ATM signalling.[1] Using phospho-specific antibodies for the indicated substrates of ATM and checkpoint kinase 2 (Chk2; KAP1-pS473), we found that after 15–30 min of IR these molecules were strongly phosphorylated in Ctrl but not in A-T hNPCs (Figure 2c). Interestingly, after IR an accumulation of cleaved poly (ADP ribose) polymerase

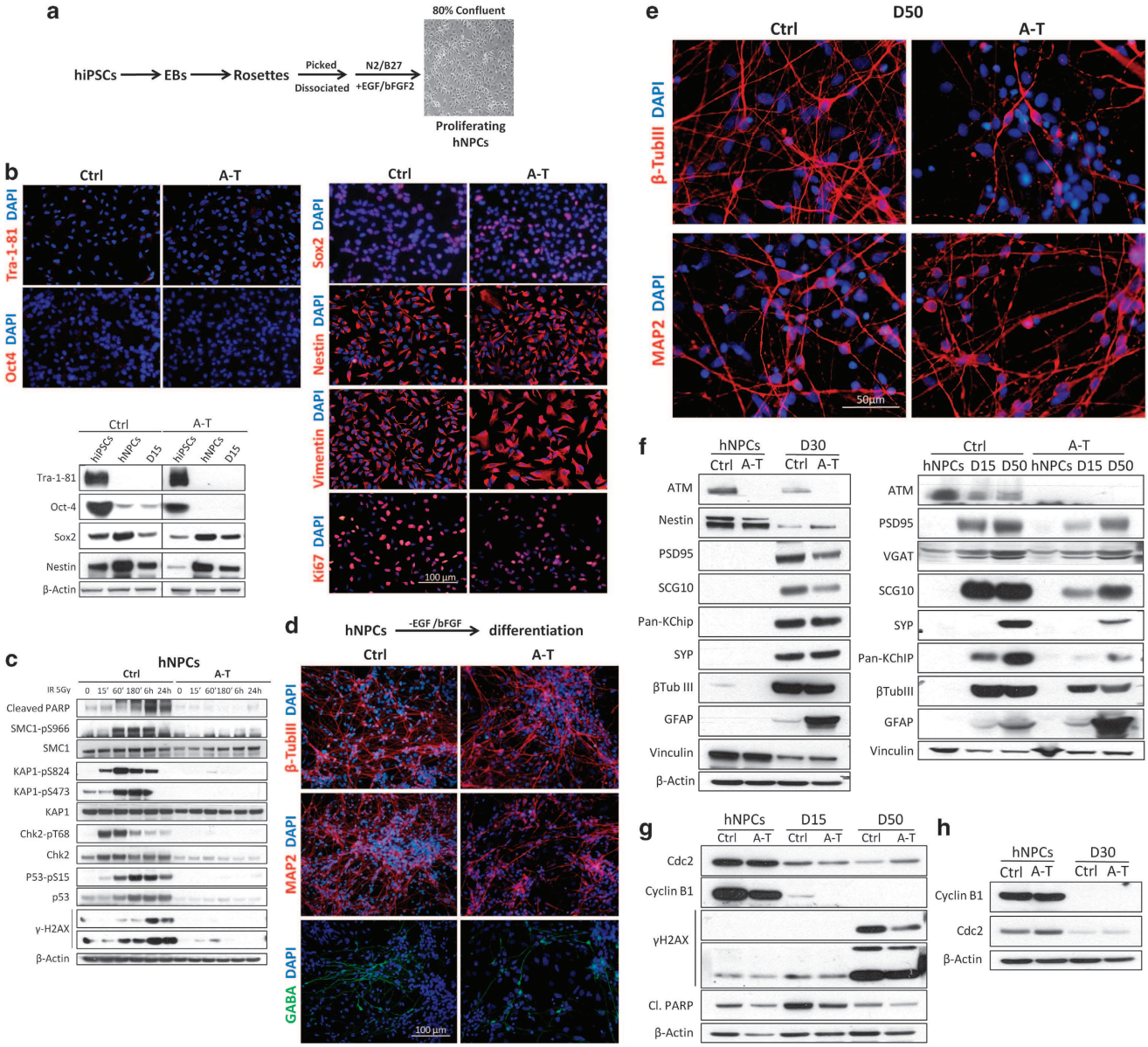

Figure 2 Generation of hNPCs from Ctrl and A-T hiPSCs. To obtain stable and proliferating hNPCs, we followed the protocol depicted in **a** and a representative image of the cell culture obtained is shown. In **b**, the characterization of the hNPCs by immunofluorescence demonstrates the loss of the pluripotency markers Tra-1-81 and Oct3/4, the expression of neural markers (Sox2, Nestin and Vimentin) and the proliferation ability (Ki67). A comparative analysis between hiPSCs and proliferating (hNPCs) and differentiated (D15) hNPCs was performed by western blot. In **c**, proliferating hNPCs were exposed to IR (5 Gy), and the time-dependent DDR activation was evaluated by analyzing the phosphorylation of the indicated ATM substrates, and of cleaved PARP. β-Actin was used as a loading control. The real capacity of hNPCs to differentiate into neurons is shown in **d**, where a high number of MAP2+, β-tubulin III+ and GABA+ cells are detected at D15 and D50 (**e**). hNPCs and neurons at 15–30 or 50 days of differentiation were collected and analyzed by western blot for the expression of differentiation and maturation markers (**f**) or for the indicated proteins (**g** and **h**)

(PARP), a marker of apoptosis, was detected in Ctrl but not in A-T hNPCs, suggesting that ATM deficiency confers radioresistance in proliferative cells (Figure 2c). When hNPCs were induced to differentiate, they acquired a neuronal-like morphology and at day 15 of differentiation (D15) were positive for β-tubulin III or MAP2, with a fraction of cells also expressing the marker of inhibitory neurons γ-aminobutyric acid (GABA; Figure 2d), which we were no longer able to detect at D50 in mature neuronal cells[18] expressing β-tubulin III or MAP2 (Figure 2e). Western blot analysis confirmed the downregulation of the stem cell marker Nestin, the upregulation of the neuronal marker β-tubulin III at D30 (Figure 2f, left) and at D15 and D50 (Figure 2f, right), and the expression of the postsynaptic marker PSD95 postsynaptic density protein 95, the inhibitory synapse marker vesicular GABA transporter (VGAT), the neuronal growth-associated protein SCG10 and the potassium channel-interacting proteins (KChIPs). At D30 and D50, but not D15, cells also expressed the pre-synaptic marker Synaptophysin (SYP). We detected no obvious differences between Ctrl and A-T hNPCs concerning the generation of neuronal cells, but A-T neurons displayed deficits in the expression of SYP and PSD95 as well as of SCG10 and KChIP, and higher amounts of glial fibrillary acidic protein (GFAP; Figure 2f).

The post-mitotic status of the differentiated cells was confirmed by the downregulation in D15–D50 (Figure 2h) and D30 samples (Figure 2g) of Cdc2 and cyclin B1. Concordant with our previous results,[19] cleaved poly (ADP ribose) polymerase (PARP) was higher in Ctrl than in A-T neuronal cells. To note, γH2AX (pS139) was also highly expressed at D50, and its levels were lower in A-T than in Ctrl cells (Figure 2g).

Electrophysiological characterization. Ctrl and A-T neurons at D53 $\pm$ 6 were analyzed by whole-cell patch clamp recordings in order to verify their functional maturation. Voltage clamp experiments showed similar voltage-gated potassium currents (Figure 3a) and, most importantly, voltage-gated sodium currents, selectively blocked by tetrodotoxin (TTX), which is a specific feature of mature neurons (Figure 3a, left panel). Transient peak sodium inward currents had similar amplitude in Ctrl and A-T neurons: maximal peak current density was 84.9 $\pm$ 19.6 pA/pF, $n = 10$ in Ctrl neurons, 82.7 $\pm$ 13.5 pA/pF, $n = 13$ in A-T neurons (Figure 3b). Moreover, current clamp experiments showed that both Ctrl and A-T neurons could generate discharges of action potentials in response to injection of depolarizing current steps (Figure 3c). Finally, to determine whether neurons developed functional synapses, we performed voltage clamp experiments for recording spontaneous excitatory and inhibitory postsynaptic currents (sEPSCs and sIPSCs). Both Ctrl and A-T neurons exhibited sEPSCs (Figure 3d) with similar frequencies (0.02 $\pm$ 0.01 Hz, $n = 4$ cells and 0.03 $\pm$ 0.02 Hz, $n = 4$ cells, respectively), which were blocked by application of kynurenic acid (3 mM; data not shown), but no sIPSCs (Figure 3e).

DNA damage-induced G1/S checkpoint in relation to development stage. In somatic cells, ATM mediates the G1/S checkpoint but is inactive in ESCs and iPSCs.[20,21] To further delineate this activity in relation to the developmental stage, we analyzed the cell cycle profile of primary fibroblast, hiPSCs, hNPCs and terminally differentiated neurons by flow cytometry before and 24 h after IR treatment (Supplementary Figure 2). Primary Ctrl fibroblasts displayed a normal G1/S checkpoint arrest, in contrast to A-T fibroblasts in which this checkpoint defect resulted in a significant increase in the percentage of G2 phase cells (Figure 4a). Notably, not only A-T hiPSCs, but also Ctrl hiPSCs lacked the G1/S checkpoint although, interestingly, Ctrl hNPCs regained it, whereas A-T hNPCs maintained this defect. The analysis of neurons at D30 revealed that all cells were in the G0/G1 phase and this condition was not perturbed 24 h after IR.

To better understand the implication of DDR proteins in the regulation of cell cycle arrest in fibroblasts, hiPSCs and hNPCs, Ctrl cells were harvested at the indicated time points after treatment with 5 Gy IR (Figure 4b) and the expression of ATM-pS1981, p53-pS15, CDC25A and p21^{waf1} was analyzed. Interestingly, although all cell types proficiently activated ATM and induced the accumulation of p53, hiPSCs were unable to induce p21^{waf1}, and did not express CDC25A. This could explain the incapacity of hiPSCs to regulate the cell cycle after DNA damage. We also investigated other DDR proteins such as RAD51, the MRN complex (RAD50-MRE11-NBS1) and X-ray repair cross-complementing 1 (XRCC1), and found changes in expression during the developmental stages, suggesting a different ability to repair DNA damage in the different cell types (Supplementary Figure 3).

Base excision repair capacity in undifferentiated and differentiated hNPCs. In neurons, the base excision repair (BER) pathway is essential to remove oxidative DNA damage and single-strand breaks (SSBs) generated by high levels of ROS, and defects in BER contribute to neurodegeneration.[22–25] To determine how BER is regulated in pre- and post-mitotic neurons, we analyzed the short-patch (SP) and long-patch (LP) BER subpathways.[23] Analysis of SP-BER revealed no significant differences between Ctrl and A-T both in the proliferation and post-mitotic (D15) stage (Figure 5a). To better understand this result, we analyzed the levels of the SP-BER proteins apurinic/apyridinic endonuclease 1 (APE1), DNA polymerase β (Pol-β) and XRCC1, and after differentiation (D15) only the levels of XRCC1 appear reduced (Figure 5c). Similar findings were seen in D30 neurons (data not shown).

LP-BER activity appeared markedly lower in both Ctrl and A-T post-mitotic neurons than in their respective proliferating hNPCs (Figure 5b). This finding is concordant with the reduced expression of Flap endonuclease 1, a protein involved in LP-BER in non-replicating cells (Figure 5c). Overall, these results point out differences that depend on different levels of expression or differential activation of BER enzymes in undifferentiated and differentiated cells, but appear independent of ATM.

DNA damage response and repair in post-mitotic neurons. IR-time course analysis of Ctrl neurons at D30 showed a vigorous ATM-dependent phosphorylation of SMC1-S966, KAP1-S824, Chk2-T68, p53-S15 and γ-H2AX, while this response was repressed in A-T neurons

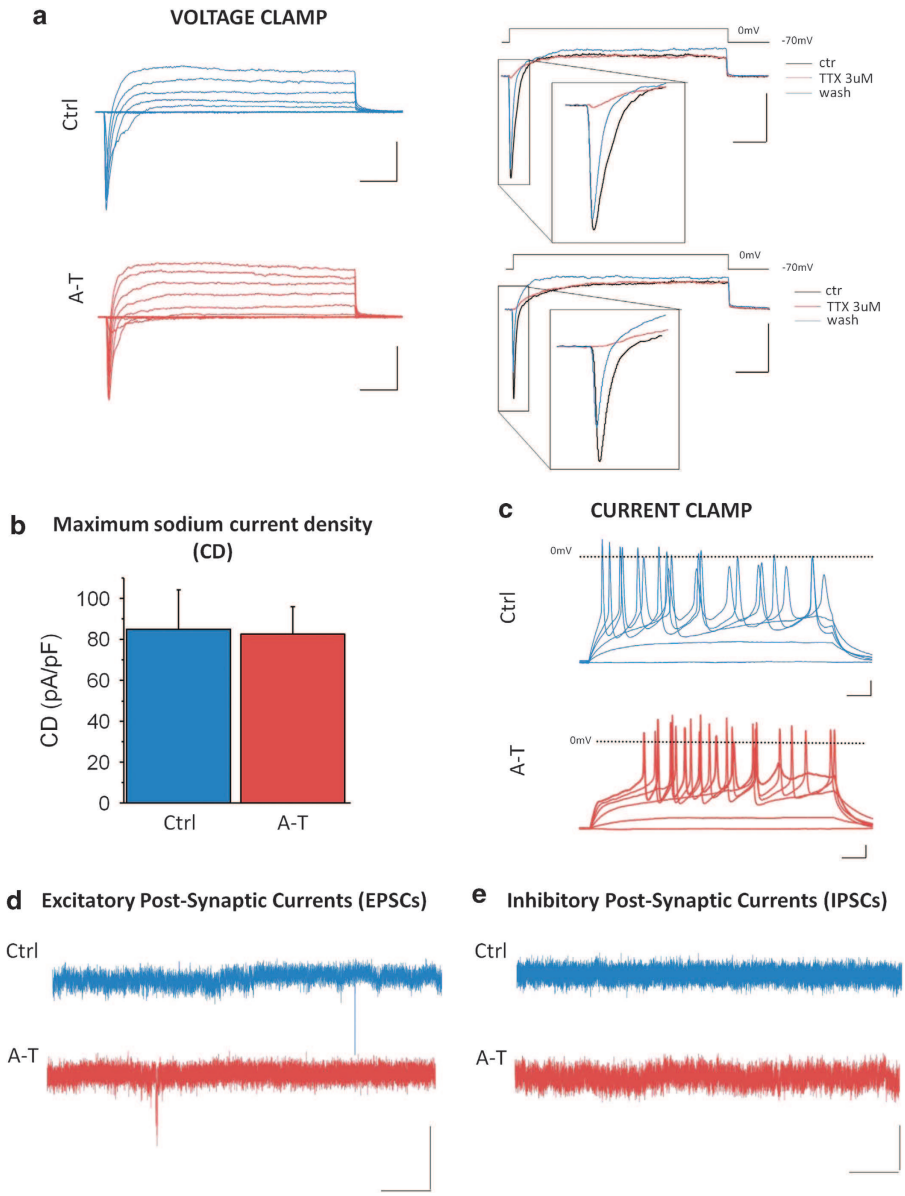

Figure 3 Functional characterization of Ctrl and A-T neurons after 50 days of differentiation. In **a**, left, patch clamp whole-cell recordings of representative total ionic currents elicited with depolarizing voltage steps between –70 and + 10 mV (10 mV increments from a holding potential of –70 mV) in Ctrl and A-T hNP-derived neurons; scale bar: 500 pA, 10 ms. In **a**, right, representative currents elicited with a depolarizing voltage step to − 10 mV in control (black), during perfusion with TTX 3 μM (red) and after washout (blue) in Ctrl (upper panels) and A-T (lower panels) hNP-derived neurons; scale bar: 500 pA, 10 ms. In **b**, bar graph of maximum sodium current densities (CD) in Ctrl and A-T hNPC-derived neurons (no statistical significant difference: unpaired *T*-test). In **c**, representative action potential discharges recorded in current clamp during injections of 1-s long depolarizing current steps from a holding potential of − 70 mV; scale bar: 10 mV, 100 ms. In **d**, traces showing sEPSCs, recorded at the holding potential of − 70 mV, while in **e** traces showing the absence of sIPSCs, recorded at the holding potential of + 30 mV; scale bar: 10 mV, 1 s

(Figure 6a). Similarly, the phosphorylation of the Chk2 substrate KAP1-S473 was abrogated in A-T neurons. Interestingly, as previously described for proliferating hNPCs (Figure 2c), 24 h after IR an accumulation of cleaved PARP was detected in Ctrl but not in A-T neurons, indicating that ATM deficiency confers short-term radio-resistance also in terminally differentiated cells (Figure 6a, upper panel). Altogether, these results indicate that normal post-mitotic neurons activate the DDR as efficiently as their proliferating precursors, and that ATM deficiency ablates this response.

The ability of post-mitotic neurons to repair SSBs and DSBs was investigated with the alkaline and neutral comet assay, respectively. Although the repair of SSBs, induced by hydrogen peroxide (H_2O_2),[26] showed no major differences between Ctrl and A-T post-mitotic neurons (Figure 6b), the repair of DSBs, induced by IR,[26] appeared defective in A-T neurons, which displayed 30% more unrepaired lesions than Ctrl cells (Figure 6c). The latter finding is consistent with a defective DDR, as shown in Figure 6a.

To investigate the role of ATM in the resolution of IR-induced DSBs in D30 neurons, we scored the time-dependent

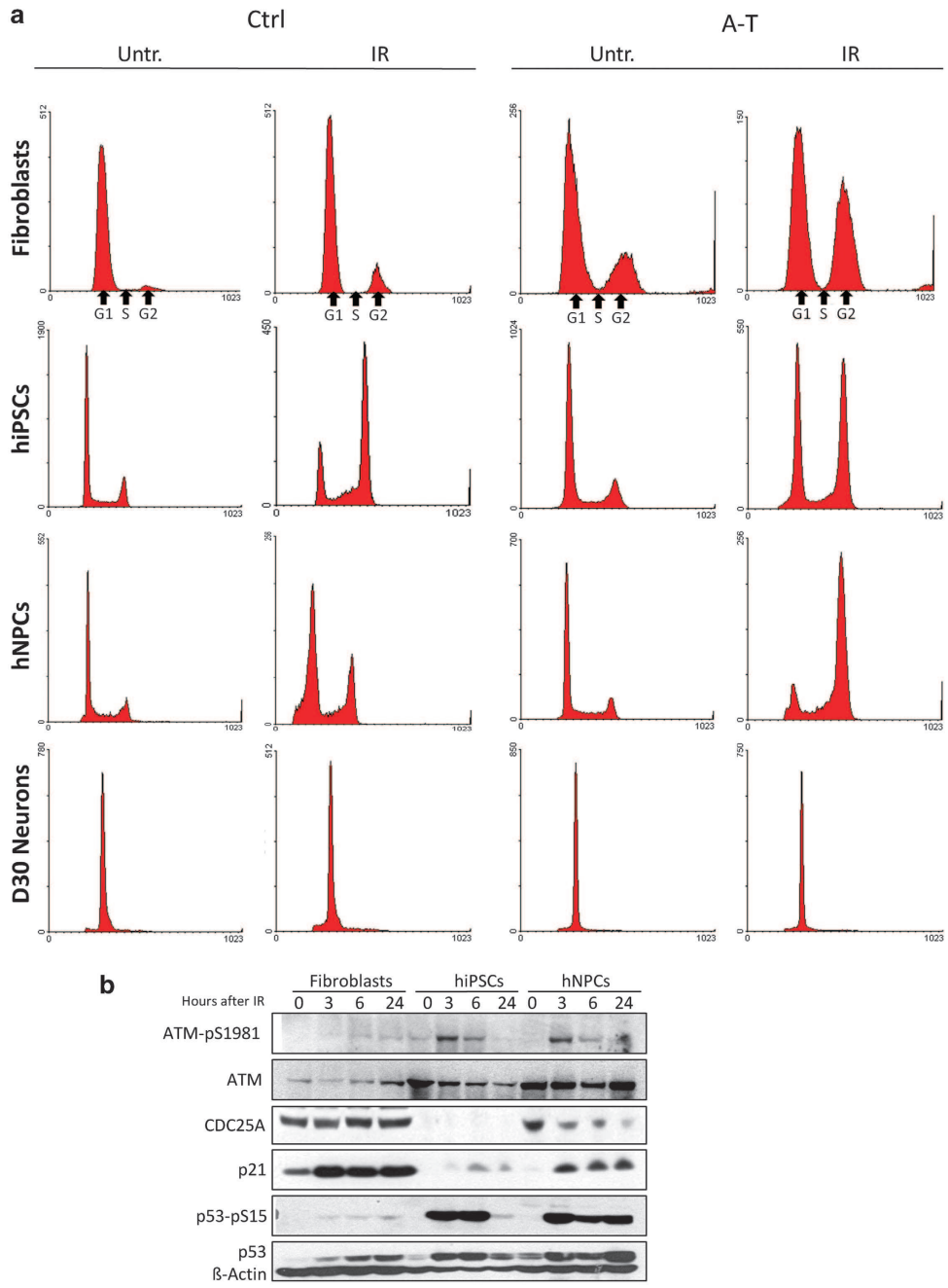

Figure 4 Cell cycle phase distribution changes after IR treatment. Ctrl and A-T cells at various developmental stages (primary fibroblasts, hiPSCs, hNPCs, D30 post-mitotic neurons) were treated with 5 Gy IR, collected after 24 h, and analyzed for DNA content by flow cytometry (**a**). In **b**, Ctrl fibroblasts, hiPSCs and hNPCs were treated with 5 Gy IR, collected at the indicated times and analyzed by western blot. β-Actin was used as a loading control

formation and clearance of γ-H2AX and 53BP1 nuclear foci by immunofluorescence, as described.[27,28] Unirradiated Ctrl D30 neurons showed a basal number of γ-H2AX and 53BP1 foci per cell (1.4 ± 1.2 and 0.9 ± 1), which increased to 13.3 ± 3.3 and 10.1 ± 2.4, respectively, after IR, to decline after 6 h and even further after 24 h (Figures 6d and e). Untreated A-T cells showed a number of foci per cell comparable to Ctrl cells, which increased more modestly, 5.6 ± 2.6 for γ-H2AX and 5.6 ± 2.1 for 53BP1 after 15 min, and persisted after 24 h (Figures 6d and e graphs). These findings indicate that A-T post-mitotic neurons show slower kinetics of DSBs repair than Ctrl, concordant with previous findings in other ATM-deficient cells.[19]

The apoptotic effect of radiation on Ctrl and A-T neurons 24 h after 5 Gy IR was assessed by flow cytometry analysis of the subdiploid DNA peak (Supplementary Figure 4). Fewer apoptotic cells were detected in IR-treated A-T cells (22.2%) than in Ctrl cells (32.3%), suggesting that ATM deficiency attenuates short-term apoptosis, concordant with the findings on cleaved PARP (Figure 6a) and our previous findings.[19,29]

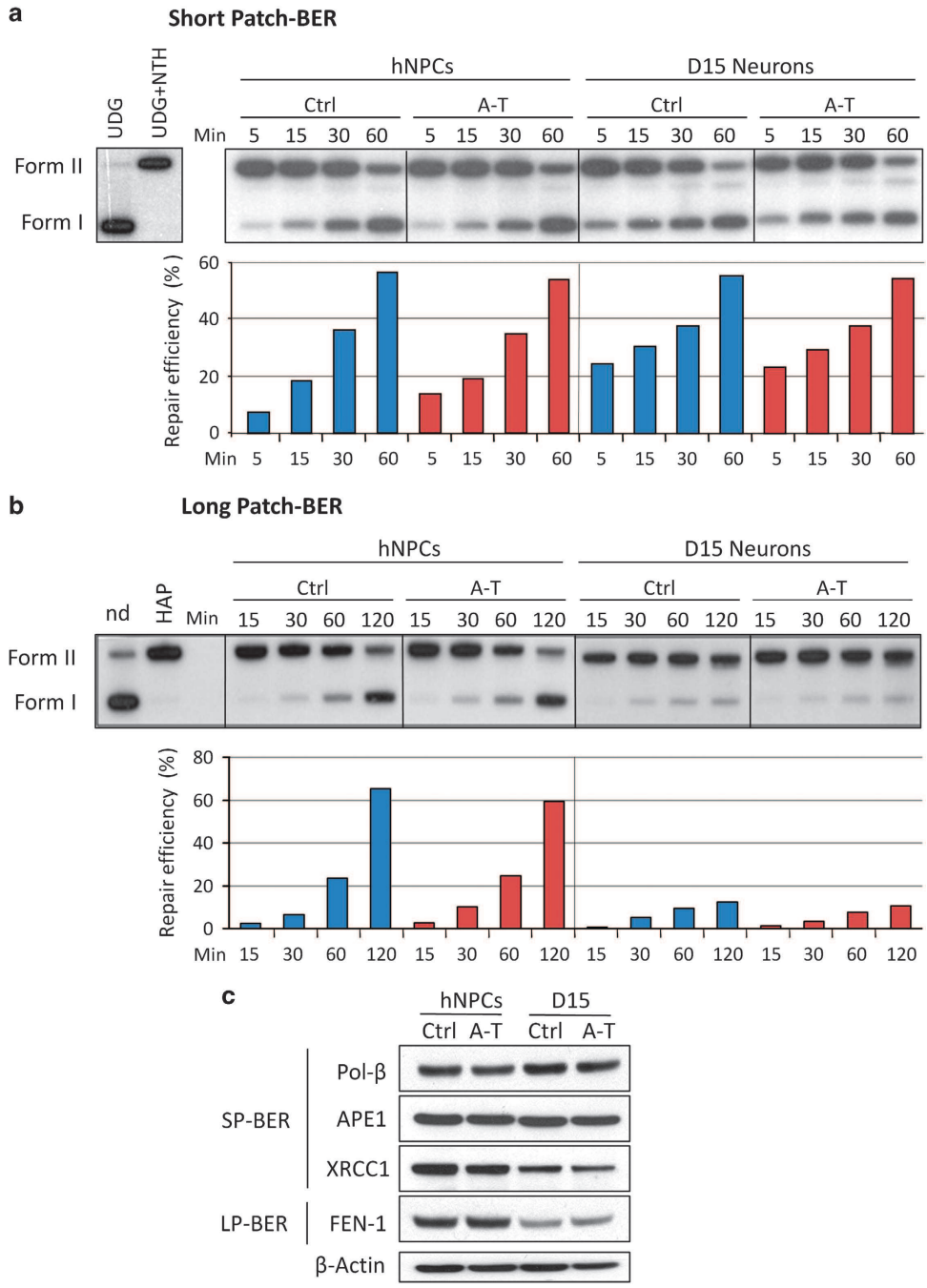

Figure 5 BER activities in proliferating and post-mitotic Ctrl and A-T neuronal cells. *In vitro* repair reactions were performed by using whole-cell extracts and as substrate a 32P-labeled circular plasmid containing a single AP site (pGEM-AP) to measure SP-BER (**a**) or a THF residue (pGEM-THF) for LP-BER (**b**). The correct insertion of a single lesion in the plasmid molecules was checked by digestion with uracil DNA glycosylase (UDG) followed by endonuclease III (NTH) for pGEM-AP (**a**), and by AP endonuclease (HAP1) for pGEM-THF (**b**). Repair kinetics of the AP site (**a**) or THF residue (**b**) by proliferating hNPCs and post-mitotic neurons (D15) were measured following incubation of the single lesion-containing plasmids with extracts from Ctrl or A-T defective neuronal cells for increasing periods of time. Repair products were analyzed by agarose gel electrophoresis and the radioactivity of the bands corresponding to nicked (form II) and supercoiled (form I) plasmids was quantified. Repair efficiency is expressed as relative amount of Form I over total radioactivity in each lane. Blue bar, Ctrl cell extracts; red bar, A-T cell extracts. The expression level of SP-BER and LP-BER proteins was evaluated by western blot in proliferating and post-mitotic neuronal cells (**c**). β-Actin was used as a loading control

Treatment of A-T and Ctrl neuronal cells with genotoxic and oxidative agents. As genotoxic agents and oxidative stress may similarly affect ATM-deficient neurons, we investigated the viability of Ctrl and A-T post-mitotic neurons (D30) upon treatment with compounds that work through different mechanisms: camptothecin (CPT), which inhibits Topoisomerase I (Top1) and traps Top1-DNA covalent complexes (Top1-ccs);[30] trabectedin, which blocks transcription factor activity;[31] Paraquat, which induces ROS through depolarization of the inner mitochondrial membrane,[32] and

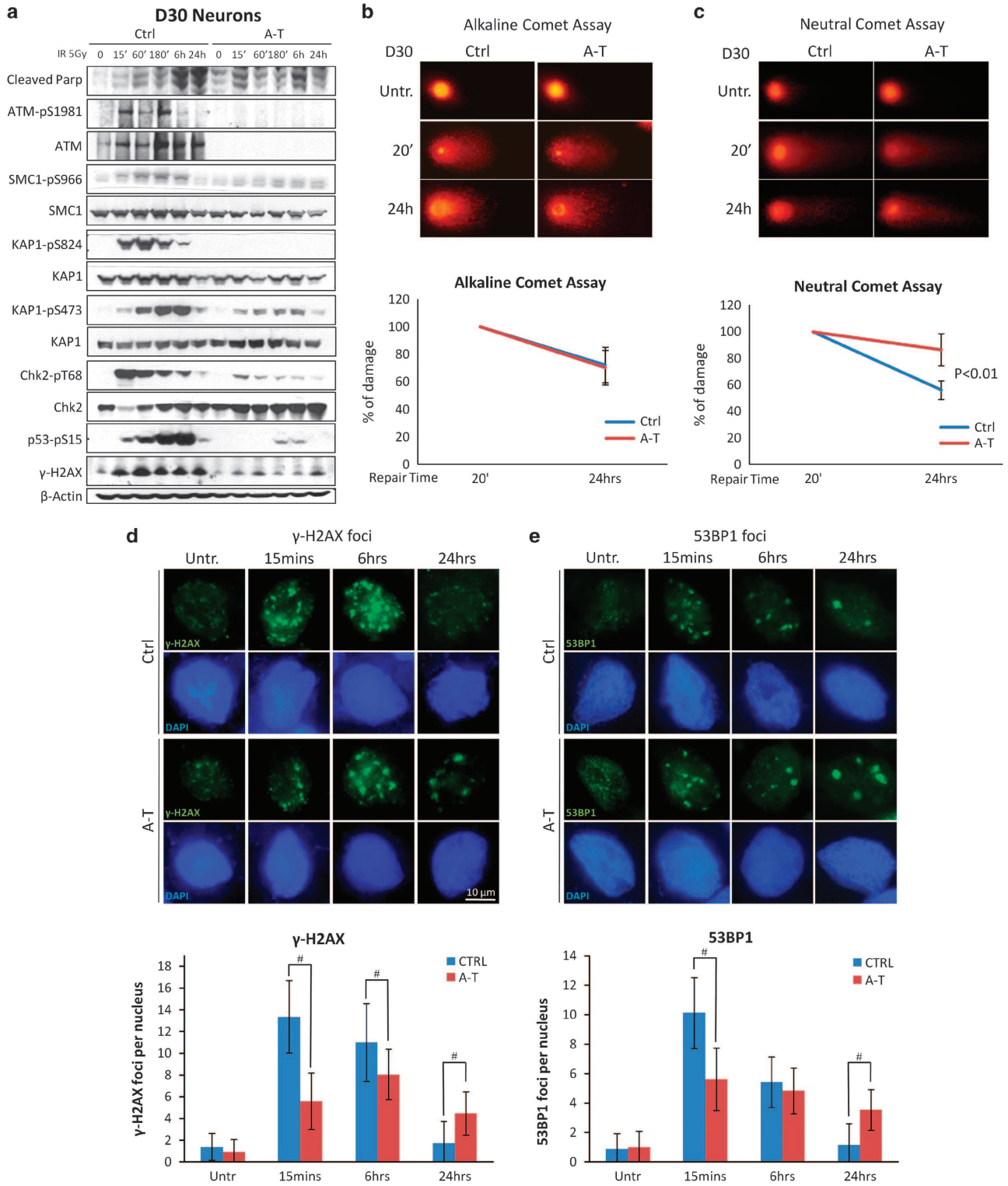

Figure 6 A-T post-mitotic neurons are defective in DDR. In **a**, D30 post-mitotic neurons (D30) were tested by western blot with antibodies specific for the various ATM phosphosubstrates and cleaved PARP at various times after treatment with 5 Gy IR. β-Actin was used as a loading control. DNA SSBs (**b**) and DSBs (**c**) were analyzed in neurons (D30) by alkaline and neutral comet assay, respectively, at two different times after treatment. 20 min after H_2O_2 or IR treatment was considered the time point with the maximum DNA damage. In **b** and **c**, representative photos of comets from untreated cells and at different time points following treatment. The ratio between treated and untreated tail moments of at least 50–70 cells per experimental point is shown in the graphs (values in %). One representative experiment out of three is shown. In **d** and **e**, formation and resolution of IR-induced nuclear foci. Neurons (D30) were irradiated with 0.5 Gy, collected at the indicated times and labeled for γ-H2AX (**d**) and 53BP1 (**e**). For each treatment, the number of foci was scored from 100 cell nuclei per duplicate preparations and from three independent experiments (mean ± S.D.) (**d** and **e**, bottom) For each time point, the difference between Ctrl and A-T was statistically significant ($^{\#}P<0.01$) (analysis performed by the Student's *t*-test)

H_2O_2. Ctrl and A-T post-mitotic neurons were equally sensitive to H_2O_2 and Paraquat (Figures 7a and b), a finding concordant with previous data[33] and with the results in Figure 6b showing that these cells have the same ability to resolve SSBs. By contrast, A-T neurons were significantly more resistant than Ctrl neurons to CPT and trabectedin by about 40% and 30%, respectively (Figures 7c and d).

Accumulation of Top1-ccs in A-T post-mitotic neurons. As in murine neural cells ATM deficiency results in accumulation of Top1-ccs and failure to recover global transcription after Top1-cc trapping,[34] we used a modified alkaline comet assay (MACA),[34] which indirectly quantifies Top1-ccs, to analyze hNPC-derived neurons (D30) untreated or treated for 45 min with 30 μM CPT (Figure 8a, left). As shown in the graph, the accumulation of Top1-ccs was much greater in A-T than in Ctrl neurons, both before and after CPT treatment. Of note, the overall levels of Top1 in proliferating and post-mitotic neurons (D30) were similar (Figure 8a, right).

To further confirm these findings, we applied the rapid approach to DNA adduct recovery (RADAR) assay that allows to directly detect Top1-ccs bound to genomic DNA.[35] D30 neurons, incubated for 1 h with 30 μM CPT, were harvested immediately or 3 h after washout of the drug to analyze the recovery of the damage. DNA was isolated, dot blotted and Top1-ccs were revealed with an anti-Top1 antibody and ECL. The levels of Top1-ccs (Figure 8b, left) were then normalized with the total amount of DNA, revealed by 4′,6-diamidin-2-fenilindolo (DAPI; Figure 8b, middle). β-Actin was used to verify that the DNA samples were free of non-covalently bound contaminating proteins (Figure 8b, right). The graph shows Top1 protein levels after normalization with DNA, and, as expected, untreated A-T neurons displayed higher accumulation of Top1-ccs than Ctrl cells, and also appeared defective in Top1-cc recovery after CPT removal.

Discussion

The mechanisms underlying neurodegeneration in A-T still remain elusive. Up to the present, ATM knockout and knockin mice[36,37] and *in vitro* ATM-deficient human neural stem cell (hNSC) models[19,38] have been useful for elucidating many aspects of the neuropathology, but animal models do not recapitulate the CNS disease,[39] while hNSCs have been argued to be very heterogeneous.[40] To obtain a more reliable *in vitro* model of neurodegeneration in A-T, two novel approaches have recently been described: the establishment of patient olfactory mucosa-derived neurospheres, which give rise to neurons,[41] and the reprogramming of patient fibroblasts to a pluripotent stage.[15,17]

As a functional analysis of the neuronal cells harboring patient-specific mutations in ATM has not yet been reported, in this study we examined hiPSC-derived A-T hNPCs and terminally differentiated neurons in culture. We found that A-T hNPCs displayed a strongly attenuated response to DSBs with respect to Ctrl hNPCs, which is concordant with our previous study on hNSCs.[19]

Moreover, terminally differentiated A-T neurons exhibited decreased expression of SYP and PSD95, which is

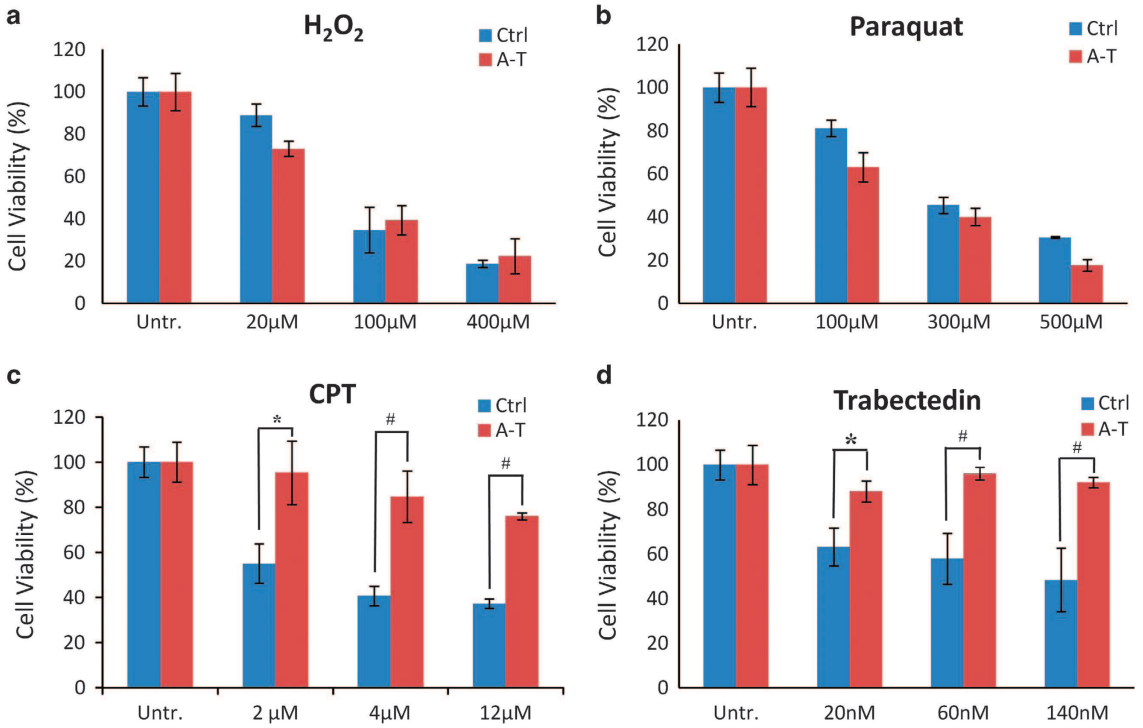

Figure 7 A-T post-mitotic cells are resistant to CPT and trabectedin treatment. Neurons at D30 grown in 96-well plates were assessed for cell viability by CellTiter-Glo 72 h after exposure to H_2O_2 for 20 min (**a**), or continuously with Paraquat (**b**), CPT (**c**) and trabectedin (**d**) at the indicated doses. All treatments were performed in triplicate wells. The graphs show mean ± S.D. and, where indicated, the difference between Ctrl and A-T was statistically significant ($^*P<0.05$; $^{\#}P<0.01$) (analysis performed by the Student's *t*-test)

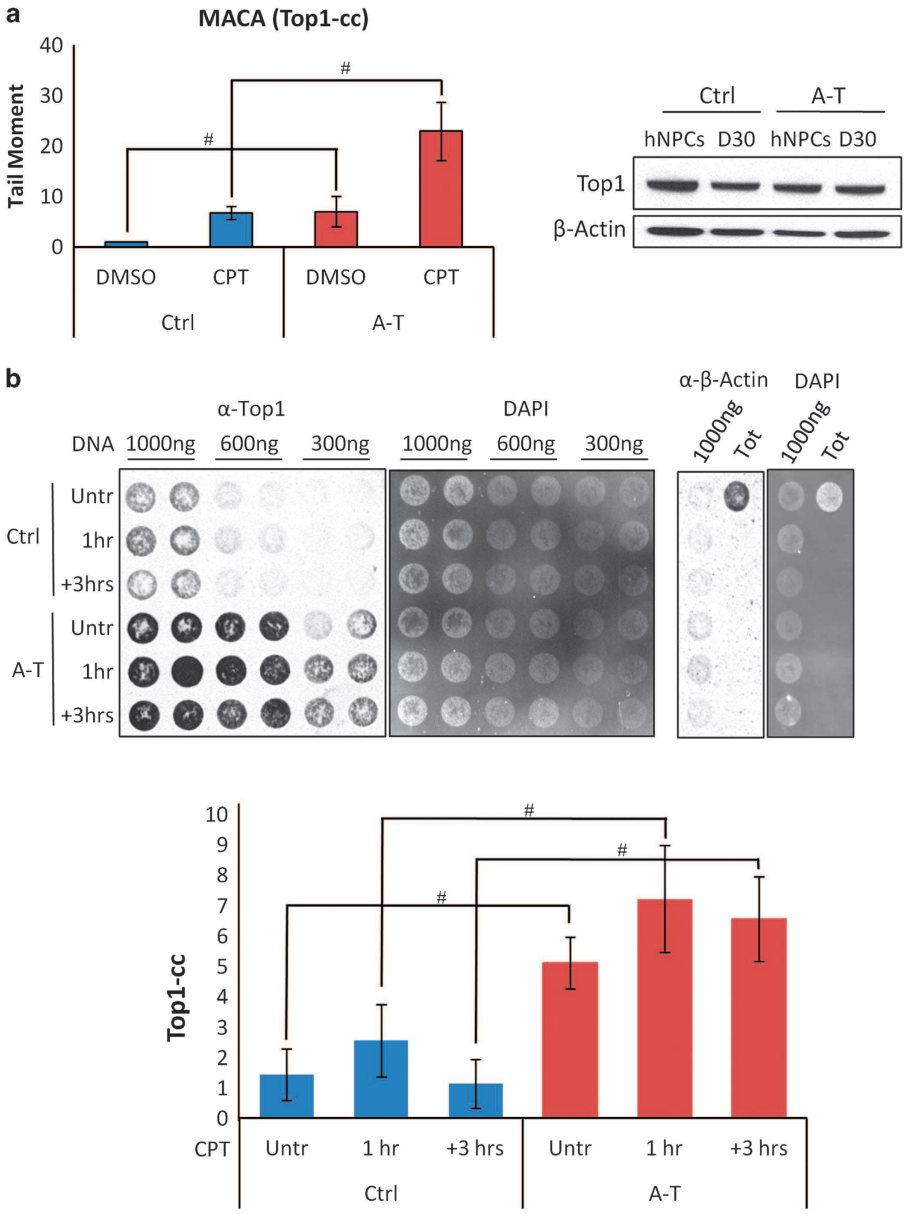

Figure 8 A-T post-mitotic neurons accumulate abnormal levels of Top1-cc. Total intracellular levels of Top1 protein were analyzed by western blot in proliferating hNPCs and post-mitotic neurons (**a** left). The levels of endogenous Top1-ccs were quantified in Ctrl and A-T post-mitotic neurons (D30) subjected to 30 μM CPT for 40 min by MACA from 50 cells per sample per experiment (**a** right). Data are the average of three independent experiments (mean ± S.D.). For each time point, the difference between Ctrl and A-T was statistically significant ($^{\#}P<0.01$) except where indicated. In **b**, Ctrl or A-T post-mitotic neuronal cells were untreated or treated with 30 μM CPT for 60 min or incubated and harvested 3 h after washing. The DNA was purified from cells after lyses with a denaturing buffer (MB) as reported in Materials and methods section. The indicated amount of DNA was vacuum blotted on a nitrocellulose membrane, which was then tested with anti-Top1 antibody and ECL (left) and with DAPI (middle). β-Actin (left) represents the control for non-covalently bound contaminant proteins. The densitometry analysis of Top1-cc signals after normalization for blotted DNA (DAPI) from three biological replicates (mean ± S.D.) is reported in the graph. Y axis represents the relative signal intensity. Where indicated the difference between Ctrl and A-T was statistically significant ($^{\#}P<0.01$; analysis performed by the Student's *t*-test)

concordant with previous works showing pre- and postsynaptic degeneration in ATM knockout mice,[42] the requirement of cytoplasmic ATM for phosphorylation of the synaptic vesicle proteins VAMP2 and Synapsin-1, and that ATM deficiency affects spontaneous vesicle release and establishment of long-term potentiation.[8] We also showed that A-T neurons are defective in the expression of SCG10 and KChip, altogether underpinning defects in neuronal maturation.

In agreement with the role of ATM in establishing the G1/S checkpoint arrest to prevent cells with damaged DNA from entering the S-phase,[1] primary Ctrl fibroblasts effectively arrested at the G1/S boundary after IR, but once reprogrammed into hiPSCs lost this G1/S checkpoint arrest to regain it at the stage of hNPCs. Instead, A-T cells showed a disrupted G1/S checkpoint, whatever the developmental stage. Notably, the absence of the G1/S checkpoint arrest in Ctrl hiPSCs is a characteristic of ESCs, where the cells

subjected to DNA damage in G1 enter S-phase to be eliminated by apoptosis, thus avoiding the propagation of mutations detrimental for the whole organism.[43,44] Accordingly, hiPSCs showed a great accumulation of p53-pS15 and faint induction of $p21^{waf1}$, compatible with a p53-dependent apoptotic response rather than with a G1/S checkpoint activation. Moreover, we found that Ctrl hiPSCs upregulate homologous recombination components such as Rad51, concordant with the fact that ESCs predominantly use this high fidelity pathway to avoid the accumulation of mutations, in contrast to somatic cells, which rely on the error-prone non-homologous end joining to repair DNA damage occurring in G1.[45]

BER is the major pathway for repair of oxidatively damaged DNA and various SSB intermediates,[22] and previous findings demonstrate that ATM and Chk2 facilitate the recruitment of downstream BER proteins to the initial damage recognition/excision step to promote BER.[46] Here, we found no significant differences in SP-BER activity between Ctrl and A-T proliferative hNPCs and post-mitotic neurons, while conversely, LP-BER activity was reduced in post-mitotic neurons. It should be noted that both SP-BER and LP-BER enzymatic efficiencies have been found to decrease, along with the respective protein components, in a neuroblastoma cell line upon differentiation,[24] and while our data on LP-BER concord with these results, those on SP-BER are clearly at variance. This could be because the expression of the SP-BER component XRCC1 is totally ablated in differentiated neuroblastoma cells,[24] while being only partially downregulated in our neurons. Regardless of this discrepancy, the variations in LP-BER activity between post-mitotic neurons and proliferative hNPCs were totally independent of ATM expression.

In accordance with our previous findings using hNSCs,[19] here we found that the DDR was vigorously activated in post-mitotic Ctrl neurons, according to the strong phosphorylation of ATM substrates, whereas in A-T post-mitotic neurons this response was almost ablated. We also highlighted relevant DSB repair defects in A-T neurons, which indicated that ATM deficiency delays the repair of DSBs, in accordance with previous reports[19,47] and with the observation that ATM is required for the repair of heterochromatic DSBs.[48] Furthermore, we demonstrated that A-T neurons show less apoptosis-related sub-diploid DNA content and a lower cleaved PARP induction after IR-treatment than Ctrl neurons. Indeed, ATM deficiency has been found to attenuate the apoptotic response to IR in A-T lymphoblastoid cells and in hNSCs[19,29] and ATM is required for the p53-mediated apoptosis of developing post-mitotic neurons exposed to IR.[49,50]

Although ATM appears involved in sensing and modulating the cellular response to ROS,[7] in our study A-T post-mitotic neurons were as sensitive to oxidative agents as Ctrl post-mitotic neurons, in agreement with the alkaline comet assays showing that these neurons equally repair SSBs, and in the case of H_2O_2, with results obtained with A-T lymphoblastoid cells.[33] By contrast, A-T post-mitotic neurons were significantly more resistant than Ctrl neurons to the genotoxic agents CPT and Trabectedin, probably because, in the absence of ATM, drug-induced DSBs in transcribed genes fail to activate a p53-dependent apoptotic response. This finding is concordant with results showing that ATM inhibition suppresses the genotoxic response in rat cerebellar granule neurons.[51]

Finally, as it has been recently shown that post-mitotic neural cells from ATM-deficient mice accumulate Top1-ccs and fail to recover global transcription after Top1-cc trapping by CPT,[34] and given that Top1-ccs can promote transcription elongation arrest and decay,[52] a phenomenon underlying neurodegeneration,[53–55] we analyzed Top1-ccs by two different assays and found greater levels of these intermediates in A-T than in Ctrl neurons. This finding, which to our knowledge has never been reported in human A-T neurons, warrants further studies to determine the impact of Top1-cc on genome-wide global transcription.

In conclusion, we have shown that A-T post-mitotic neurons display normal electrophysiological activity, defective expression of maturation markers, attenuated response to and repair of DSBs, but normal capacity to repair SSBs and normal BER activities. Strikingly, A-T neurons exhibit elevated levels of Top1-ccs, which may potentially impair transcriptional fidelity, a possibility that requires further investigation. Finally, we have shown that hiPSCs, like ESCs, provide a unique *in vitro* model to study the G1/S cell cycle checkpoint in a developmental context.

Materials and Methods

Primary cell culture. A-T patient-derived primary dermal fibroblasts (GM03487 and GM02530) were purchased from the Coriell Institute for Medical Research (Camden, NJ, USA). Both carry compound heterozygous mutations in *ATM* gene: GM03487 (c.8266A>T and c.1141_1142ins4), GM02530 (c.5675_5762del in trans with c.2251-1G>A and c.6573_6653del). Dermal fibroblasts of a healthy, ethnically matched donor and their iPSCs derivatives were previously described by us.[18] Fibroblasts were cultured at 37 °C in a 5% CO_2 in E-MEM supplemented with 15% heat-inactivated FCS, 100 units/ml penicillin, 100 μg/ml streptomycin, 100 μM non-essential amino acids and 2 mM glutamine. Primary MEFs (PMEF-CFL, Millipore, Bedford, MA, USA) were cultured in DMEM/F12 supplemented with 20% heat-inactivated FCS, 100 units/ml penicillin, 100 μg/ml streptomycin, 100 μM non-essential amino acids and 2 mM glutamine. PMEF-CFLs were mitotically inactivated (Mito-MEFs) with 1 μg/ml Mytomycin C (Kiowa Hakko Kirin, Milan, Italy) in DMEM high glucose (Euroclone, Pero, Italy) for 3 h and were then collected and plated into 0.1% gelatin-coated six-well plates at a concentration of 1.8×10^5 cells/cm^2.

hiPSC generation and culture. Human primary fibroblasts were infected with the STEMCCA Cre-Excisable Constitutive Polycistronic Lentivirus (Millipore) following the manufacturer's instructions. After 20–25 days, hiPSC clones were picked and transferred onto a Mito-MEF feeder in human embryonic stem cell (hESC) medium composed of DMEM/F12 supplemented with 20% KnockOut serum replacement (Life Technologies, Monza, Italy), 100 units/ml penicillin, 100 μg/ml streptomycin, 100 μM non-essential amino acids, 2 mM glutamine, 1 mM sodium pyruvate, 100 μM 2-mercaptoethanol and 20 ng/ml basic fibroblast growth factor (bFGF; Peprotech, Rocky Hill, NJ, USA). For passaging, hiPSCs were incubated with DMEM/F12 containing 1 mg/ml collagenase IV (Sigma, Milan, Italy) at 37 °C for 10 min. Cells were then scraped, collected and transferred at a split ratio of 1 : 3 to a new plate on Mito-MEFs in hESC medium. For feeder-free culture, hiPSCs were seeded on Matrigel (hESC-qualified matrix, BD Biosciences, San Jose, CA, USA)-coated plates in Nutristem culture medium (Stemgent, Cambridge, MA, USA) supplemented with 100 units/ml penicillin and 100 μg/ml streptomycin. For differentiation into derivatives of all three primary germ layers, hiPSCs were collected as for passaging and transferred to a gelatin-coated plate in DMEM/F12 supplemented with 20% heat-inactivated FCS, 100 units/ml penicillin, 100 μg/ml streptomycin, 100 μM non-essential amino acids and 2 mmol/l glutamine.

Generation of hNPCs and terminal differentiation. hiPSC colonies were harvested as for passaging, resuspended in hESC medium without bFGF and plated into a 6 cm low binding dish (HydroCell, Nunc, Cornaredo, Italy) for floating cultivation. After 5 days in suspension culture, EBs were collected and plated into a Matrigel (growth factor reduced, BD Biosciences)-coated dish for

additional 7 days in hESC media supplemented with 1X N2 (Gibco, Monza, Italy). After 7 days, rosettes were manually picked, mechanically dissociated into single cells and resuspended in Neural Precursor Medium (NPMedium) composed of DMEM/F12 supplemented with 2 mM glutamax, 100 units/ml penicillin, 100 μg/ml streptomycin, 1 : 500 B27 (Gibco), 1X N_2, 20 ng/ml epidermal growth factor (EGF) and 20 ng/ml bFGF (Società Italiana Chimici, Roma, Italy) and plated into Matrigel-coated flasks. NPMedium was changed every 2 days. For passaging, 90% confluent cells were detached using Accutase (PAA; Piscataway, NJ, USA) and split at a ratio of 1 : 4. hNPCs displayed a homogenous population starting at passage 3. To obtain terminally differentiated neurons, proliferating hNPCs were plated in NPMedium at a concentration of 5×10^3 cells/cm^2; 24 h later medium was changed to NPMedium without bFGF and EGF and replaced every 2–3 days thereafter.

Western blotting. Western blot analysis was performed as previously described.[56] Briefly, cells were lysed in Laemmli buffer (0.125 M Tris-HCl pH 6.8, 5% SDS) and lysates were sonicated, size-fractionated by SDS-PAGE and electroblotted onto PVDF membranes (Millipore), which were then incubated with primary antibodies and binding detected by ECL (Pierce, Rockford, IL, USA) on autoradiographic films. Bands were acquired with a digital scanner. The primary mouse monoclonal antibodies used were against the following molecules: OCT3/4(clone C-10), p53, Cdc2 (p34), p21^{waf1} (Santa Cruz Biotechnology, Inc., Dallas, TX, USA), β-tubulin III (clone 2G10), SYP, Vinculin, β-actin (Sigma), Tra-1-81 (eBioscience, San Diego, CA, USA), anti-Sox2, CDC25A (Abcam, Cambridge, UK), cyclin B1 (clone GNS-1, BD Pharmigen, Franklin Lakes, NJ, USA), γH2AX (H2AX-pSer139, clone JBW301, Millipore), PSD95, SCG10, Pan-KChIP, SYP (NeuroMab, Davis, CA, USA), Nestin, MAP2 (clone AP20, Chemicon International, Billerica, MA, USA), KAP1 (TIF1β, clone 4E1, Cell Signaling Technology, Danvers, MA, USA), Chk2 (clone DCS270-273, MBL Intl Corp., Des Plaines, IL, USA) and Top1 (BD Biosciences); rabbit antibodies specific for ATM (clone Y170, Epitomics, Burlingame, CA, USA), ATM pS1981 (Rockland Inc., Gilbertsville, PA, USA), cleaved PARP, XRCC1, KAP1-pS824, Chk2-pThr68, p53-pSer15 (Cell Signaling Technology), GFAP (Millipore), VGAT (Synaptic System, Goettingen, Germany), Polβ, Fen1 (Abcam), APE1 (Santa Cruz Biotechnology, Inc.), SMC1, SMC1-pSer966 (Bethyl Laboratories, Inc., Montgomery, TX, USA) and KAP1-pS473 (Biolabs, San Diego, CA, USA).

Immunofluorescence. Cells grown on coverslips were fixed in 4% buffered paraformaldehyde and permeabilized with 0.1% Triton X-100 in PBS for 10 min.[19] After blocking with PBS plus 10% normal goat serum for 40 min, cells were incubated overnight with primary antibodies at 4 °C. The following primary antibodies were used: monoclonal anti-Oct 3/4 (Clone C-10, Santa Cruz Biotechnology, Inc.), anti-SSEA4 (eBioscience), anti-Tra-1-81 (eBioscience), anti-α-SMA (clone 1A4, Sigma), anti-Sox17 (clone 245013, R&D System, Minneapolis, MN, USA), anti-β-tubulin III (clone TUJ1, Covance, Princeton, NJ, USA), anti-Nestin, anti-MAP2 (clone AP20, Chemicon International), anti-Vimentin (DAKO, Cernusco sul Naviglio, Italy), and polyclonal anti-GFAP (Millipore), anti-GABA, and anti-Ki67 (Thermo Scientific, Milan, Italy). After three washes with PBS, cells were incubated with Alexa fluor-labeled goat anti-mouse or anti-rabbit antibodies (Life Technologies) for 45 min. Cells were washed, counterstained with DAPI, mounted on glass-slides with Prolong Gold Antifade (Life Technologies) and analyzed using an Eclipse E1000 Nikon fluorescence microscope equipped with a DMX1200F CCD camera (Torino, Italy). For the assessment of nuclear foci, cells on coverslips were washed with 0.9% NaCl, air dried, fixed in 3% buffered paraformaldehyde and permeabilized for 5 min at 4 °C in 0.5% Triton. Cells were then blocked in PBS containing 5% BSA and 0.2% Tween20, labeled with antibodies specific for H2AX-pS139 antibody (clone JBW301, Upstate Biotechnology, New York, NY, USA) and 53BP1 (NB100-304; Novus Biologicals, Cambridge, UK) and foci from three independent experiments and duplicate slides were enumerated.

Electrophysiology analysis. Electrophysiological recordings were done as reported[18,57] at room temperature (22–25 °C) using a Multiclamp 700 A patch clamp amplifier and pClamp 10.2 software (Molecular Devices, Sunnyvale, CA, USA). Recordings usually started 5 min after the rupture of the membrane patch, to allow intracellular dialysis with the pipette solution. External bath solution consisted of 129 mM NaCl, 1.25 mM NaH_2PO_4, 35 mM glucose, 1.8 mM $MgSO_2$, 1.6 mM $CaCl_2$, 3 mM KCl and 10 mM HEPES, pH 7.4 with NaOH. The internal pipette solution consisted of 120 mM K gluconate, 15 mM KCl, 2 mM $MgCl_2$, 0.2 mM EGTA, 10 mM HEPES, 20 mM P-creatine, 2 mM ATP-Na_2, 0.2 mM GTP-Na_2 and 0.1 mM Leupeptine, pH 7.2 with KOH. Cell capacitance and series resistance errors were carefully compensated ($\sim$85%) throughout the experiment. The remaining linear capacity and leakage currents were eliminated online using a P/4 subtraction paradigm. Pipette resistance was between 2.6 and 3.0 MΩ. For the recordings of total voltage-gated ion currents, signals were filtered at 10 kHz and sampled at 100 kHz. For the recordings of postsynaptic currents, signals were filtered at 3 kHz and sampled at 10 kHz. When we switched the amplifier to current clamp mode, we applied the bridge balance compensation and held the resting potential at -70 mV by injecting the appropriate holding current. Neuronal firing was recorded injecting depolarizing current pulses of increasing amplitude. The neurons with unstable resting potential and/or unstable firing were discarded. In current clamp mode signals were filtered at 10 kHz and sampled at 20 kHz.

Cell cycle phase analysis. Cells at different developmental stages were irradiated with 5 Gy IR, incubated for 24 h and then fixed with 70% ethanol, washed, treated PBS-RNAse A, at 37 °C for 30 min and finally stained with propidium iodide. Cells were analyzed with a FACSCalibur flow cytofluorimeter instrument fitted with a Cell Quest software package (Becton Dickinson, Sunnyvale, CA, USA).

***In vitro* BER assay.** Whole-cell extracts for BER assays were prepared from 15×10^6 cells that were harvested, resuspended in 400 μl buffer I (10 mM Tris pH 7.8, 200 mM KCl) and then lysed by adding an equal volume of Buffer II (10 mM Tris pH 7.8, 200 mM KCl, 2 mM EDTA, 40% glycerol, 0.2% Nonidet-P40, 2 mM DTT and protease inhibitors). After stirring for 1 h at 4 °C and centrifugation, the supernatant was aliquoted and stored at -80 °C. Closed circular DNA molecules containing a single lesion were constructed as described[58] by priming single-stranded pGem-3Zf(+) DNA with the oligonucleotides containing the modified base of interest (uracil and tetrahydrofuran (THF). These oligonucleotides were [γ-32P]ATP 5′ end-labeled. The *in vitro* DNA synthesis was performed by using DNA T4 DNA polymerase holoenzyme, single-stranded DNA-binding protein, dNTPs and T4 DNA ligase. The plasmid DNA containing a single uracil residue was digested with UDG to produce a single abasic site. Repair of the plasmid DNA containing the lesions (pGEM-AP/THF) was conducted as described.[58] Briefly, reaction mixtures (50 μl) contained 40 mM HEPES/KOH (pH 7.9), 75 mM KCl, 5 mM $MgCl_2$, 0.5 mM dithiothreitol, 50 μM of each dNTP, 2 mM ATP, 40 mM phosphocreatine, 2.5 μg of creatine phosphokinase (type I), 3.4% glycerol, 18 μg of bovine serum albumin and 50 μg of cell extracts. After incubation at 30 °C, the plasmid DNA was recovered and loaded onto agarose gels. The relative yield of the different plasmid forms was measured. All experiments were repeated at least three times, and representative experiments are shown.

Comet assay and MACA. To prepare the Comet slides, the day before analysis microscope glass slides were washed with methanol, air dried and immersed in molten Normal Melting-Agarose (1%) to obtain the first agarose layer, before being stored overnight at 4 °C. To evaluate DNA strand breaks, post-mitotic neurons were incubated with 20 μM H_2O_2 (Sigma) for 20 min or irradiated with 5 Gy. After treatment with Accutase, the cell suspension was added to 180 μl of molten Low Melting-Agarose (0.7% LM-agarose) at 37 °C, and immediately layered onto Comet slides, covered with a coverslip and stored at 4 °C in the dark. After 25 min, the coverslip was removed and a second LM-Agarose layer was layered onto the slides. The slides were then transferred to a pre-chilled lysis solution (2.5 M NaCl, 100 mM EDTA, 10 mM Tris-base, 300 mM NaOH, pH 10, and 1% freshly added Triton X-100) for 2 h at 4 °C in the dark. In the alkaline condition, the slides were placed in a horizontal electrophoresis chamber and the denaturation step was performed in pre-chilled electrophoresis solution (300 mM NaOH, 1 mM EDTA, pH $>$ 13) at 4 °C in the dark. After 20 min, the slides were electrophoresed (1 V/cm, 300 mA) for 20 min, and washed with neutralization buffer (0.4 M Tris-HCl, pH 7.4). In the neutral condition, after the lysis the slides were washed twice with 1 $\times$ Tris-borate EDTA buffer solution pH 8.3 (TBE) for 10 min. Electrophoresis was carried out at the rate of 1.0 V/cm for 20 min. The slides were then washed in deionized water for 5 min. MACA on post-mitotic neurons was performed as described.[34] After electrophoresis, Comet slides were fixed with pre-chilled methanol, air dried overnight, stained with ethidium bromide (0.1 mg/ml) for 10 min, and images acquired with an Eclipse E1000 Nikon fluorescence microscope equipped with a DMX1200F CCD camera. Comet images were processed with Comet Score software (v1.5; TriTek Corporation, Sumerduck, VA, USA).

Rapid approach to DNA adduct recovery. Post-mitotic neurons (D30) were incubated with or without 30 μM CPT for 1 h. Following treatment, part of the cells was immediately lysed, while the remaining washed with PBS and incubated in fresh medium for 3 h before lysis. For DNA–protein covalent complexes isolation, cells were lysed in the culture plates by addition of 2 ml of MB lysis reagent (6 M GTC, 10 mM Tris-HCl, pH 6.5, 20 mM EDTA, 4% Triton X100, 1% Sarkosyl and 1% dithiothreitol) and processed as described.[35] Purified DNA was vacuum blotted on nitrocellulose membranes and Top1 detected using a mouse monoclonal anti-Top1 antibody (BD Biosciences) and ECL. Sample loadings were normalized for DNA content using DAPI.

Neuronal viability assay. Neuronal viability was evaluated using the Cell Titer-Glo luminescent assay (Promega, Madison, WI, USA). Briefly, hNPCs were seeded into Matrigel-coated 96-well plates (10 000 cells per well) and let to differentiate for 30 days, after which they were treated in triplicate with CPT, H_2O_2, Paraquat (all from Sigma) or trabectedin (Yondelis; ET-743) for 72 h. H_2O_2 was removed after 20 min. Afterward, a volume of CellTiter-Glo Reagent was added to each well and luminescence measured using a Tecan Genios instrument (Männedorf, Switzerland).

Conflict of Interest

The authors declare no conflict of interest.

Acknowledgements. This work was financially supported by Comitato Telethon Fondazione Onlus (grant # GGP10066 to DD) and by the Italian Association for Cancer Research (AIRC) (grant # IG-10248 to DD). Dr. Carlessi Luigi is recipient of a post-doctoral fellowships award from Fondazione Umberto Veronesi. We wish to thank Dr. Sherif El-Kamisy, Department of Molecular Biology and Biotechnology, Sheffield University, UK, for kindly providing the detailed MACA protocol, and Dr. Christian Unger, Centre for Stem Cell Biology, Sheffield University, UK, for providing training (to DL) and expertise in the field of iPSCs, as well as reagents.

1. Shiloh Y, Ziv Y. The ATM protein kinase: regulating the cellular response to genotoxic stress, and more. *Nat Rev Mol Cell Biol* 2013; **14**: 197–210.
2. Ambrose M, Gatti RA. Pathogenesis of ataxia-telangiectasia: the next generation of ATM functions. *Blood* 2013; **121**: 4036–4045.
3. McKinnon PJ. DNA repair deficiency and neurological disease. *Nat Rev Neurosci* 2009; **10**: 100–112.
4. Verhagen MM, Martin JJ, van Deuren M, Ceuterick-de Groote C, Weemaes CM, Kremer BH *et al.* Neuropathology in classical and variant ataxia-telangiectasia. *Neuropathology* 2012; **32**: 234–244.
5. Barzilai A, Rotman G, Shiloh Y. ATM deficiency and oxidative stress: a new dimension of defective response to DNA damage. *DNA Repair* 2002; **1**: 3–25.
6. Liu N, Stoica G, Yan M, Scofield VL, Qiang W, Lynn WS *et al.* ATM deficiency induces oxidative stress and endoplasmic reticulum stress in astrocytes. *Lab Invest* 2005; **85**: 1471–1480.
7. Guo Z, Kozlov S, Lavin MF, Person MD, Paull TT. ATM activation by oxidative stress. *Science* 2010; **330**: 517–521.
8. Li J, Han YR, Plummer MR, Herrup K. Cytoplasmic ATM in neurons modulates synaptic function. *Curr Biol* 2009; **19**: 2091–2096.
9. Siddoway B, Hou H, Yang H, Petralia R, Xia H. Synaptic activity bidirectionally regulates a novel sequence-specific S-Q phosphoproteome in neurons. *J Neurochem* 2014; **128**: 841–851.
10. Li J, Chen J, Ricupero CL, Hart RP, Schwartz MS, Kusnecov A *et al.* Nuclear accumulation of HDAC4 in ATM deficiency promotes neurodegeneration in ataxia telangiectasia. *Nat Med* 2012; **18**: 783–790.
11. Li J, Hart RP, Mallimo EM, Swerdel MR, Kusnecov AW, Herrup K. EZH2-mediated H3K27 trimethylation mediates neurodegeneration in ataxia-telangiectasia. *Nat Neurosci* 2013; **16**: 1745–1753.
12. Barzilai A. The neuro-glial-vascular interrelations in genomic instability symptoms. *Mech Ageing Dev* 2011; **132**: 395–404.
13. Borghesani PR, Alt FW, Bottaro A, Davidson L, Aksoy S, Rathbun GA *et al.* Abnormal development of Purkinje cells and lymphocytes in Atm mutant mice. *Proc Natl Acad Sci USA* 2000; **97**: 3336–3341.
14. Takahashi K, Tanabe K, Ohnuki M, Narita M, Ichisaka T, Tomoda K *et al.* Induction of pluripotent stem cells from adult human fibroblasts by defined factors. *Cell* 2007; **131**: 861–872.
15. Nayler S, Gatei M, Kozlov S, Gatti R, Mar JC, Wells CA *et al.* Induced pluripotent stem cells from ataxia-telangiectasia recapitulate the cellular phenotype. *Stem Cells Transl Med* 2012; **1**: 523–535.
16. Carlessi L, Fusar Poli E, De Filippis L, Delia D. ATM-deficient human neural stem cells as an in vitro model system to study neurodegeneration. *DNA Repair (Amst)* 2013; **12**: 605–611.
17. Carlessi L, Fusar Poli E, Delia D. Brain and induced pluripotent stem cell-derived neural stem cells as an in vitro model of neurodegeneration in ataxia-telangiectasia. *Exp Biol Med (Maywood)* 2013; **238**: 301–307.
18. Verpelli C, Carlessi L, Bechi G, Fusar Poli E, Orellana D, Heise C *et al.* Comparative neuronal differentiation of self-renewing neural progenitor cell lines obtained from human induced pluripotent stem cells. *Front Cell Neurosci* 2013; **7**: 175.
19. Carlessi L, De Filippis L, Lecis D, Vescovi A, Delia D. DNA-damage response, survival and differentiation in vitro of a human neural stem cell line in relation to ATM expression. *Cell Death Differ.* 2009; **16**: 795–806.
20. Momilovic O, Choi S, Varum S, Bakkenist C, Schatten G, Navara C. Ionizing radiation induces ataxia telangiectasia mutated-dependent checkpoint signaling and G2 but not G1 cell cycle arrest in pluripotent human embryonic stem cells. *Stem Cells* 2009; **27**: 1822–1835.
21. Momcilovic O, Knobloch L, Fornsaglio J, Varum S, Easley C, Schatten G. DNA damage responses in human induced pluripotent stem cells and embryonic stem cells. *PLoS One* 2010; **5**: e13410.
22. Xu G, Herzig M, Rotrekl V, Walter CA. Base excision repair, aging and health span. *Mech Ageing Dev* 2008; **129**: 366–382.
23. Fortini P, Ferretti C, Pascucci B, Narciso L, Pajalunga D, Puggioni EMR *et al.* DNA damage response by single-strand breaks in terminally differentiated muscle cells and the control of muscle integrity. *Cell Death Differ* 2012; **19**: 1741–1749.
24. Sykora P, Yang JL, Ferrarelli LK, Tian J, Tadokoro T, Kulkarni A *et al.* Modulation of DNA base excision repair during neuronal differentiation. *Neurobiol Aging* 2013; **34**: 1717–1727.
25. Hegde ML, Hegde PM, Rao KS, Mitra S. Oxidative genome damage and its repair in neurodegenerative diseases: function of transition metals as a double-edged sword. *J Alzheimers Dis* 2011; **24**(Suppl 2): 183–198.
26. Benitez-Bribiescal L, Sanchez-Suarez P. Oxidative damage, bleomycin, and gamma radiation induce different types of DNA strand breaks in normal lymphocytes and thymocytes: a comet assay study. *Ann. N Y Acad Sci* 1999; **887**: 133–149.
27. Riballo E, Kuhne M, Rief N, Doherty A, Smith GC, Recio MJ *et al.* A pathway of double-strand break rejoining dependent upon ATM, Artemis, and proteins locating to gamma-H2AX foci. *Mol Cell* 2004; **16**: 715–724.
28. Schultz LB, Chehab NH, Malikzay A, Halazonetis TD. p53 binding protein 1 (53BP1) is an early participant in the cellular response to DNA double-strand breaks. *J Cell Biol* 2000; **151**: 1381–1390.
29. Takagi M, Delia D, Chessa L, Iwata S, Shigeta T, Kanke Y *et al.* Defective control of apoptosis, radiosensitivity, and spindle checkpoint in ataxia telangiectasia. *Cancer Res* 1998; **58**: 4923–4929.
30. Liu LF, Desai SD, Li T, Mao Y, Sun M, Sim S. Mechanism of action of camptothecin. *Ann N Y Acad Sci* 2000; **922**: 1–10.
31. Minuzzo M, Marchini S, Broggini M, Faircloth G, D'Incalci M, Mantovani R. Interference of transcriptional activation by the antineoplastic drug ecteinascidin-743. *Proc Natl Acad Sci USA* 2000; **97**: 6780–6784.
32. McCarthy S, Somayajulu M, Sikorska M, Borowy-Borowski H, Pandey S. Paraquat induces oxidative stress and neuronal cell death; neuroprotection by water-soluble coenzyme Q10. *Toxicol Appl Pharmacol* 2004; **201**: 21–31.
33. Suraweera A, Becherel OJ, Chen P, Rundle N, Woods R, Nakamura J *et al.* Senataxin, defective in ataxia oculomotor apraxia type 2, is involved in the defense against oxidative DNA damage. *J Cell Biol* 2007; **177**: 969–979.
34. Alagoz M, Chiang SC, Sharma A, El-Khamisy SF. ATM deficiency results in accumulation of DNA-topoisomerase I covalent intermediates in neural cells. *PLoS One* 2013; **8**: e58239.
35. Kiianitsa K, Maizels N. A rapid and sensitive assay for DNA–protein covalent complexes in living cells. *Nucleic Acids Res* 2013; **41**: e104.
36. Spring K, Cross S, Li C, Watters D, Ben-Senior L, Waring P *et al.* Atm knock-in mice harboring an in-frame deletion corresponding to the human ATM 7636del9 common mutation exhibit a variant phenotype. *Cancer Res* 2001; **61**: 4561–4568.
37. Elson A, Wang Y, Daugherty CJ, Morton CC, Zhou F, Campos-Torres J *et al.* Pleiotropic defects in ataxia-telangiectasia protein-deficient mice. *Proc Natl Acad Sci USA* 1996; **93**: 13084–13089.
38. Biton S, Gropp M, Itsykson P, Pereg Y, Mittelman L, Johe K *et al.* ATM-mediated response to DNA double strand breaks in human neurons derived from stem cells. *DNA Repair* 2007; **6**: 128–134.
39. Lavin MF. The appropriateness of the mouse model for ataxia-telangiectasia: neurological defects but no neurodegeneration. *DNA Repair (Amst)* 2013; **12**: 612–619.
40. Jakel RJ, Schneider BL, Svendsen CN. Using human neural stem cells to model neurological disease. *Nat Rev Genet* 2004; **5**: 136–144.
41. Stewart R, Kozlov S, Matigian N, Wali G, Gatei M, Sutharsan R *et al.* A patient-derived olfactory stem cell disease model for ataxia-telangiectasia. *Hum Mol Genet* 2013; **22**: 2495–2509.
42. Kuljis RO, Xu Y, Aguila MC, Baltimore D. Degeneration of neurons, synapses, and neuropil and glial activation in a murine Atm knockout model of ataxia-telangiectasia. *Proc Natl Acad Sci USA* 1997; **94**: 12688–12693.
43. Abdelalim EM. Molecular mechanisms controlling the cell cycle in embryonic stem cells. *Stem Cell Rev* 2013; **9**: 764–773.

44. Momcilovic O, Navara C, Schatten G. Cell cycle adaptations and maintenance of genomic integrity in embryonic stem cells and induced pluripotent stem cells. *Results Probl Cell Differ* 2011; **53**: 415–458.
45. Tichy ED, Pillai R, Deng L, Liang L, Tischfield J, Schwemberger SJ *et al.* Mouse embryonic stem cells, but not somatic cells, predominantly use homologous recombination to repair double-strand DNA breaks. *Stem Cells Dev* 2010; **19**: 1699–1711.
46. Chou WC, Wang HC, Wong FH, Ding SL, Wu PE, Shieh SY *et al.* Chk2-dependent phosphorylation of XRCC1 in the DNA damage response promotes base excision repair. *EMBO J* 2008; **27**: 3140–3150.
47. Adams BR, Golding SE, Rao RR, Valerie K. Dynamic dependence on ATR and ATM for double-strand break repair in human embryonic stem cells and neural descendants. *PLoS One* 2010; **5**: e10001.
48. Woodbine L, Brunton H, Goodarzi AA, Shibata A, Jeggo PA. Endogenously induced DNA double strand breaks arise in heterochromatic DNA regions and require ataxia telangiectasia mutated and Artemis for their repair. *Nucleic Acids Res* 2011; **39**: 6986–6997.
49. Herzog K, Chong MJ, Kapsetaki M, Morgan JI, McKinnon PJ. Requirement for Atm in ionizing radiation-induced cell death in the developing central nervous system. *Science* 1998; **280**: 1089–1091.
50. Lee Y, Chong MJ, McKinnon PJ. Ataxia telangiectasia mutated-dependent apoptosis after genotoxic stress in the developing nervous system is determined by cellular differentiation status. *J Neurosci* 2001; **21**: 6687–6693.
51. Tian B, Yang Q, Mao Z. Phosphorylation of ATM by Cdk5 mediates DNA damage signalling and regulates neuronal death. *Nat Cell Biol* 2009; **11**: 211–218.
52. Solier S, Ryan MC, Martin SE, Varma S, Kohn KW, Liu H *et al.* Transcription poisoning by Topoisomerase I is controlled by gene length, splice sites, and miR-142-3p. *Cancer Res* 2013; **73**: 4830–4839.
53. Glass D, Vinuela A, Davies MN, Ramasamy A, Parts L, Knowles D *et al.* Gene expression changes with age in skin, adipose tissue, blood and brain. *Genome Biol* 2013; **14**: R75.
54. Berchtold NC, Coleman PD, Cribbs DH, Rogers J, Gillen DL, Cotman CW. Synaptic genes are extensively downregulated across multiple brain regions in normal human aging and Alzheimer's disease. *Neurobiol Aging* 2013; **34**: 1653–1661.
55. Lu T, Pan Y, Kao SY, Li C, Kohane I, Chan J *et al.* Gene regulation and DNA damage in the ageing human brain. *Nature* 2004; **429**: 883–891.
56. Carlessi L, Buscemi G, Fontanella E, Delia D. A protein phosphatase feedback mechanism regulates the basal phosphorylation of Chk2 kinase in the absence of DNA damage. *Biochim Biophys Acta* 2010; **1803**: 1213–1223.
57. Cestele S, Schiavon E, Rusconi R, Franceschetti S, Mantegazza M. Nonfunctional NaV1.1 familial hemiplegic migraine mutant transformed into gain of function by partial rescue of folding defects. *Proc Natl Acad Sci USA* 2013; **110**: 17546–17551.
58. Frosina G, Cappelli E, Ropolo M, Fortini P, Pascucci B, Dogliotti E. *In vitro* base excision repair assay using mammalian cell extracts. *Methods Mol Biol* 2006; **314**: 377–396.

Supplementary Information accompanies this paper on Cell Death and Disease website (http://www.nature.com/cddis)